Autophagy and Extracellular Vesicle Secretion in the Prion-like Spreading of Amyloid beta

by

Anissa Marie Viveiros

A thesis submitted in partial fulfillment of the requirements for the degree of

Master of Science

Department of Pharmacology

University of Alberta

Abstract

Alzheimer's disease (AD) is characterized by the accumulation of amyloid beta (Aβ) peptide. It has been proposed that AD pathology is transmissible by a "prion-like" mechanism through extracellular vesicles (EVs) that contain Aβ. In this context, EVs describe both microvesicles and exosomes, which are derived from the outward budding of the plasma membrane and from multivesicular bodies (MVBs) respectively. MVBs can either be targeted to the lysosome as intermediates of autophagic degradation, or to the plasma membrane for exosome release. Autophagy is an essential cellular process and impairments in this pathway occur in AD. Our laboratory has discovered that Aβ inhibits autophagy by reducing protein prenylation: a post-translational modification necessary for lysosomal targeting in autophagy. Despite evolving research in EVs as a vehicle for Aβ spreading, the regulation of EV-mediated Aβ transfer is unknown. We propose that Aβ-induced autophagy blockade increases the cellular release of EVs, thus contributing to the "prion-like" spreading of Aβ aggregates.

Prior to assessing the effects of Aβ, we optimized the methods for collection, separation and analysis of EVs derived from cultured cells. We analyzed EVs by image flow cytometry, nanoparticle tracking analysis and transmission electron microscopy. We characterized EV subtypes by image flow cytometry with EV markers CD9 and AnnexinV.

We compared differential ultracentrifugation, which is the most common method employed in the field, to size exclusion chromatography for EV separation. Our results corroborated reports that high-speed centrifugation causes aggregation of EVs, thus we determined size exclusion chromatography to be the optimal separation

method.

We found that Aβ blocked autophagy and increased EV secretion. Further, Aβ treatment induced the secretion of different EV subtypes than untreated cells. We next developed a cell-to-cell transfer paradigm of EVs derived from labeled N2aAPP^{swe} donor cells fed to N2a recipient cells to determine the transmission of fluorescently labeled EVs and Aβ. Image flow cytometry revealed a proportion of recipient cells contained EVs, and this was enhanced by blocked autophagy in the donor cells. However, under our experimental conditions, we could not detect a corresponding increase in Aβ transfer to recipient cells. Nevertheless, based on the indication that different modes of autophagy blockade caused an increase of selective EV subtypes, it is possible that the lack of increased cell-to-cell transfer of Aβ was due to the paradigm that we employed.

Overall, we validated the use of Image Flow Cytometry to determine EV secretion and EV subtypes. The novelty of our work is to identify dysfunctional autophagy as critical for the intercellular spreading of Aβ and give insight, based on previous work, as impaired protein prenylation as a possible mechanism. Further, we aimed to identify and address problems in the field, as many conclusions are derived based on ultracentrifugation procedures that may hamper physiological relevance. We proposed image flow cytometry as the optimal technique to derive conclusions on EV secretion.

Acknowledgements

I was fortunate for the opportunity to perform graduate studies within the Department of Pharmacology at the University of Alberta. There are several people that have made this work possible, and I am glad to thank them.

First of all, thank you to my supervisor Dr. Elena Posse de Chaves for accepting me into her laboratory and for the guidance throughout my Masters program. Elena has taught me invaluable lessons in critical thinking, understanding how to comprehend and disseminate scientific knowledge, as well as offering technical assistance in experimental protocols. I have learned an incredible amount both in the laboratory and beyond the bench, and that is thanks to her.

Thank you to the rest of my supervisory committee, Dr. Simonetta Sipione and Dr. Satyabrata Kar. I appreciate all of your suggestions, insightful comments, and constructive advice throughout my Masters program. Thank you to Dr. David Westaway for being my external examiner.

Thank you to the present and former members of the Posse de Chaves laboratory, specifically Sarah Samuelson, Dr. Qian Wang and Jennifer Ling for the assistance in completion of this thesis, scientific discussions and for providing an always enjoyable work and learning environment. In addition, I am fortunate for the collaborative opportunities I have had with Dr. Sipione's laboratory and their troubleshooting assistance, teaching of specific techniques, and/or being a part of the brainstorming of new ideas within our EV team namely Dr. Luis Carlos, Vaibhavi Kadam, John Monyror and Dr. Danny Galleguillos.

Thank you to the Alberta Prion Research Institute for funding this project and offering opportunities to present my research.

Finally, I am thankful to my family and friends for the unending support and for reminding me I always have them to fall back on.

Table of Contents

Chapter 1 1

1. Introduction 1
- **1.1 Alzheimer's Disease** 2
- **1.2 Prions and Prion-like diseases** 6
- **1.3 Autophagy** 10
- **1.4 Protein Prenylation** 14
- **1.5 Unconventional Secretion** 19
- **1.6 Extracellular Vesicles** 21
- **1.7 Biogenesis of Extracellular Vesicles** 22
  - *1.7.1 Microvesicles* 22
  - *1.7.2 Exosomes* 24
- **1.8 Regulation of Extracellular Vesicles Secretion** 28
- **1.9 Extracellular Vesicles in Neurodegenerative Diseases** 29
- **1.10 Methods for the Study of Extracellular Vesicles** 30
  - *1.10.1 Characterization of Extracellular Vesicles* 31
  - *1.10.2 Analysis of Extracellular Vesicles* 32
  - *1.10.3 Separation of Extracellular Vesicles* 37
- **1.11 Hypothesis and Objectives** 40

Chapter 2 42

2. Materials and Methods 42
- **2.1 Materials** 43
- **2.2 Cell Culture** 43
- **2.3 Cell Labeling with DiI** 44
- **2.4 Oligomeric Aβ Preparation** 45
- **2.5 Cell Treatments** 45
- **2.6 EV Collection** 46
- **2.7 Immunoblot Analysis** 46
- **2.8 Immunoblot for Aβ** 47
- **2.9 Dotblot** 48
- **2.10 Protein precipitation** 49
- **2.11 Aβ ELISA** 49
- **2.12 Protein Quantification** 49
- **2.13 Differential Ultracentrifugation (UC)** 50
- **2.14 Iodixanol Flotation Gradient** 50
- **2.15 Size Exclusion Chromatography (SEC)** 51
- **2.16 Image Flow Cytometry (IFC)** 52
  - *2.16.1 EVs Labeling* 52
  - *2.16.2 Acquisition and Data Analysis* 52
- **2.17 Nanoparticle Tracking Analysis (NTA)** 54
- **2.18 Transmission Electron Microscopy (TEM)** 55
- **2.19 Analysis of Autophagic flux using tandem mCherry-GFP-LC3 (tLC3)** 55
- **2.20 Aβ Localization in EVs** 58
- **2.21 Cell-to-cell Transfer** 59
- **2.22 Determination of Protein Prenylation in Cell Lysates** 60
- **2.23 Statistics** 62

Chapter 3 63

3. Methods for Separation and Analysis of EVs Released by Cultured Cells 63
3.1 Introduction 64
3.2 Results 66
3.2.1 EVs labeling 66
3.2.2 Selection of Culture Medium for EV Collection 67
3.2.3 Methods of EV Separation and Analysis 74
3.3 Discussion 84
3.4 Conclusion 91

Chapter 4 93

4. Effect of Autophagy on EV Secretion and Cell-to-cell Transfer of Aβ 93
4.1 Introduction 94
4.2 Results 95
4.2.1 Regulation of EV secretion detected by IFC 95
4.2.2 Aβ blocks autophagic flux 96
4.2.3 Aβ increases EV secretion 100
4.2.4 Aβ is loaded in EVs 107
4.2.5 Blocking autophagy increases EV transfer 107
4.2.6 Blocking autophagy does not increase the cell-to-cell transfer of Aβ 111
4.2.7 EVs are highly internalized by recipient cells 111
4.3 Discussion 115
4.4 Conclusion 122

References 124

Appendices 142

List of Figures

Figure 1	Page 5
Figure 2	Page 7
Figure 3	Page 11
Figure 4	Page 12
Figure 5	Page 16
Figure 6	Page 20
Figure 7	Page 23
Figure 8	Page 26
Figure 9	Page 33
Figure 10	Page 36
Figure 11	Page 57
Figure 12	Page 68
Figure 13	Page 69
Figure 14	Page 72
Figure 15	Page 73
Figure 16	Page 75
Figure 17	Page 77
Figure 18	Page 78
Figure 19	Page 80
Figure 20	Page 81
Figure 21	Page 82
Figure 22	Page 83
Figure 23	Page 97
Figure 24	Page 99
Figure 25	Page 101
Figure 26	Page 102
Figure 27	Page 104
Figure 28	Page 105
Figure 29	Page 106
Figure 30	Page 108
Figure 31	Page 109
Figure 32	Page 110
Figure 33	Page 112
Figure 34	Page 113

List of Abbreviations

AAV	Adeno-associated virus
AD	Alzheimer's Disease
AICD	APP intracellular C-terminal domain
Akt	Protein kinase B
APP	Amyloid precursor protein
ATG	Autophagy-related genes
Atg	Autophagy-related proteins
AV	Autophagic vacuoles
Aβ	Amyloid beta
BafA1	Bafilomycin A1
BCA	Bicinchoninic acid
BGS	Bovine growth serum
BSA	Bovine serum albumin
CCD	Charge-coupled device
CFSE	5,6-carboxy-succinimidyl-fluoresceine ester
CNS	Central nervous system
Cryo-EM	Cryogenic electron microscopy
CSF	Cerebrospinal fluid
CTF	Carboxy-terminal fragment
DMEM	Dulbecco's modified eagle medium
ER	Endoplasmic Reticulum
EVs	Extracellular vesicles
FBS	Fetal bovine serum
FPP	Farnesyl-farnesyl pyrophosphate
FTase	Farnesyltransferase
GDI	GDP-dissociation inhibitor
GFP	Green fluorescent protein
GGPP	Geranylgeranyl pyrophosphate
GGTase-I	geranylgeranyltransferase type 1
GGTase-II	geranylgeranyltransferase type 2
IFC	Image Flow Cytometry
ILVs	Intraluminal vesicles
LC3	Microtubule-associated protein light chain 3
LEVs	Large EVs
MCI	Mild cognitive impairment
MTOC	Microtubule organizing centre

mTOR	Mammalian target of rapamycin
MVB	Multivesicular body
NFT	Neurofibrillary tangles
NT	Neuropil threads
NTA	Nanoparticle tracking analysis
$oA\beta_{42}$	Amyloid beta oligomers
PBS	Phosphate buffered saline
PE	Phosphatidylethanolamine
PEG	Polyethylene glycol
PrP	Prion protein
PS	Phosphatidylserine
RabGGTase	Rab geranylgeranyl transferase
SEC	Size exclusion chromatography
SEVs	Small EVs
SN	Supernatant
SREBP2	Sterol regulatory element-binding protein-2
SSC	Side scatter
tLC3	mCherry-GFP-LC3 fluorescent protein
TDI	Time delay integration
TGN	Trans-Golgi Network
TEM	Transmission electron microscopy
UC	Differential ultracentrifugation
UCM	Unconditioned media

Chapter 1

Introduction

1.1 Alzheimer's Disease

Alzheimer's disease (AD) is the most common cause of age-related dementia and accounts for 60-80% of all cases (Barker et al., 2002; Gaugler et al., 2019; Holtzman et al., 2011). With an increased aging population, AD is becoming more prevalent than ever. By 2038, an estimated 2.8% of Canadians will be diagnosed with dementia and the cumulative economic burden is expected to reach 153 billion. The financial burden of dementia extends beyond affected individuals and includes both direct and indirect costs of care, loss of caregivers' wages, in addition to affecting the health care system as a whole (Alzheimer Society, 2010). Therefore, the need for treatments that alters disease course is critical, however the lack of understanding of the biological mechanisms of AD is a major obstacle in treatment development (Buckholtz et al., 2012).

AD is inherently progressive with clinical manifestations of memory decline, language and executive dysfunction, and personality changes among other symptoms (Blennow et al., 2006; Holtzman et al., 2011). The intra-individual decline follows in stages: mild AD dementia, moderate and severe. In the mild stage, those close to the affected individual generally notice changes in behaviour, however the individual may appear unimpaired to acquaintances (Holtzman et al., 2011). In the moderate stage of disease, patients exhibit overt diminished memory recall, and gradual loss of independence, requiring more assistance in daily tasks. Severe stage is characterized by complete dependence and inevitable death by disease (Holtzman et al., 2011). Elucidating the mechanism of progression depends on understanding the biological etiology and pathogenesis of AD.

The initial histopathological findings by Alois Alzheimer described macroscopic changes such as cortical atrophy, and microscopic changes including abnormal tangles of neurofibrils in place of degenerated neurons and 'miliary foci' composed of an unknown substance (Alzheimer et al., 1995). These neuropathological hallmarks are now recognized as cytoplasmic neurofibrillary tangles composed of hyperphosphorylated microtubule-binding protein tau and extracellular plaques. Integral to plaque formation is the accumulation and subsequent aggregation of amyloid beta (Aβ) peptide (Holtzman et al., 2011). Intraneuronal oligomeric Aβ accumulation precedes plaque formation, has been demonstrated to confer toxicity in AD mouse models, and correlates with the severity of AD neurodegeneration (LaFerla et al., 2007; McLean et al., 1999). In addition, other alterations present in AD include increased oxidative stress and inflammation (Beal, 2005; Heneka et al., 2015; Selkoe, 2001; Torres et al., 2011).

Aβ is derived from the intramembrane proteolytic processing of the amyloid precursor protein (APP), a type I transmembrane protein with a long extracellular N-terminal domain and a short cytoplasmic C-terminal tail (Kang et al., 1987; O'Brien and Wong, 2011; Selkoe, 2008a) (**Figure 1**).

In the non-amyloidogenic pathway, that takes place mostly at the cell surface, APP is cleaved by α-secretase at a region that precludes formation of Aβ (Lys16-Leu17) (Allinson et al., 2003) generating sAPPα and a membrane-bound C-terminal fragment (α-CTF or C83) that is further processed by γ-secretase to release an extracellular p3 peptide and the cytoplasmic APP intracellular C-terminal domain (AICD) fragment (Thinakaran and Koo, 2008) (**Figure 1A**). The sAPPα, was demonstrated to be

neuroprotective against excitotoxicity in hippocampal slices, Aβ toxicity and glucose deprivation (Furukawa et al., 1996) and to improve memory in a mouse model of amnesia (Meziane et al., 1998).

The amyloidogenic processing of APP involves the sequential cleavage by β and γ secretases. β-site APP cleaving enzyme 1 (BACE1) is the principal enzyme *in vivo* to generate the sAPPβ by cleaving the extracellular domain of APP within the endocytic pathway (Koo and Squazzo, 1994; Thinakaran and Koo, 2008). The resulting membrane bound fragment, β-CTF or C99, is cleaved by γ-secretase to generate cytoplasmic peptide AICD and Aβ predominately as a 40-42 amino acid peptide (Thinakaran and Koo, 2008) (**Figure 1B**). Therefore, γ-secretase dictates Aβ toxicity, as the $A\beta_{42}$ product is markedly more toxic than $A\beta_{40}$ (Klein et al., 1999). The majority of Aβ produced (>90%) is Aβ40. Intriguingly, mutations in APP or subunits of the γ-secretase complex (presenilin-1 or presenilin-2) preferentially yield $A\beta_{42}$ (Thinakaran and Koo, 2008). Mutations in APP are a cause of familial AD, which provided initial evidence that Aβ plays a role in AD pathogenesis (Bateman et al., 2011; Kennedy et al., 1993; St George-Hyslop et al., 1987; Thinakaran and Koo, 2008). The majority of known APP mutations that confer risk of AD reside near the putative site of γ-secretase cleavage (amino acid residues 714-717) (Bateman et al., 2011; Bertram and Tanzi, 2004). Only one mutation, the Swedish mutation (APP KM670/671NL), increases Aβ production by increasing β-secretase cleavage of APP (Bateman et al., 2011; Citron et al., 1992; Haass et al., 1995; Thinakaran et al., 1996).

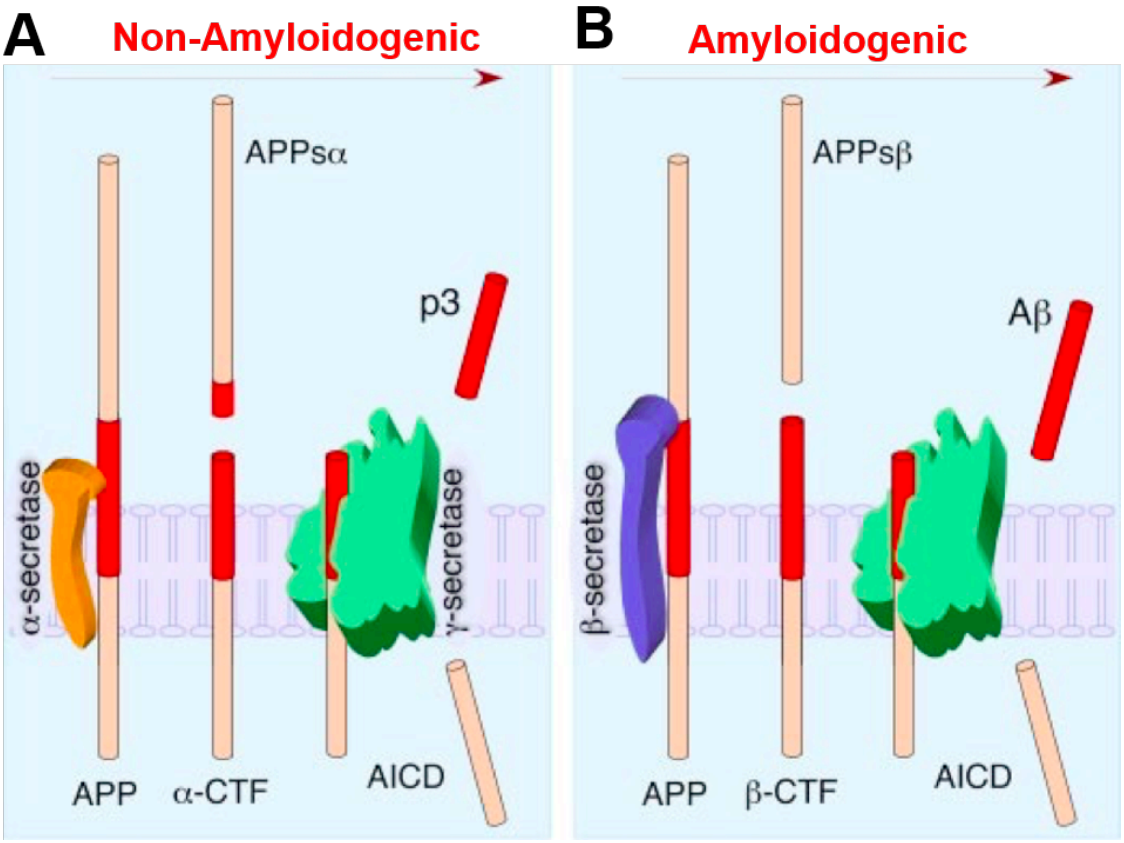

Figure 1. Schematic of the non-amyloidogenic (A) and amyloidogenic (B) processing of APP. The Aβ domain is depicted in red. **(A)** α-secretase processing cleaves APP, releasing sAPPα and α-CTF remaining in the membrane. α-secretase cleavage precludes Aβ generation. Next, γ-secretase cleavage results in the release of p3 and AICD. **(B)** β-secretase cleaves to release sAPPβ and membrane bound β-CTF. γ-secretase sequentially cleaves to generate Aβ and AICD. *Adapted from Thinakaran, G. and E. H. Koo (2008). "Amyloid precursor protein trafficking, processing, and function." J Biol Chem **283**(44): 29615-29619.*

The pathological accumulation of Aβ and neurofibrillary changes follows a characteristic pattern in post-mortem AD brains (Braak and Braak, 1991). Six stages under three headings have been identified based on neurofibrillary changes (neurofibrillary tangles and neuropil threads): the transentorhinal stages during which pathology is confined to a single layer of this region (stages I-II), limbic stages with involvement of both the transentorhinal and entorhinal layers (stages III-IV) and the isocortical stages marked by cortical destruction (stages V-VI) (Braak and Braak, 1991) (**Figure 2A**). Three stages were determined for amyloid deposition, namely stages A-C (**Figure 2B**) (Braak and Braak, 1991). Importantly, the spreading of tau pathology and behavioural symptoms mirror a clinically defined pattern (Braak and Braak, 1991; Holtzman et al., 2011). Aβ-deposition also follows a spatiotemporal pattern, specifically with the sequential involvement of the neocortex and spreading to subcortical regions along neuronal projections in AD cases (Guo and Lee, 2014; Thal et al., 2002). Concordantly, neuronal connections are also implicated in the neuron-to-neuron transmission of oAβ_{42} (Nath et al., 2012). Therefore, Aβ is suspected to spread by a prion-like mechanism (Hasegawa et al., 2017).

1.2 Prions and Prion-like diseases

Prior to discussing prion-like spreading, one must first understand the primary tenants of prion disease more generally. Prion diseases are transmissible spongiform encephalopathies affecting both humans and animals, causing dementia (Creutzfeldt-Jakob Disease), ataxia (Scrapie, Bovine Spongiform Encephalopathy), neuronal loss (all) and brain abnormalities, invariably leading to death (Prusiner, 1998; Wells et al., 1987).

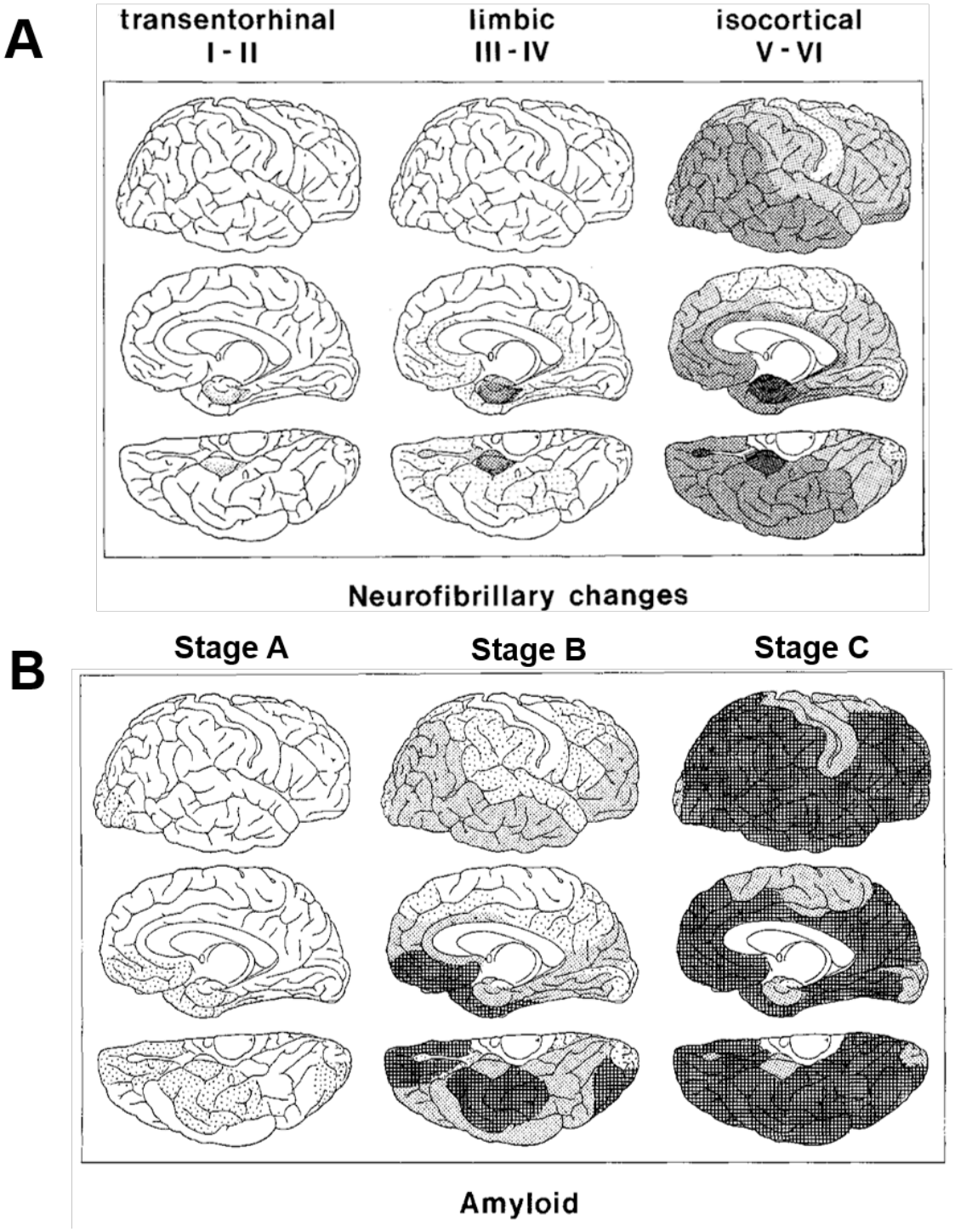

Figure legend on next page

Figure 2. Neuropathological staging of AD (A) Pattern of neurofibrillary changes include neurofibrillary tangles (NFT) and neuropil threads (NT). Stages I-II changes are confined to the transentorhinal region and progresses to isocortical destruction (Stages V-VI). Intensity of shading corresponds to density/severity of accumulated pathology. **(B)** Amyloid deposition is separated into three stages (stages A-C). Stage A is characterized by low-density amyloid deposition in the basal isocortex. The hippocampus is visually absent of amyloid. Stage B involves medium density amyloid deposition spread to virtually all isocortical regions with only minor hippocampal involvement. Stage C denotes high density of amyloid deposition in all of the isocortex. Hippocampal involvement at this stage is similar to stage B. *Adapted from Braak, H. & Braak, E. Neuropathological stageing of Alzheimer-related changes. Acta Neuropathol* ***82****, 239-259 (1991).*

Although clinical presentation may vary, at their foundation, prion diseases involve the aberrant accumulation of a conformationally altered prion protein. At the molecular level, prion disease arises from the misfolding of host cellular prion protein (PrP^{C}) to the pathological isoform PrP scrapie (PrP^{Sc}) (Aguzzi et al., 2001; Prusiner, 1998) (**Figure 3**). PrP^{Sc} has the ability to spread within tissue, across tissue, and between organisms as an infectious agent (Eisele and Duyckaerts, 2016).

As indicated previously, soluble oligomeric Aβ spreads from neuron-to-neuron and induces toxicity in the recipient cell (Hallbeck et al., 2013; Nath et al., 2012). Intracerebral inoculation of AD patient brain lysate (Meyer-Luehmann et al., 2006) or synthetic Aβ or purified Aβ aggregates (Stohr et al., 2012) in APP23 mice that overexpress human APP with the Swedish mutation, causes cerebral amyloidosis that spreads beyond the initial site of injection. More recently, it has been discovered a knock-in mouse model of modified murine APP containing the Swedish (K670N, M671L) and Iberian (I716F) mutations and a humanized Aβ region in the $APP^{NL\text{-}F/NL\text{-}F}$ mice can be induced to accumulate Aβ upon inoculation of AD patient brain homogenates, therefore the overexpression of APP may not be a prerequisite for amyloid deposition (Ruiz-Riquelme et al., 2018). Further, Aβ (oligomers or protofibrils for example) may act as a seed for the formation of distinct, higher order species that matches the conformation of the introduced protein seed (Eisele and Duyckaerts, 2016; Guo and Lee, 2014; Paravastu et al., 2009; Petkova et al., 2005). A few models of the spreading of misfolded seeds have been suggested, specifically the extrusion of naked proteins by the donor neuron to be endocytosed by or passively translocate across membranes in recipient neurons, the transfer of misfolded protein by packaging into

exosomes and subsequent uptake of exosomes by the recipient neuron, or a direct physical interaction of donor and recipient neurons by tunnelling nanotubes (reviewed in (Guo and Lee, 2014)). Overall, the prion-like characteristic of Aβ in AD denotes similarities with the molecular conversion of native to misfolded protein and in intercellular transmissibility (Eisele and Duyckaerts, 2016). Relevant to our studies, in both AD and prion disease, misfolded proteins accumulate in multivesicular bodies (MVBs), an intermediate organelle of two interrelated pathways we will discuss below: autophagy and extracellular vesicles (EVs) secretion (Takahashi et al., 2002; Yim et al., 2015).

1.3 Autophagy

Macroautophagy (herein referred to as autophagy) is an indispensable pathway to maintain cellular homeostasis by degrading long-lived proteins, lipid droplets, glycogen, ferritin, dysfunctional organelles, etc (Kaur and Debnath, 2015). There are four steps in autophagic flux, namely nucleation, elongation and closure, docking and fusion and degradation (Klionsky, 2005; Yang and Klionsky, 2010) (**Figure 4**).

The first step involves the formation of the isolation membrane (phagophore). The next step is elongation and closure, whereby the phagophore surrounds cytosolic material to form a double membrane autophagosome. The elongation reaction involves the recruitment to the isolation membrane of autophagy-related gene (*ATG*)-encoded proteins (Atg proteins) that form the ubiquitin-like protein conjugation systems (Green and Levine, 2014). These proteins work in concert on the protein LC3I, which is generated by ATG4-dependent proteolytic cleavage of LC3.

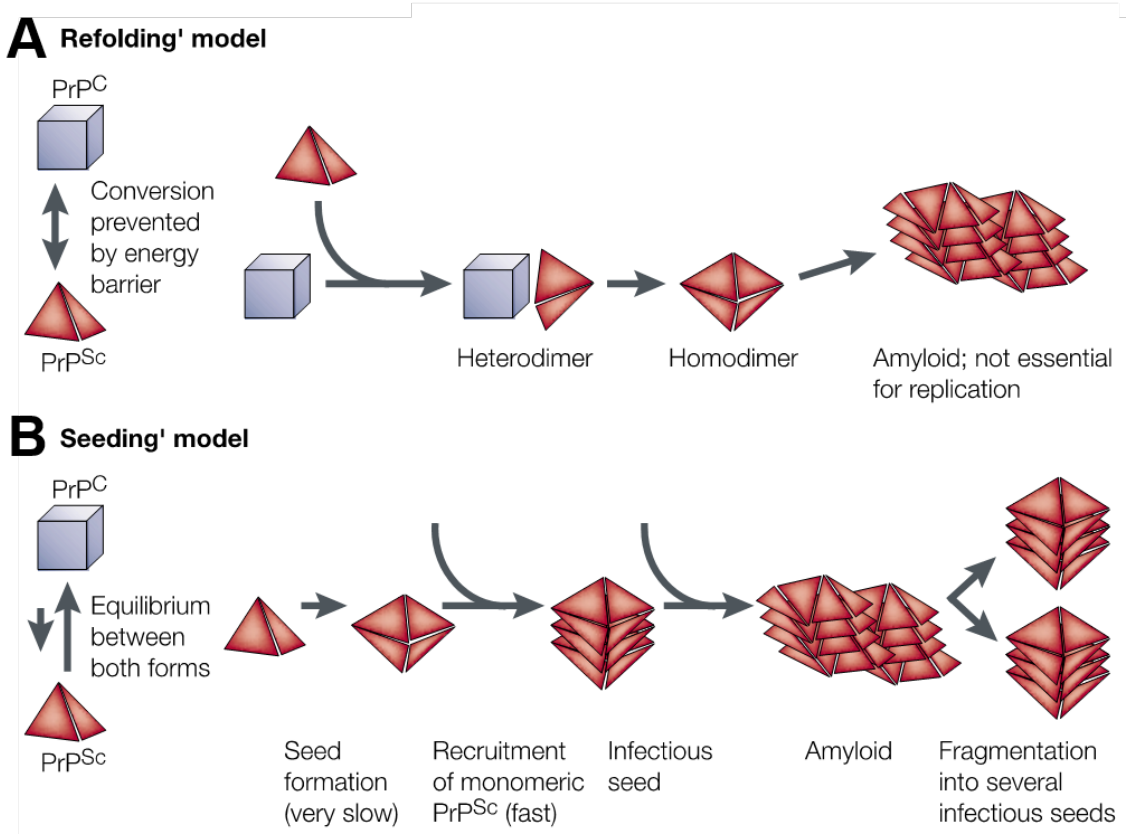

Figure 3. Models for the conversion of PrP^{C} to PrP^{SC} (A) The refolding model proposes that exogenous PrP^{Sc} induces the conversion of endogenous PrP^{C}. A high-energy barrier between each conformation exists and prevents spontaneous conversion. **(B)** The seeding model postulates that PrP^{C} and PrP^{Sc} isoforms exist at thermodynamic equilibrium. The equilibrium shifts when monomeric PrP^{Sc} accumulates and aggregates forming an infectious seed, which can further aggregate into an amyloid, then fragment again into multiple seeds thus multiplying pathology. The PrP^{Sc} isoform is stabilized in this interaction. *Adapted from Aguzzi, A., Montrasio, F. & Kaeser, P. S. Prions: health scare and biological challenge. Nature reviews. Molecular cell biology 2, 118-126, doi:10.1038/35052063 (2001).*

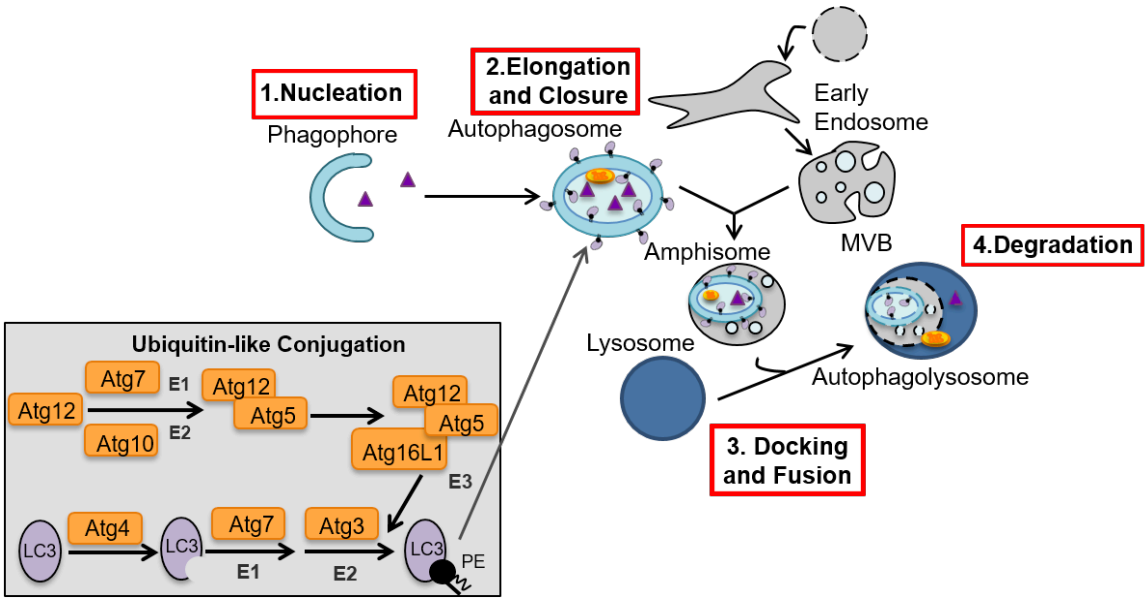

Figure 4. Autophagy pathway. Autophagy comprises 4 stages: Nucleation, Elongation and Closure, Docking and Fusion and Degradation. The nucleation phase involves the formation of the isolation membrane (phagophore). The C terminal cleavage of LC3 generates LC3I, which is conjugated to phosphatidylethanolamine (PE) through the actions of the ubiquitin-like conjugation system with Atg proteins to form LC3II at the autophagosome membrane. LC3II is critical for the elongation phase of autophagy. Closure of the phagophore forms the double membrane bound autophagosome. The autophagosome can either fuse with the lysosome directly or with the multivesicular body (MVB) first, forming the amphisome, then fuse with the lysosome to form the autophagolysosome. Exposure of lysosomal hydrolases to autophagosome content results in its degradation.

In a ubiquitin-like reaction, these proteins conjugate phosphatidylethanolamine (PE) to LC3I to form LC3II at the autophagosome membrane and subsequently seal the double membrane (Green and Levine, 2014; Yang and Klionsky, 2010). The phosphatidylethanolamine-conjugated form of the LC3 is the only autophagy protein that stably associates with the mature autophagosome (Klionsky et al., 2012). Next, the autophagosome fuses either with the MVB to form the amphisome, which will fuse with the lysosome for degradation, or the autophagosome fuses with the lysosome directly forming an autophagolysosome. Inside the autophagolysosomes, lysosomal hydrolases degrade the autophagosome cargo (Green and Levine, 2014) (**Figure 4**).

Neurons depend on autophagy to maintain their large cytoplasm and membranes associated with axons and dendrites without the aid of cell division (Nixon and Yang, 2012). Therefore, autophagy is constitutively active in neurons (Nixon and Yang, 2011) and the clearance of autophagic vacuole intermediates is remarkably efficient (Boland et al., 2008; Nixon, 2007). Neuron-specific abrogation of basal autophagy in mice by deletion of autophagy-related genes (*ATGs*) results in neurodegeneration in the absence of any disease-associated proteins, suggesting that impaired autophagy contributes to the pathophysiology of neurodegenerative diseases (Hara et al., 2006; Komatsu et al., 2006).

Dysfunctional autophagy has been implicated in both prion disease and AD (Aguib et al., 2009; Heiseke et al., 2010). Nixon *et al* reported accumulation of autophagic vacuoles upon biopsy of AD brain specimens (Nixon et al., 2005). At physiological levels of autophagy induction, Aβ may be formed within a subpopulation of autophagic vacuoles and would be rapidly degraded upon lysosomal hydrolase

exposure, however in AD the maturation of autophagic vacuoles is compromised such that autophagy induction favours the accumulation of intraneuronal Aβ (Yao et al., 2013; Yu et al., 2005). Concordantly, several studies have demonstrated that promoting autophagy without a concomitant increase in autophagic flux may induce further accumulation of autophagosomes and $A\beta_{42}$ generation in cellular and animal models of AD (Yu et al., 2005; Zhang et al., 2010). However, it has also been demonstrated that rapamycin may reduce accumulation of $A\beta_{42}$ and tau pathology by promoting their clearance, thus improving learning and memory in experimental AD mice (3xTg-AD and PDAPP) (Bove et al., 2011; Caccamo et al., 2010; Spilman et al., 2010). Therefore, there is contradictory evidence in the beneficial or deleterious effects of promoting autophagy in AD by rapamycin (reviewed in (Bove et al., 2011)).

In prion disease, the accumulation of autophagic vacuoles was reported in experimental animal models of Creutzfeldt-Jakob's disease (Boellaard et al., 1989). Activation of autophagy by rapamycin, trehalose, or lithium induces clearance of misfolded prion protein and delays disease onset in mice (Aguib et al., 2009; Fader et al., 2008; Heiseke et al., 2009; Heiseke et al., 2010). Impaired autophagic flux may contribute to prion disease development, and promotes the lateral transfer of prion protein in cellular models (Abdulrahman et al., 2018; Yao et al., 2013).

1.4 Protein Prenylation

Protein prenylation is the covalent attachment of isoprenoid lipids, namely farnesylpyrophosphate (FPP) and geranylgeranylpyrophosphate (GGPP) to the C-terminus of selective proteins (Casey and Seabra, 1996). FPP and GGPP are synthesized by the mevalonate pathway through sequential enzymatic reactions from precursor

acetyl CoA. The pathway diverges into two separate branches: the non-sterol isoprenoids and the sterol pathway ultimately forming cholesterol (Bloch, 1965; Panda et al., 2011) (**Figure 5**).

Farnesylation and monogeranylgeranylation of proteins are achieved by the action of farnesyltransferase (FTase) and geranylgeranyltransferase type 1 (GGTase-I) respectively. Proteins that are farnesylated or monogeranylgeranylated contain C-terminal CAAX motifs, whereby the amino acid at position X confers specificity for lipid attachment (Desnoyers et al., 1996). In addition, the enzyme geranylgeranyltransferase type 2 (GGTase-II) or Rab geranylgeranyltransferase (RabGGTase) catalyzes the addition of two geranylgeranyl moieties to Rabs, a family of Ras-related small GTPases, at two (or one) carboxy-terminal cysteine residues (Pereira-Leal and Seabra, 2000). The covalent attachment of the lipophilic isoprenyl group(s) enables prenylated proteins to anchor to cell membranes, which is a requirement for biological function (McTaggart, 2006).

Although various heterotrimeric G protein subunits and nuclear lamins are prenylated, the largest group is the small GTPases (McTaggart, 2006). All small GTPases are able to specifically bind GDP and GTP, being inactive when bound to GDP (cytosolic location) and active when bound to GTP (membrane location). They also have an intrinsic GTPase activity to hydrolyze bound GTP to GDP and phosphate (Pi) (Bento et al., 2013).

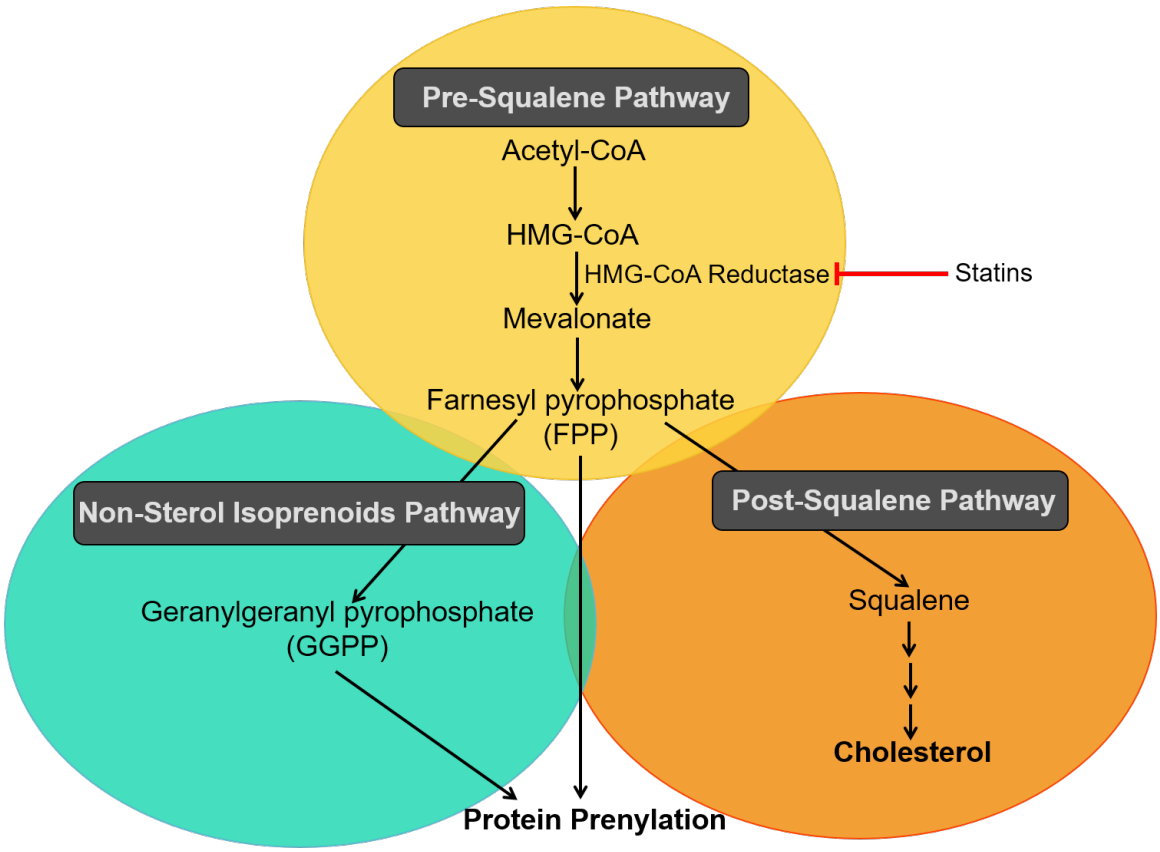

Figure 5. Simplified flow chart of the mevalonate pathway and the connection to protein prenylation. The isoprenoid and cholesterol branches are enclosed in green and orange backgrounds respectively. The non-sterol isoprenoid pathway results in the formation of GGPP, an essential mediator of protein prenylation in addition to FPP. Statins inhibit HMG-CoA Reductase, the rate limiting enzyme of the formation of mevalonate, thus cholesterol and isoprenoid lipids. The degree of inhibition of mevalonate production determines the depletion of isoprenoid lipids.

Rabs are regulators of intracellular membrane trafficking and control membrane identity, vesicle targeting, motility and docking/fusion (Takai et al., 2001). In the central nervous system (CNS), Rabs participate in retrograde transport of growth factors, axonal endocytosis, synaptic functions such as exocytosis, and polarized neurite growth (Ng and Tang, 2008). Rab5 and Rab7 have been linked to AD. Expression profiling studies showed that in cholinergic basal forebrain neurons microdissected from postmortem brains of individuals with mild cognitive impairment (MCI) and AD there is selective upregulation of *rab4*, *rab5*, *rab7*, and *rab27* genes that correlated with cognitive decline and neuropathological criteria for AD (Ginsberg et al., 2011). Rab5 and Rab7 protein levels were regionally increased within the frontal cortex and hippocampus but not in the less susceptible cerebellum and striatum in MCI and AD (Ginsberg et al., 2010). The elevation of Rab7 and Rab5 in AD brains has been interpreted as increased activity of the endocytic pathway (Ginsberg et al., 2010). Further, increased levels of Rab7 have been measured in cerebrospinal fluid (CSF) from AD patients, thus may offer a novel, AD specific, CSF biomarker (Armstrong et al., 2014). Unpublished data from our laboratory demonstrated increased levels of Rab7 in the cortex of TgCRND8 mice, which encode a double mutant form of APP with the Swedish (KM670/671NL) and Indiana (V717F) mutations (Chishti et al., 2001; Smith, 2016).

Recent studies have shown that several Rabs are important in autophagy (Ao et al., 2014; Bento et al., 2013; Chua et al., 2011; Hyttinen et al., 2013). There is extensive evidence indicating that Rab7 is required for normal autophagic flux in mammals (Ao et al., 2014; Bento et al., 2013; Bucci et al., 2000; Cantalupo et al., 2001; Gutierrez et al., 2004; Hyttinen et al., 2013; Jager et al., 2004; Johansson et al., 2007; Kimura et al., 2007;

Vanlandingham and Ceresa, 2009; Wang et al., 2011; Zhou et al., 2013). Rab7 localization to autophagosomes, late endosomes and lysosomes is pivotal for Rab7 function in autophagy (Bucci et al., 2000; Feng et al., 1995; Gutierrez et al., 2004; Jager et al., 2004; Kimura et al., 2007; Press et al., 1998; Saxena et al., 2005; Vanlandingham and Ceresa, 2009; Wang et al., 2011). Rab7 plays an essential role in the movement of autophagosomes randomly formed in the cytoplasm toward the microtubule-organization centre (MTOC) where lysosomes are abundant (Kimura et al., 2007). Under stress conditions, lysosomes also move toward the MTOC to engage autophagosomes even more efficiently (Korolchuk et al., 2011). The bidirectional transport of autolysosomes in non-neuronal cells depends on kinesin/dynein mechanisms (Yang et al., 2011). LC3-positive autophagosomes forming in axons rapidly acquire late endosome marker Rab7 and lysosomal LAMP1 and undergo predominant retrograde movement (Lee et al., 2011). To perform these functions, Rab7 serves as scaffold for the sequential assembly of effectors required for vesicular intracellular trafficking (Bento et al., 2013; Hyttinen et al., 2013; Nixon, 2013; Wang et al., 2011). Previous work in our laboratory revealed a novel mechanism of Aβ-induced neurotoxicity: o$A\beta_{42}$ reduces sterol regulatory element-binding protein-2 (SREBP2) activation, which is an essential transcriptional regulator of the mevalonate pathway, through protein kinase B (Akt) inhibition, thereby reducing isoprenoid synthesis and protein prenylation (Mohamed et al., 2012; Mohamed et al., 2018). The initial findings were extended to show that Rab7 is mislocalized to the cytosol in neurons due to Rab7 hypoprenylation (Smith, 2016).

1.5 Unconventional Secretion

Unconventional secretion denotes any form of secretion that bypasses the classical endoplasmic reticulum (ER)-to-Golgi pathway. Classical secretion is mediated by a hydrophobic, N-terminal signaling peptide (leader sequence) that directs proteins to the ER, then proteins are captured in COPII-coated vesicles and sorted through the Golgi network, ultimately destined for secretion at the plasma membrane (Palade, 1975; Schatz and Dobberstein, 1996). However, proteins that lack a signaling peptide and/or are secreted independently of the ER-Golgi pathway were discovered, thus leading to the concept of unconventional protein secretion.

There are four types of unconventional secretion (**Figure 6**). Type I unconventional secretion describes the non-vesicular translocation of leaderless proteins across membranes through *de novo* pore formation (e.g. HIV TAT). Type II, or ABC transporter based-secretion, is another non-vesicular mechanism to secrete lipidated (prenylated, acylated), leaderless peptides (e.g. yeast pheromone a-factor). Type III comprises vesicular-based secretion of leaderless protein, whereby different vesicular intermediates fuse with the plasma membrane and release cargo as free hydrophilic proteins into the extracellular space (e.g. Interleukin 1β) (Rabouille, 2017; Rabouille et al., 2012). These vesicular intermediates include late endosomes, secretory lysosomes, secretory autophagosomes and amphisomes (Zhang and Schekman, 2013). The final type of unconventional secretion termed Type IV involves proteins that, despite having a signaling peptide, bypass the Golgi (e.g. K+ voltage gated channel Kv4) (Rabouille, 2017; Rabouille et al., 2012; Zhang and Schekman, 2013).

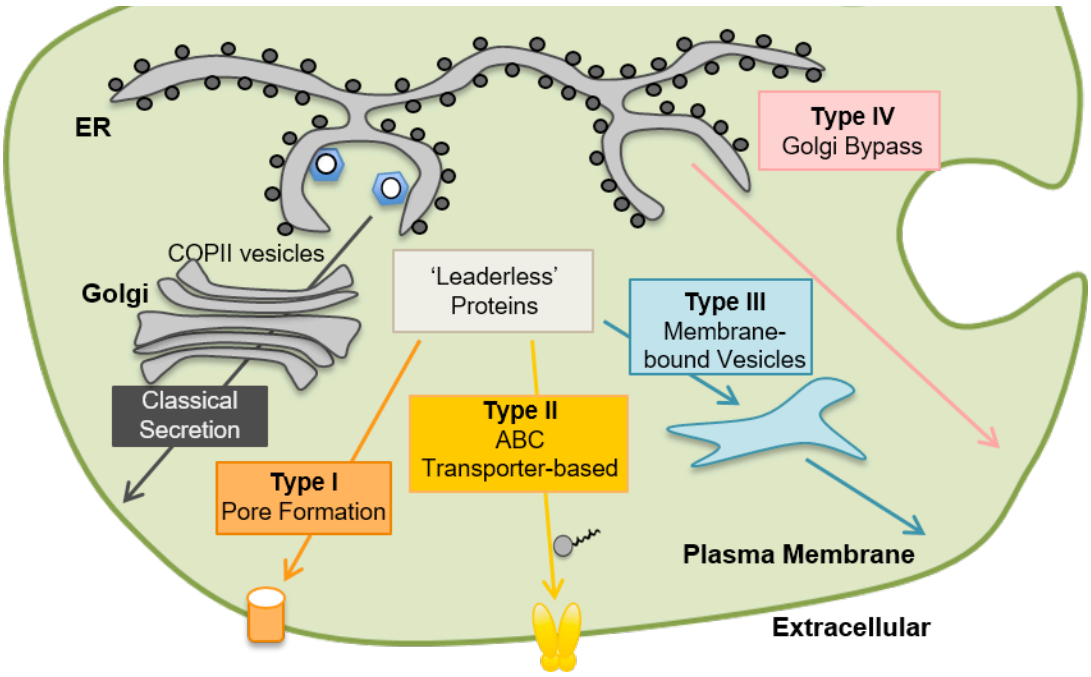

Figure 6. Pathways of conventional and unconventional secretion. Classical secretion (dark grey) involves proteins sequestered in COPII coated vesicles and delivered to the membrane for secretion following trafficking through the Golgi. Type I secretion (orange) involves release of hydrophobic proteins through the formation of a pore in the membrane. Type II (yellow) is ABC transporter-based secretion, and is the extrusion of lipidated proteins. Type III (blue), involves membrane bound vesicles that bind with the plasma membrane, releasing their contents to the extracellular space. Type IV (pink) denotes a mechanism that bypasses the Golgi for secretion and generally involves membrane resident proteins.

Leaderless proteins are also released from the cells after being incorporated into extracellular vesicles (EVs) that derive from multivesicular bodies or from shedding from the plasma membrane. This type of secretion shares some common aspects with Type III unconventional secretion, however it has recently been proposed to be classified as a distinct pathway because proteins are delivered as membrane-enclosed proteins and not free proteins (Nickel and Rabouille, 2018). The work described here focuses on this type of unconventional secretion.

1.6 Extracellular Vesicles

EVs are membrane-enclosed particles of cellular origin involved in intercellular signaling (Basso and Bonetto, 2016; Budnik et al., 2016; Fevrier and Raposo, 2004). EVs contain nucleic acids and protein cargo, thus have garnered much research interest as biomarkers for disease (Hornick et al., 2015; Melo et al., 2015), exploitation for drug delivery (Usman et al., 2018; Vader et al., 2016), and potential role in spreading of pathological proteins (Danzer et al., 2012; Eisele and Duyckaerts, 2016; Zhang et al., 2016).

Classically, based on their origin, EVs have been classified as apoptotic bodies, microvesicles and exosomes (**Figure 7**). Apoptotic bodies (800-5000nm) result from membrane blebbing of dying cells and contain fragmented nuclei and cytoplasmic organelles. Microvesicles are derived from the outward budding of the plasma membrane (100-1000nm), and exosomes from the endocytic pathway (30-150nm) (Colombo et al., 2014). However, reproducible separation of each population is extremely difficult, and EV isolates generally comprise a mixture of EVs of different cellular origins (Lotvall et al., 2014). Therefore, as a response to inaccurate

nomenclature as well as to promote consistency in the field, the more appropriate designation is to classify EVs based on size: small EVs (sEV) and large EVs (LEVs) and the cut-off to be clearly defined in each particular study (Gould and Raposo, 2013; Thery et al., 2018). We will discuss the biology using the terminology of microvesicles and exosomes, however experimentally we will use the nomenclature of small and large EVs.

1.7 Biogenesis of Extracellular Vesicles

1.7.1 Microvesicles

Microvesicles are derived from the outward budding of the plasma membrane. This is a heterogeneous group of EVs, comprised of a phospholipid bilayer with transmembrane proteins surrounding a core containing cytosolic components (VanWijk et al., 2003). Microvesicles were first recognized as a product of platelet activation ('platelet-dust'), thereby as lipid rich particles that exert pro-coagulant effects (Wolf, 1967). Later, it was discovered that shedding of plasma membrane-derived vesicles occurred in many other cell types, such as neutrophils (Stein and Luzio, 1991), fibroblasts (Lee et al., 1993), and tumour cells amongst others (Cocucci et al., 2009).

A primary feature of microvesicles is the loss of phospholipid asymmetry of their membranes, causing exposure of negatively charged phospholipids on the vesicular surface (Akers et al., 2013; Morel et al., 2011). Membrane phospholipid asymmetry is physiologically essential for cells and is maintained in an ATP-dependent manner, such that the outer leaflet is enriched with phosphatidylcholine and sphingomyelin, and the cytoplasmic side contain phospholipids phosphatidylethanolamine (PE) and phosphatidylserine (PS).

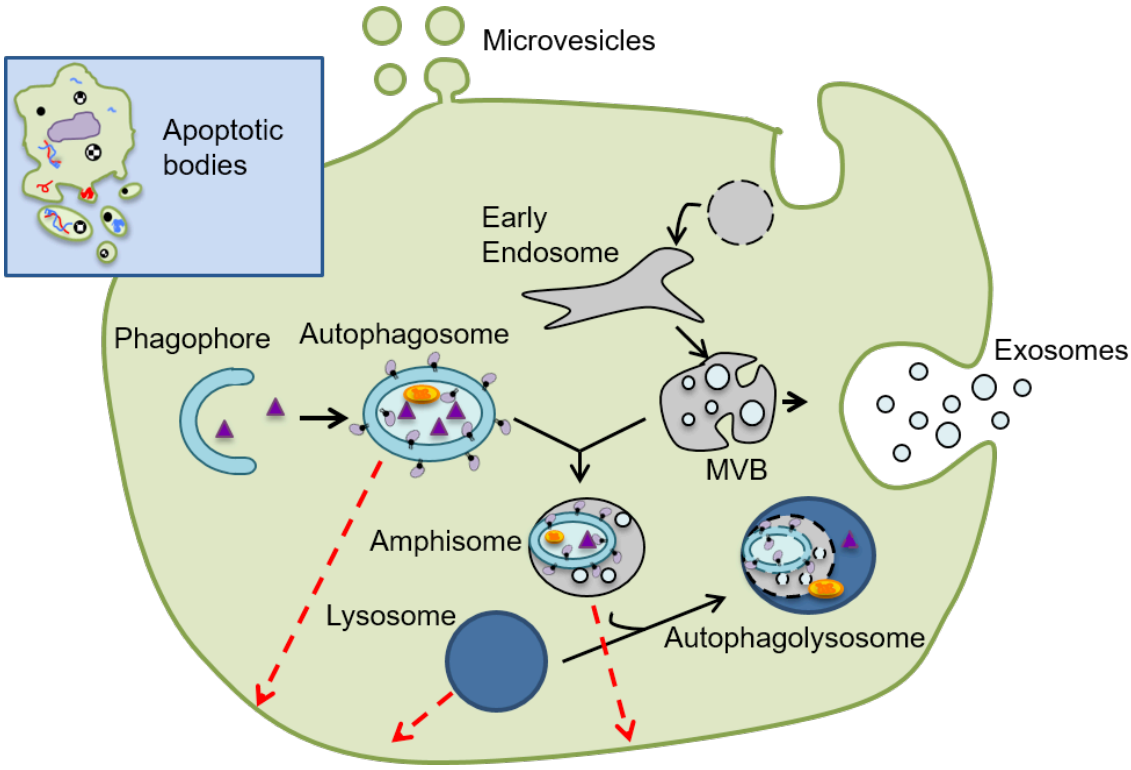

Figure 7. EV types and their regulation by autophagy. Apoptotic bodies are derived from cells undergoing programmed cell death. Microvesicles result from the outward budding of the plasma membrane. Exosomes are formed within the endocytic pathway. Autophagic flux and exosome secretion are coordinated mechanisms, whereby the MVB is an intermediate in both pathways. The MVB derives from invaginations of the early endosome membrane, forming intraluminal vesicles. The MVB can be directed to the autophagy-lysosome pathway for the subsequent degradation of its cargo, or to the plasma membrane for the extracellular release of exosomes. Corresponding to type III unconventional secretion, secretory autophagosomes, amphisomes and lysosomes may be directed to the plasma membrane for the release of free proteins (red dashed arrows).

Complementary lipid transporters contribute to asymmetry; 'flippases' translocate lipids inward, and 'floppases' promotes the outward movement of lipids (Morel et al., 2011). Further, the 'scramblase', which is activated by an influx of calcium ions, promotes the bidirectional movement of lipids. This transporter has been implicated in exposing PS on the outer leaflet of the plasma membrane during cellular activation or stress, specifically in platelets, for production of procoagulant microvesicles (Fadeel and Xue, 2009). Phospholipid reorganization originally seemed common to the production of all microvesicles, whereby PS is exposed on the outer leaflet of the plasma membrane, and membrane budding and fission are completed through contraction of cytoskeletal proteins (Akers et al., 2013). This mechanism has been described in a melanoma model. Translocation of PS to the outer leaflet initiates a signaling cascade, beginning with the activation of GTP-binding protein ribosylation factor (ARF6), phospholipase D (PLD) activation, concluding with phosphorylation of myosin-light chain and microvesicle release (Akers et al., 2013; Muralidharan-Chari et al., 2009) (**Figure 8**). The presence of PS exposure at the surface of microvesicles can be examined by binding of AnnexinV, a protein with high affinity for PS (Dacharyprigent et al., 1993). However, subsets of microvesicles that do not expose PS have been described, as determined by lack of AnnexinV labeling (Connor et al., 2010). The release mechanism of PS-negative microvesicle that maintain phospholipid asymmetry has not yet been elucidated.

1.7.2 Exosomes

Johnstone *et al* first recognized exosomes when characterizing the maturation of reticulocytes (Johnstone et al., 1987). Dr. Johnstone followed transferrin receptor by

electron microscopy and immunogold labeling, as she found previously this receptor was lost in mature erythrocytes and was found in isolated vesicles. From these initial observations, Dr. Johnstone captured elegant images of what she termed multivesicular elements (and we refer to as MVBs), fusing with the plasma membrane and releasing a relatively uniform population (average 30-50nm) of membrane-enclosed vesicles into the culture medium (Pan et al., 1985).

More recently, the precise biogenesis of exosomes has been elucidated along with the signaling cascade that culminates in their secretion (**Figure 8**). Exosomes are derived from the endocytic pathway, beginning with the early endosome.
The early endosomes arise from the fusion of multiple endocytic vesicles, and are identified by the association of Rab5. Interaction with Rab5 mediates the movement of early endosomes along the microtubule network (Hessvik and Llorente, 2018; Huotari and Helenius, 2011; Nielsen et al., 1999). Exchange of Rab5 with Rab7, whereby Rab7 is then recruited and activated with concomitant Rab5 inactivation and dissociation from the membrane, determines the maturation of the early endosome to late endosomes (Ao et al., 2014; Mizuno-Yamasaki et al., 2012). While this maturation process is occurring, formation of intraluminal vesicles begins through invagination of the early endosomal membrane. Intraluminal vesicle formation, thus MVB maturation, involves two processes. The first requires tetraspanin-enriched membrane microdomain formation, where it has been suggested that tetraspanins may recruit specific protein cargo for inclusion into intraluminal vesicles (Kowal et al., 2014; Lane et al., 2018).

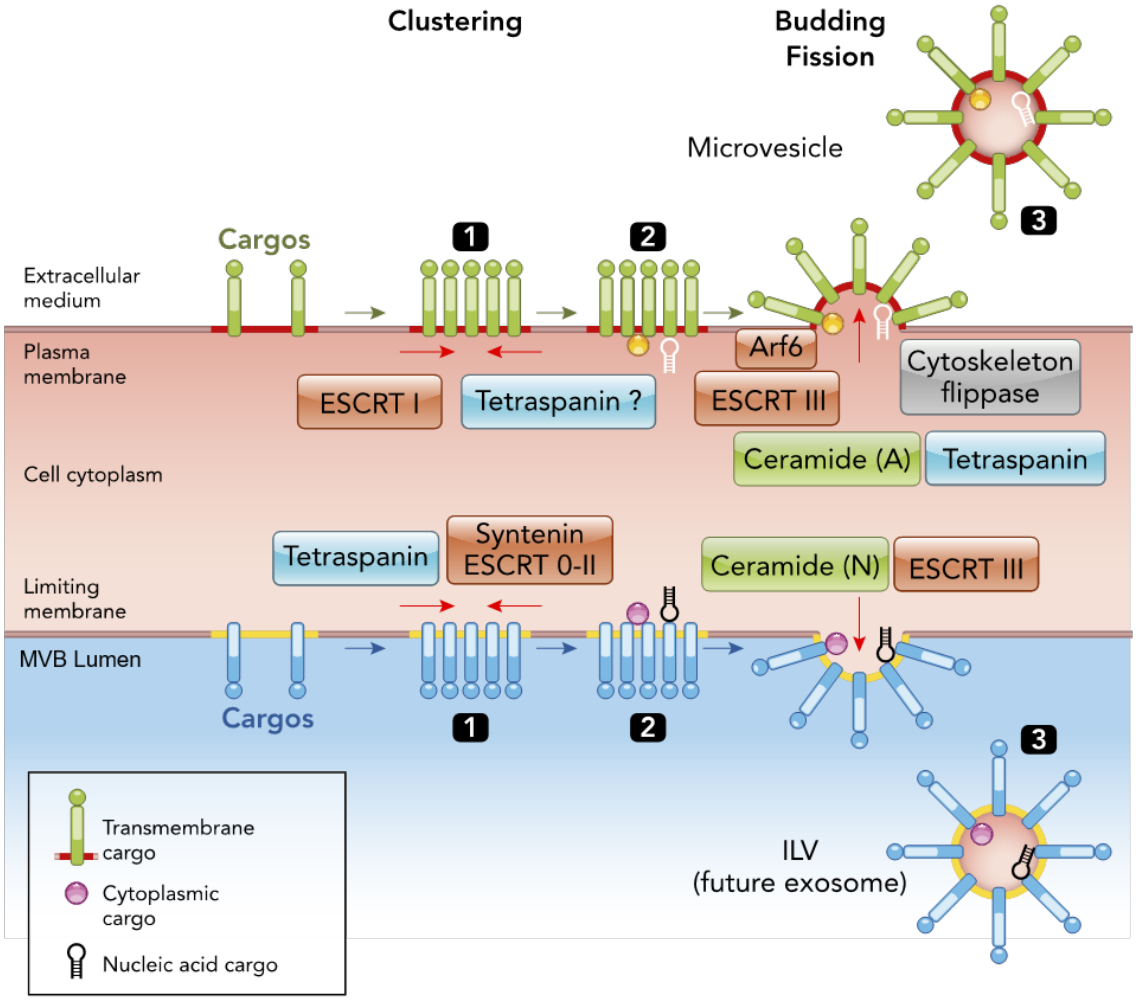

Figure 8. Biogenesis of microvesicles and intraluminal vesicles (future exosomes). Pathways of the formation of intraluminal vesicles (ILVs) within the MVB (bottom, blue panel) and outward budding vesicles from the plasma membrane (top, orange panel). Each pathway requires (1) clustering of cargo, (2) budding and scission and (3) release from the membrane. For the process of microvesicle formation and release, ESCRT complexes recognize and cluster cargo. Next, PS is translocated to the outer membrane leaflet, initiating the outward budding of the plasma membrane. Arf6 initiates a signaling cascade that culminates in the scission and release of microvesicles. The formation of intraluminal vesicles, which will result in the release of exosomes downstream, involves ESCRT complexes for biogenesis. ESCRT0-II recognizes and binds cargo and each other to form a cargo-enriched zone. ESCRTII initiates ESCRTIII assembly, inducing vesicle budding and release. *Adapted from Stahl, P. D. and G. Raposo (2019). "Extracellular Vesicles: Exosomes and Microvesicles, Integrators of Homeostasis." Physiology (Bethesda) **34**(3): 169-177.*

Further, reorganization of tetraspanins CD9 and CD63 have been proposed to be the initial step for intraluminal vesicle biogenesis (Akers et al., 2013). However, the most recognized involvement is with the endosomal sorting complex required for transport (ESCRT) machinery. ESCRT complexes are evolutionarily conserved and comprise approximately twenty proteins assembled into four complexes, specifically ESCRT-0, -I, -II, and –III (Akers et al., 2013; Raposo and Stoorvogel, 2013). ESCRT-0 is involved in the ubiquitin-dependent recognition of cargo. Next, ESCRT-I and –II are recruited, initiating membrane budding and cargo sequestration. Accessory protein ALIX facilitates the recruitment of ESCRT-III through concomitant binding of Tsg101 of ESCRT-I and CHMP4 of ESCRT-III (Akers et al., 2013; Henne et al., 2011; McCullough et al., 2008). ESCRT-III recruits deubiquitination machinery, facilitates cargo packaging into mature vesicles, and promotes scission and release of intraluminal vesicles (Henne et al., 2011) (**Figure 8**). Finally, MVBs are directed to the plasma membrane for the extracellular release of newly formed exosomes, which may involve soluble NSF-attachment protein receptor (SNARE) complexes (Kowal et al., 2014).

The discovery that inhibition of key proteins in ESCRT machinery failed to completely inhibit intraluminal vesicle formation led to the discovery of ESCRT-independent pathways, indicating the existence of a subgroup of MVBs (Stuffers et al., 2009). In an attempt to delineate ESCRT-independent mechanisms, a neutral sphingomyelinase inhibitor (GW 4869) was used to inhibit ceramide production, a lipid proposed to be required for the inward curvature of membranes thus intraluminal vesicle formation. This drug dramatically reduced exosome secretion, however Kowal *et al* cautions the interpretation of results, as altering lipid composition will affect plasma

membrane-derived EVs and other cellular functions (Kowal et al., 2014; Trajkovic et al., 2008).

1.8 Regulation of Extracellular Vesicles Secretion

The regulation of EV secretion is cell-type dependent. For a non-exhaustive list of specific examples, red blood cells secrete MVB-derived EVs during maturation (Johnstone et al., 1987), B cells and T cells upon activation of cell surface receptors (Thery et al., 2009), and tumour cells release EVs constitutively (Lane et al., 2018). Due to its effect on plasma membrane remodelling, elevated intracellular calcium determines plasma membrane EV shedding in erythrocytes, platelets, monocytes and neutrophils (Thery et al., 2009). More broadly, environmental deviations, such as stress conditions, increase EV secretion (Chettimada et al., 2018; Thery et al., 2009). Another broad mechanism is the coordinated regulation of EV secretion and autophagy.

EV secretion and autophagy are inherently linked cellular homeostatic mechanisms. The first evidence for the link between the two pathways came from Fader *et al*, whereby they demonstrated that autophagy induction by rapamycin promoted the fusion of MVBs with autophagosomes, and consequently reduced exosomes secretion in cells (Fader et al., 2008). Therefore, autophagy plays a critical role in the fate of MVBs, and thus in the fate of the intraluminal vesicles within them. MVBs can be directed toward the lysosome as intermediates of autophagic degradation, or the plasma membrane for the extracellular release of exosomes (Baixauli et al., 2014; Eitan et al., 2016; Fader and Colombo, 2009; Hessvik et al., 2016; Raposo and Stoorvogel, 2013). Exosomes secretion in the nervous system is proposed as an alternative disposal pathway to ameliorate cellular stress when autophagy is impaired, thus facilitating

degradation of cargo by non-neuronal cells (Baixauli et al., 2014; Yuyama et al., 2012), or promoting progression of neurodegenerative diseases as 'Trojan horses' in spreading of pathological proteins (Ghidoni et al., 2008; Joshi et al., 2015).

1.9 Extracellular Vesicles in Neurodegenerative Diseases

EVs are considered a double-edged sword in neurodegenerative diseases, as they may exert beneficial or detrimental effects depending on their fate within the brain. The beneficial clearance of pathological proteins is mediated by microglia, the resident immune cells of the CNS (Kreutzberg, 1996). In separate studies, it has been demonstrated that oligodendrocyte-derived exosomes are preferentially taken up by microglia, and microglial uptake of exosomes can promote Aβ clearance (Fitzner et al., 2011; Yuyama et al., 2012). However, the functionality of microglia dampens with age and with the progressive accumulation of pathological proteins in AD, such that microglia themselves may promote degeneration (Blume et al., 2018; Clayton et al., 2017). Further, microglia-derived EVs have been suggested to promote neurotoxicity by mobilizing toxic Aβ oligomers (Joshi et al., 2014). Therefore, the beneficial effect of microglial degradation is likely negated when these cells are dysfunctional and Aβ-loaded EVs are alternatively taken up by neurons, thus propagating the spread of pathology.

The EV-mediated detrimental spreading of pathological proteins is dependent on EV uptake by neurons. In APP overexpressing neuroblastoma cells, Aβ generated in early endosomes was localized to MVBs, and released in association with exosomes (Rajendran et al., 2006). Exosomal proteins ALIX and flotillin-1 were found associated with neuritic plaques in post mortem AD brains and in a mouse model of AD

respectively, suggesting a potential role of Aβ-loaded exosomes in plaque formation (Kokubo et al., 2005; Rajendran et al., 2006; Vingtdeux et al., 2012). Further, exosomes separated from AD patient brains were internalized by cultured cells and reduced their viability (Sinha et al., 2018).

In a cellular model of Parkinson's disease, exosomes loaded with α-synuclein were taken up by cells, and this mechanism is dependent on intact vesicles (Danzer et al., 2012). Further, the uptake of vesicles containing α-synuclein reduces cell viability in culture (Danzer et al., 2012; Emmanouilidou et al., 2010).

In models of prion disease, exosomes containing PrP^{Sc} were sufficient initiators of prion propagation, and brain-inoculated EVs derived from PrP^{Sc} infected cells induce disease in healthy mice (Fevrier et al., 2004; Vella et al., 2007).

Inhibition of autophagic flux has been suggested to favour the spreading of pathological proteins (Abdulrahman et al., 2018; Danzer et al., 2012; Lee et al., 2013) and creates an inflammatory and neurotoxic microenvironment (Lee et al., 2013; Poehler et al., 2014).

In summary, EVs are implicated in neurodegeneration, and autophagy status regulates EV secretion. Delineating the precise role of autophagy manipulation on secretion necessitates the analysis and separation of EVs.

1.10 Methods for the Study of Extracellular Vesicles

As stated previously, the nomenclature of EVs has been amended to classify small and large EVs rather than identifying the specific subcellular origins of vesicles (Thery et al., 2018). Therefore, this terminology will be used when discussing EV characterization, analysis and separation. The following list of EV methods is not

exhaustive, and particular focus is placed on techniques we have utilized in the thesis. It will become evident that multiple approaches must be used in concert to readily define a population of EVs, and to determine the regulation of EV secretion. Therefore, although no technique is universally applicable, they are employed in accordance with the goals of each experiment.

1.10.1 Characterization of Extracellular Vesicles

EV characterization discerns the physical properties of EVs, including morphology and density. This can be achieved by two methods: electron microscopy and density gradient centrifugation. In electron microscopy, accelerated electrons serve as the source of radiation to visualize the specimen. Electrons are scattered after passing through the sample, and are focused by electromagnetic lenses. As the wavelength of the electron beam is substantially less than that of light from an optical microscope, the resolution power is much higher (Milne et al., 2013). Two applications of electron microscopy have been utilized for EVs, namely cryogenic electron microscopy (cryo-EM) and transmission electron microscopy (TEM) (Thery et al., 2006; Yuana et al., 2013). Cryo-EM involves the imaging of vitrified samples (frozen in a layer of glass-like ice) and maintained at liquid nitrogen and/or helium temperatures, thus absolving the need for desiccation and fixation as required in conventional TEM (Milne et al., 2013; Yuana et al., 2013). Both cryo-EM and TEM have been applied to image, count and phenotype EVs, although cryo-EM is preferred to maintain the native state of EV membranes (Erdbrugger and Lannigan, 2016; Yuana et al., 2013). Electron microscopy combined with immunogold labeling allows for classifying EV subtypes (Erdbrugger and Lannigan, 2016; Thery et al., 2006; Yuana et al., 2013). However,

phenotyping is limited, the sample preparation for EM is labour intensive and high throughput analysis is not possible (Erdbrugger and Lannigan, 2016).

Iodixanol gradient centrifugation is a useful tool to determine EV density. In principle, membranous vesicles will reach equilibrium and float at a specific density within the gradient that matches their buoyant density (Brakke, 1953). The original reported density of exosomes was 1.15 to 1.19g/mL; however, recent publications highlighted the heterogeneity of EVs density and determined it to be highly dependent on the source of EVs (Colombo et al., 2014; Thery et al., 2006). In light of further experimentation, the density is more accurately reported as 1.09 to 1.15g/mL, however cell type specificity is a very important determinant and will affect this range (Greening et al., 2015; Tauro et al., 2013).

1.10.2 Analysis of Extracellular Vesicles

EV analysis encompasses techniques to determine EV properties such as size and phenotypic markers, without necessarily separating EVs from their milieu. For the purpose of this thesis, we will discuss Nanoparticle Tracking Analysis (NTA), Imaging Flow Cytometry (IFC), and, briefly, Dynamic Light Scattering (DLS).

NTA monitors the Brownian movement of particles in solution based on laser scatter with a charge-coupled device (CCD). It tracks the velocity of single particles and calculates the particle size according to the Strokes-Einstein equation (Filipe et al., 2010; Shao et al., 2018) (**Figure 9**). NTA detects 30 to 1000nm particles, with the lower limit of detection relying on the refractive index of the biological vesicles (Filipe et al., 2010).

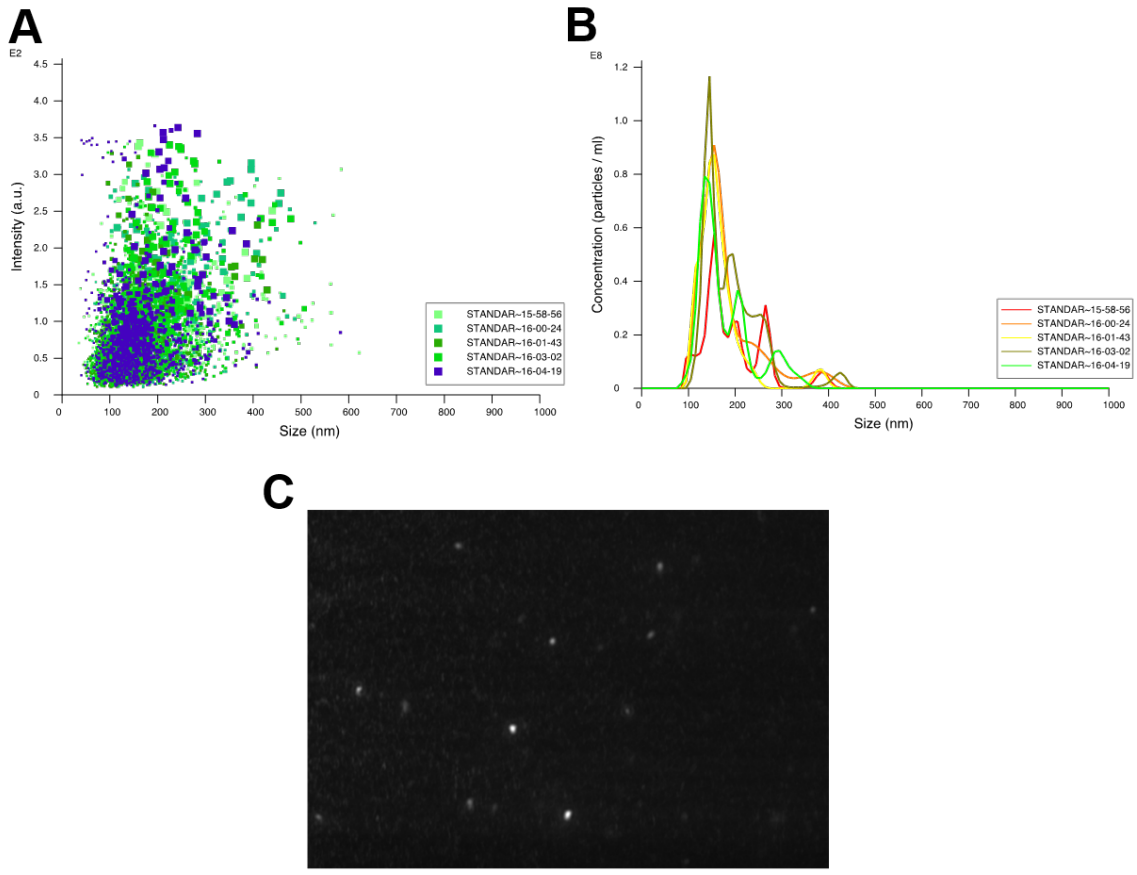

Figure 9. Nanoparticle Tracking Analysis (NTA) (A) NTA tracks individual particles in Brownian motion based on scatter. Each dot represents a single tracked particle, and each colour represents particles tracked within the replicate. Five replicates are measured for each sample **(B)** Example of NTA curve based on size. Each coloured curve represents one (of five) replicates. **(C)** Screenshot from a one-minute movie of particles tracked by NTA. Five movies are captured for each sample.

DLS correlates the interference of bulk light scattered by particles in Brownian motion as a function of time and calculates particle size with the Strokes-Einstein equation (Filipe et al., 2010; Frisken, 2001; Shao et al., 2018).

Both DLS and NTA enumerate vesicles and NTA determines concentrations of particles within a sample, as there is no inherent feature to determine concentration by DLS. Although techniques have been implemented to determine sample concentration by DLS based on the linear dependency of the mean size of silver nanoparticles on the pH of solution, techniques are complex and obtain a relative rather than absolute concentration (Vysotskii et al., 2009; Vysotsky et al., 2009).

Filipe *et al* (Filipe et al., 2010) compared NTA and DLS using polystyrene beads of known sizes. With beads of the same size, NTA and DLS were accurate in determining the size of the beads, although a slight overestimation was found with DLS. However, when the samples were spiked with larger beads, only NTA was able to accurately resolve the different populations, whereas DLS reported a mean size of the beads rather than identifying each peak of the heterogeneous population (Filipe et al., 2010). Further, although NTA was able to detect all three peaks, the proportion of small beads detected was markedly reduced when the sample was spiked with large beads; the small beads were underestimated (Erdbrugger and Lannigan, 2016; Filipe et al., 2010). Overall, for enumeration of a polydisperse and heterogeneous samples as EVs, NTA is more suitable than DLS.

Flow cytometry has been explored for analysis of submicron particles, however optimizing a technique originally made to analyze cells was initially very challenging. Traditional flow cytometry detects events based on scatter, thus the scatter intensity

must be of a magnitude sufficient to resolve above background levels. This was not achievable for small nanoparticles (Erdbrugger and Lannigan, 2016). The solution came from detecting fluorescent nanoparticles (Erdbrugger and Lannigan, 2016), yet, the problem remained that the limit of detection was low employing conventional flow cytometry (likely lower limit of 400-800nm) (Erdbrugger and Lannigan, 2016; Lannigan and Erdbruegger, 2017). With the advent and implementation of imaging cytometry to nanoparticle analysis, this limit of detection was improved. In fact, detection of fluorescent liposomes of a known size, which have a similar refractive index to EVs, was resolved to 100-200nm (Erdbrugger et al., 2014).

Imaging flow cytometry (IFC) combines the speed and power of flow cytometry with the resolution of microscopy (Erdbrugger and Lannigan, 2016). The ImageStream uses a CCD that acquires data from six channels with a single event. Coincident images are compiled from brightfield (transmitted light), darkfield (side scatter) and four fluorescent channels (Ortyn et al., 2006). As a readout from the CCD, the ImageStream uses Time Delay Integration (TDI) and a lengthened signal integration time, thus, in combination with a slower flow rate, has increased sensitivity over conventional flow cytometry (Lannigan and Erdbruegger, 2017). IFC offers the advantage to both analyze EVs phenotypically, as well as determine basic morphology (**Figure 10**). Therefore, with use of captured images, IFC is able to discriminate EVs from beads, particulate matter and cells (Erdbrugger and Lannigan, 2016).

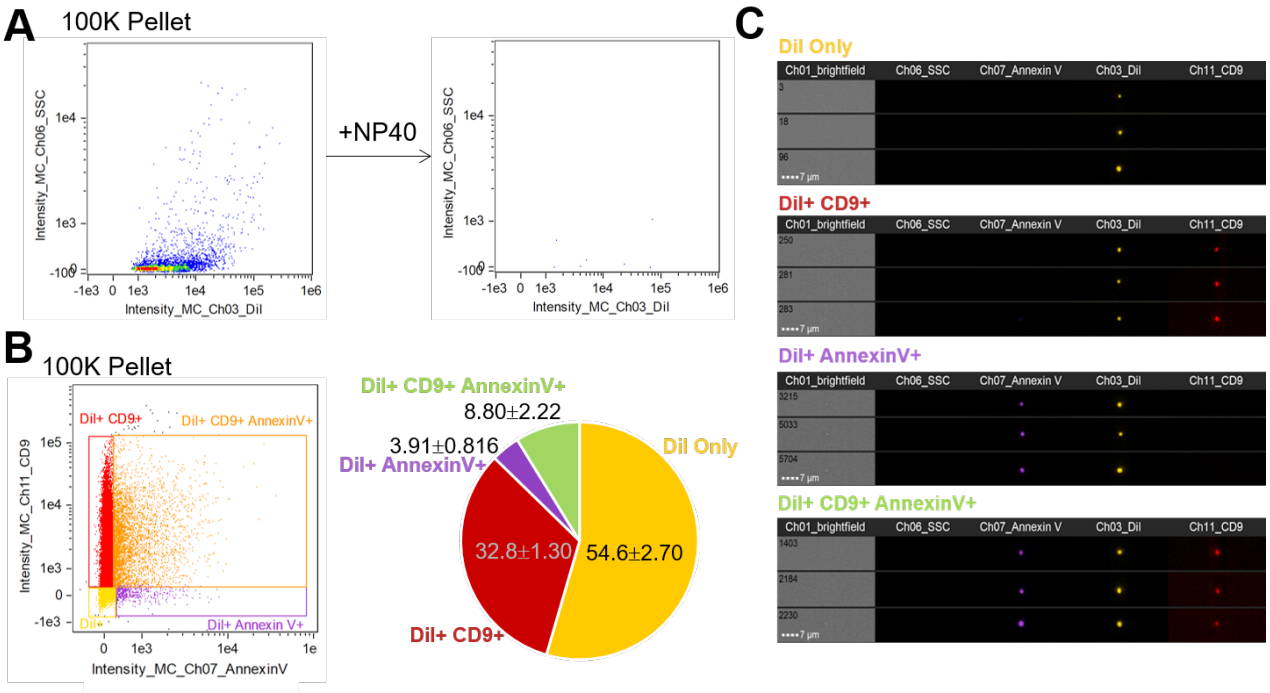

Figure 10. Image Flow Cytometry to visualize fluorescent small particles (A) Representative dotplot of the 100K Pellet obtained by differential ultracentrifugation. Samples were incubated with NP40 detergent (0.5%) for 30 minutes at room temperature to demonstrate that particles are EVs. **(B)** IFC can be employed to characterize EV subtypes. The 100K Pellet derived from differential ultracentrifugation was labeled with CD9 and AnnexinV prior to IFC. **(C)** Representative images of each subtype. From left to right: Channel 01_brightfield, Channel 06_side scatter (SSC), Channel 07_AnnexinV, Channel 03_DiI and Channel 11_CD9.

However, the potential limitations of IFC include the requirement of small volumes, therefore concentration of samples may be necessary prior to analysis to achieve the same power as conventional flow cytometry (Lannigan and Erdbruegger, 2017). Further, size determination by IFC is not an inherent feature of the instrument. Nevertheless, a reasonable size range may be achieved with fluorescently labeled liposomes, which will have a similar refractive index to EVs rather than traditional polystyrene beads that scatter substantially more light than lipid-enclosed vesicles (Lannigan and Erdbruegger, 2017).

1.10.3 Separation of Extracellular Vesicles

Separation of EVs from biological samples may still be necessary for certain experimental goals. Therefore, a few methods have been employed: differential ultracentrifugation (UC), polymer-based precipitations, immunoaffinity capture, and size-exclusion chromatography (SEC).

UC is the most commonly used method to separate EVs. UC separates EVs based on buoyant density, and involves sequential centrifugation steps, which, in theory, selectively sediment apoptotic bodies (2000xg), microvesicles (10,000xg) and exosomes (100,000xg) (Konoshenko et al., 2018; Thery et al., 2006).

As the density of particles remaining in the supernatant (SN) is progressively lower following each centrifugation, a higher centrifugation force and duration is required to pellet the smaller and less dense particles (Livshits et al., 2015). However, because the distribution of differently sized particles in the sample is homogenous, co-sedimentation of small EVs with larger particles is inevitable and isolation of a pure population is not achievable (Anderson, 1966; Livshits et al., 2015). Therefore, caution

is recommended in the interpretation of EVs separated by UC. Major concerns when using UC include possible aggregation of particles, lack of reproducibility, and inefficient separation from non-exosomal components (Konoshenko et al., 2018). Further, UC causes loss of material, or alternatively may generate events artificially due to the harsh pelleting procedure (Erdbrugger and Lannigan, 2016).

Polymer-based precipitation exploits the hydrophilicity of polyethylene glycol (PEG) to reduce EVs solubility and allow them to pellet at low speed centrifugation (Konoshenko et al., 2018; Shao et al., 2018). For certain experimental purposes, polymer-based precipitations offer an inexpensive, simple and quick method to separate EVs (Andreu et al., 2016). However, retention of the polymer and PEG-mediated co-precipitation of proteins, lipoproteins and aggregates are disadvantages (Konoshenko et al., 2018; Shao et al., 2018). Consequently, EVs separated by this method reduce cell viability when provided to recipient cells (Gamez-Valero et al., 2016).

Immunoaffinity capture relies on antibody-antigen interaction to separate a pure population of EVs based on a chosen marker. Tetraspanins are a common marker for EVs when using this separation method. Methodological disadvantages include the challenge of dissociating EVs from the immobilized antibody prior to downstream analysis, which may affect EVs if harsh elution buffers are used. Further, nonspecific binding may be a source of contamination (Konoshenko et al., 2018; Taylor and Shah, 2015). Overall, this approach offers the possibility of selecting a highly specific group of EVs, which is both an advantage and downfall. As no pan-label for EVs has been discovered, separating EVs based on a single marker prevents analysis of

heterogeneous populations, potentially offering an incorrect picture of EV secretion. Therefore, this approach is problematic in assessment of general EV secretion (Taylor and Shah, 2015). On the other hand, if analyzing a select population, immunoaffinity is a useful tool, such as the potential diagnostic application for identifying and isolating tumour cell-derived EVs based on specific markers (Rana et al., 2012; Taylor and Shah, 2015).

SEC separates a biological solution based on the size, thus the hydrodynamic radius of its components. Porous beads composed of neutral cross-linked polymers are packed into a column. The suspension of particles is loaded onto the column, they are eluted with buffer and fractions are collected (Taylor and Shah, 2015). Particles and molecules pass through the heteroporous beads and are excluded or included in the beads dependent on their hydrodynamic radius and the matrix pore size. The smaller hydrodynamic radius of the molecule allows greater access to pores, increasing the dwell time within the column. Contrary, larger molecules will access less pores and move around the beads, thus eluting in early fractions (Shao et al., 2018; Taylor and Shah, 2015). Size exclusion-based methods offer high yield of EVs free of soluble protein contamination, preventing aggregation of EVs, preserving membrane integrity, and rendering an EV preparation that is compatible for the feeding of recipient cells. The primary limitation is the high cost of purchase of commercially available columns, and the time dedication required to process multiple samples (Konoshenko et al., 2018; Lobb et al., 2015).

In conclusion, there are several well-developed techniques to separate and analyze EVs. The chosen method to employ for each experimental purpose should be determined, and multiple techniques should be utilized.

1.11 Hypothesis and Objectives

Aβ localizes to MVBs and ILVs and is released in association with EVs (Bellingham et al., 2012; Danzer et al., 2012; Rajendran et al., 2006; Sinha et al., 2018; Yuyama and Igarashi, 2017). EVs from AD patients' brains contain increased levels of Aβ oligomers (Sinha et al., 2018). EVs secretion is regulated by autophagy (Baixauli et al., 2014; Eitan et al., 2016; Vingtdeux et al., 2012). Autophagy induction inhibits EV release by directing MVBs to the autophagic pathway (Fader et al., 2008). Conversely, autophagy inhibition promotes EV release and contributes to the spread of misfolded proteins (Abdulrahman et al., 2018; Lee et al., 2013; Poehler et al., 2014). Our laboratory has discovered that Aβ inhibits protein prenylation and blocks autophagic flux (Mohamed et al., 2012; Mohamed et al., 2018; Smith, 2016). Based on this evidence and on our findings that Rabs prenylation is significantly reduced in Aβ-treated neurons and in brains of TgCRDND8 mice we hypothesize:

Hypothesis: Aβ increases EV secretion and promotes the cell-to-cell transfer of Aβ by a mechanism that involves blockade of autophagy flux.

Objectives:

1. To select the most appropriate methods of EV separation and analysis based on the purpose of our studies

2. To investigate the regulation of EV release by Aβ and other agents that alters autophagy.
3. To assess the uptake of Aβ-containing EVs by recipient cells.

Chapter 2

Materials and Methods

2.1 Materials

$A\beta_{42}$ was purchased from rPeptide (Cat# A-1163-2) (Watkinsville, GA, USA). Hylite fluorescent Aβ was purchased from Anaspec (Cat# 60479-01). Opti-MEM® reduced-serum medium, Dulbecco's modified eagle medium (DMEM), penicillin-streptomycin, BGS and Geneticin® were from Gibco. Protease inhibitor cocktail tablets were from Roche. Clarity™ Western ECL Substrate (Cat# 170-5060) and nitrocellulose membranes were purchased from Bio-Rad. Bicinchoninic acid (BCA) protein assay kit and Vybrant™ DiI (Invitrogen™ V22885) were from Thermo Fisher Scientific (Montreal, QC, Canada). All horseradish peroxidase-conjugated secondary antibodies were from Amersham Biosciences. OptiPrep™ was purchased from Axis-Shield (Oslo, Norway). qEV columns (SP1) were from Izon (Christchurch, New Zealand). Enzyme-linked immunosorbent assay (ELISA) kit for human $A\beta_{1-42}$, and Immobilon PVDF was purchased from Millipore Sigma (Ontario, Canada). Amicon Ultra-15 100K MWCO, Amicon Ultra-4 10K MWCO, and Amicon Ultra-0.5 10K MWCO were from Millipore Sigma (Ontario, Canada). Glutathione Sepharose 4B beads (17075601) were purchased from GE Healthcare (Chicago, Illinois, United States). Staurosporine (S6942) and Bafilomycin A1 (B1793) were purchased from Millipore Sigma. Chemicals were purchased from Millipore Sigma.

2.2 Cell Culture

The mouse neuroblastoma cell line, Neuro2a (N2a) was obtained from ATCC (CCL-131) and cultured in OptiMEM:DMEM (1:1), 10% bovine growth serum (BGS), 1% penicillin/streptomycin, 2mM L-Glutamine and 0.11g/L Sodium Pyruvate (N2a Growth Media). N2a cells stably overexpressing the human APP harbouring the Swedish

mutation (K670N, M671L) (N2aAPP^{swe}) were kindly provided by Dr. Thinakaran (University of Chicago, USA) (characterized in (Thinakaran et al., 1996)). N2aAPP^{swe} cells were cultured in OptiMEM:DMEM (1:1), 10% bovine growth serum (BGS), and 1% penicillin/streptomycin, 2mM L-Glutamine, 0.11g/L Sodium Pyruvate and 0.4% Geneticin. Geneticin was kept in media for only the first two passages, then N2aAPP^{swe} cells were switched to N2a growth media. Cells were kept in culture for no more than fifteen passages. N2a cells with a CRISPR/Cas9 knock-out of ATG5 (N2a ATG5 KO) were kindly provided by Dr. Hermann Schaetzl (University of Calgary, Canada) (details in (Abdulrahman et al., 2018)). Cells were cultured in N2a growth media. All cells were maintained at 37°C with 5% CO_2 and passaged every two days. Experiments were performed on day 2 after plating of cells, including treating cells (if required), then EV collection.

2.3 Cell Labeling with DiI

Cells were labeled with Vybrant™ DiI cell labeling solution according to manufacturer's instructions. Briefly, cells were detached with 0.25% trypsin-EDTA, counted and re-suspended in serum-free media (OptiMEM:DMEM (1:1), 1% penicillin/streptomycin, 2mM L-Glutamine and 0.11g/L Sodium Pyruvate). A volume of cell suspension that corresponds to 1.8×10^6 cells per 10cm^2 plate for N2a cells (1.5×10^6 cells per 10cm^2 for N2aAPP^{swe}, 2.0×10^6 for N2a ATG5KO) was brought to a concentration of 1×10^6 cells/mL in serum-free media and 5µL/mL of labeling solution was added. The seeding densities were determined as to achieve the same confluence of all cells at the end of the experiment (~80%). After incubation at 37° for 20 minutes, cells were centrifuged at 300×g for five minutes. The cellular pellet was re-suspended

and washed in N2a growth media and centrifuged again. Cells were washed a total of three times to remove free dye prior to plating. Cells were maintained in culture for a minimum of 18 hours before treatment(s). DiI secretion was measured as a proxy for EV secretion.

2.4 Oligomeric Aβ Preparation

Oligomeric Aβ was prepared referring to a published protocol (Dahlgren et al., 2002). The same lot was used throughout the study. Lyophilized Aβ was reconstituted to 1mM with hexafluoroisopropanol (HFIP), and pipetted into sterile, low protein binding microfuge tubes. HFIP was dried down with a constant stream of nitrogen gas and desiccated under vacuum for one hour. The resulting Aβ film was stored at -80°C until required. To prepare oligomers of Aβ, the peptide was resolubilized with Me_2SO to a concentration of 5mM and rapidly brought to 100μM with Leibovitz's L-15 CO_2 medium (phenol red-free, antibiotic-free, and serum-free). The resulting solution was incubated at 4°C for 24 hours to allow oligomerization of the protein. The $oA\beta_{42}$ preparation was characterized as in previous work (Dahlgren, Manelli et al. 2002, Saavedra, Mohamed et al. 2007) and showed to contain monomers and oligomers of Aβ but not fibrils. Hylite fluorescent Aβ was prepared the same way. The same lot was used throughout the study.

2.5 Cell Treatments

Cells were treated with autophagy modulator bafilomycin (150nM, 4 hours) or $oA\beta_{42}$. Treatments with 20μM $oA\beta_{42}$ were performed for 20-24 hours as in our previous work (Mohamed et al., 2012; Mohamed et al., 2018). $oA\beta_{42}$ was provided in serum-free medium (OptiMEM:DMEM (1:1), 1% penicillin/streptomycin, 2mM L-Glutamine and

0.11g/L Sodium Pyruvate), and bafilomycin was provided to cells in N2a growth media. Treatments were initiated at a cell confluency of approximately 50%. After the treatment period, cells were washed with N2a growth media and incubated with fresh N2a growth media for one hour. Next, cells proceeded for EV collection.

2.6 EV Collection

After plating cells and performing treatments, the media was replaced for EV collection. We tested four mediums for EV collection: classical EV-depleted media (EVd) (OptiMEM:DMEM 1:1, 1% penicillin/streptomycin, 2mM L-Glutamine and 0.11g/L Sodium Pyruvate with 10% EV-depleted serum), serum-free media supplemented with N2 (N2) (OptiMEM:DMEM 1:1, 1% penicillin/streptomycin, 2mM L-Glutamine and 0.11g/L Sodium Pyruvate with 1x N2), serum-free media supplemented with B27 (B27) (OptiMEM:DMEM 1:1, 1% penicillin/streptomycin, 2mM L-Glutamine and 0.11g/L Sodium Pyruvate with 1xB27) and OptiMEM alone (Opti). BGS was centrifuged at 100,000×g for 16 hours to prepare EV-depleted serum (Thery et al., 2006). After 24 hours, the medium was harvested and centrifuged at 2000×g for 10 minutes and the supernatant (2K SN) obtained. The 2K SNs were normalized based on cellular protein content when comparing treatment groups.

2.7 Immunoblot Analysis

Cells were harvested in 1×RIPA buffer (140mM NaCl, 20mM Tris, 1% SDS, 0.1% NP40, 0.5% Sodium deoxycholine, pH 7.4) with protease inhibitor cocktail and sonicated. A BCA assay was performed, and cells normalized to achieve the same amount of protein in each sample (20-40μg). When analyzing EV samples, the volume of each 2K SN was adjusted based on the amount of protein in the secreting cells (i.e., EVs

are derived from the same number of cells). Normalized samples were denatured with 5x sample buffer (60mM Tris, 25% glycerol, 2% SDS, 5% 2-Mercaptoethanol, 0.1% bromophenol blue pH 6.8) and boiled for five minutes prior to loading and running gels. Proteins were resolved by SDS-PAGE with 16% gels containing 0.1% SDS. Gels were transferred to PVDF membranes overnight at 4°C in 25mM Tris, 192mM glycine and 20% methanol, (pH 8.3). Membranes were washed three times with TBS (200mM Tris, 1.37M NaCl, pH 7.4) with 0.1% Tween 20 (TTBS) then blocked for one hour in TTBS containing 5% non-fat milk (blocking buffer). Membranes were probed for EV enriched markers using the following primary antibodies: ALIX (AIP1) (1:250) (BD Biosciences, 611621), CD9 (1:1000) (Abcam, ab92726), and Flotillin-1 (1:1000) (BD Biosciences, 610820) or LC3 (1:500) (Novus Biologicals, NB100-2220) and Actin (1:2000) (Cell Signaling Technology, 4957S) overnight at 4°C. All primary antibodies were diluted in TTBS containing 5% bovine serum albumin (BSA), with the exception of LC3 and Actin, which were diluted in blocking buffer. The next day, membranes were washed twice with TBS, twice with TTBS and twice again with TBS followed by a one-hour incubation with secondary antibody (1:2000 in blocking buffer) at room temperature with gentle agitation. Membranes were washed again two times for five minutes with TBS, TTBS and TBS respectively. Immunoreactivity was detected with Clarity™ Western ECL Substrate (Bio-Rad) and visualized with Li-COR C-DiGit western blot scanner. Bands were quantified with Image Studio.

2.8 Immunoblot for Aβ

Proteins were resolved by Tris-Tricine gel electrophoresis with 12% Tris-Tricine gels and 3% cross-linker containing 0.1% SDS. Tricine-SDS-PAGE is superior to

Laemmli SDS-PAGE for resolving small proteins (Schagger, 2006). Samples were prepared with 5× sample buffer without loading dye (60mM Tris, 25% glycerol, 2% SDS, 5% 2-Mercaptoethanol, pH 6.8). Gels were run with a cathode buffer between gels (100mM Tris, 100mM Tricine, 0.1% SDS, pH~8.25), and anode buffer on the outside (100mM Tris, 100mM Tricine, 22.5 mM HCl, pH 8.9). Gels were transferred to PVDF membranes in CAPS buffer (500mM 3-[cyclohexylamin-1-propanesulfonic acid] (CAPS), 10% methanol, pH 11) overnight at 90mA, 4°C. Two PVDF membranes were used to capture proteins that may transfer through the initial membrane. Membranes were washed and blocked as previously described and incubated in anti-Aβ 4G8 antibody (1:1000) (Biolegend, 800701) made up in 5% BSA. Membranes were visualized as previously described.

2.9 Dotblot

Sample volume was adjusted with TBS with protease inhibitors to achieve 100µL per well in the dotblot (minimum 200µL when running in duplicate). Nitrocellulose membrane (0.45µm standard, 0.2µm for Aβ) and filter paper were prewashed in TBS for 10 minutes prior to dotblot assembly. Dotblot was assembled from bottom to top, with filter paper and membrane respectively between. Screws were tightened crosswise and membranes washed with TBS under vacuum prior to loading samples. After sample application, the membrane was washed with two volumes of TBS under vacuum. The membrane was removed and allowed to dry. When detecting Aβ, membranes were washed in two volumes of mild stripping buffer for 10 minutes prior to primary antibody incubation (200mM glycine, 0.1% SDS, 1% Tween 20, pH 2.2). Membranes were washed and blocked as previously described and incubated in anti-Aβ

4G8 antibody (1:1000) (Biolegend, 800701) made up in 5% BSA. Membranes were washed and visualized as previously described. Quantification was performed with Image J.

2.10 Protein precipitation

For protein precipitation of supernatants for immunoblot, both acetone and tricholoroacetic acid (TCA) were used. For acetone precipitation, samples were vortexed upon addition of 4 volumes of acetone and proteins allowed to precipitate overnight. Precipitated proteins were centrifuged (15,000×g, 4°C), and the pellet washed 3 times with acetone prior to re-suspension in RIPA buffer with protease inhibitors. For TCA precipitation, 10% TCA was added to samples for 30 minutes on ice. Samples were centrifuged at 15,000×g for 15 minutes at 4°C. Supernatants were removed and pellets were washed with acetone and centrifuged again at 15,000×g for 10 minutes at 4°C. Pellets were washed three times to remove all residual TCA then re-suspended in RIPA buffer with protease inhibitors.

2.11 Aβ ELISA

ELISA for $A\beta_{42}$ was performed according to the manufacturer's instructions (Millipore, EZHS42). Absorbance was measured using SpectraMax® i3x Multi-Mode Microplate Reader at 450nm (signal) and 590nm (background).

2.12 Protein Quantification

BCA assay was performed according to manufacturer's instructions (Bio-Rad). Absorbance was measured using SpectraMax® i3x Multi-Mode Microplate Reader at 562nm.

2.13 Differential Ultracentrifugation (UC)

100K Pellets (EVs) were obtained in accordance with previously described protocols with minor adjustments (Lobb et al., 2015). In experiments in which EV release will be investigated, volumes of the 2K SNs were adjusted based on cellular protein content and centrifuged at 100,000×g for 90 minutes with the Optima™ MAX-XP Ultracentrifuge in 10.4mL polycarbonate tubes (Beckman). The supernatant (denoted 100K SN) was retained and the pellet washed with 1mL of phosphate buffered saline (PBS) (137mM NaCl, 2.7mM KCl, 10mM Na_2HPO_4, 1.8mM KH_2PO_4, pH 7.4) and centrifuged again at 100,000×g for 90 minutes in 2mL centrifuge tubes (Qiagen). The pellet of the 100,000×g centrifugation (100K Pellet) was then re-suspended in PBS and analyzed by IFC or immunoblot. The 100K Pellet was obtained from a minimum of four plates per treatment group for immunoblot. The normalized samples were blotted alongside 20-40µg of corresponding cell lysates.

2.14 Iodixanol Flotation Gradient

Iodixanol (Optiprep™, Axis-Shield, Oslo, Norway) gradients were performed according to previously described protocols with minor adjustments (Greening et al., 2015). Briefly, 5%, 10%, 20% and 40% iodixanol solutions were freshly prepared in serum-free media (DMEM:OptiMEM 1:1) and rotated end-over-end at 4° for 30 minutes. A discontinuous gradient was carefully layered by adding 3mL of 40%, 3mL of 20%, 3mL of 10%, and 2mL of 5%, solutions in a 16.8 mL open-top polyallomer tube (Beckman Coulter, Fullerton, California, USA). Integrity of gradients was visually examined to ensure no mixing of layers prior to sample addition. Proteins from normalized 2K SN were concentrated using Amicon Ultra-15 100K MWCO filters

according to manufacturer's instructions. The resulting retentate (i.e., volume retained on top of the filter) was brought up to 1mL with serum-free media (DMEM:OptiMEM 1:1) and layered gently on the prepared gradient at 4°C. Gradients were centrifuged using SW 41-Ti swinging bucket rotor (Beckman Coulter, Fullerton, California, USA) for 18 hours at 100,000×g (24,200rpm). After the centrifugation, twelve 1mL fractions were collected from top to bottom. The entire protocol, including sample additions, gradient formation and centrifugations were performed at 4°C. With immunoblot analysis, 10% of each fraction was precipitated with 4 volumes of ice-cold methanol overnight at −20°C. Precipitated proteins were centrifuged (16,000×g for 15 minutes at 4°C), and the pellet washed one time with methanol, and centrifuged again. The methanol was aspirated, and protein pellet allowed to air dry for 5 minutes maximum to prevent excessive drying. The protein-containing pellet was re-suspended in RIPA buffer with protease inhibitors. Note that acetone precipitation is not compatible with iodixanol fractions. Fraction precipitation was not required for dotblot analysis thus samples were loaded directly.

2.15 Size Exclusion Chromatography (SEC)

Normalized 2K SNs were concentrated using 100K MWCO filters and the resulting retentates brought up to 550µL with N2 media (OptiMEM:DMEM 1:1, 1% penicillin/streptomycin, 2mM L-Glutamine and 0.11g/L Sodium Pyruvate with 1x N2). A 50µL aliquot was used for DiI measurements and the remaining 500µL loaded onto the qEV column. Fractions were eluted with 0.1µm filtered PBS and 500µL fractions were obtained. Twenty fractions were collected. DiI fluorescence and absorbance at 280nm were measured in all fractions and the peak of DiI was pooled (generally

fractions 6-9). Fractions were concentrated with Amicon Ultra-4 or Amicon Ultra-0.5 10K MWCO filters depending on the volume of the peak obtained.

2.16 Image Flow Cytometry (IFC)

2.16.1 EVs Labeling

EVs present in different preparations were analyzed, and obtained as previously described (2K SNs, OR EVs separated by UC or SEC). An aliquot of supernatants or re-suspended pellets were first diluted 1:1 with 2× AnnexinV binding buffer (10 mM HEPES, 140 mM NaCl, and 2.5 mM $CaCl_2$, pH 7.4). The first label, Alexa Fluor® 647 conjugated CD9 antibody (BioLegend, Cat#124810), was diluted 1:10 with 0.1µm filtered PBS, and added to the sample at a final concentration of 2.5µg/mL. Samples were incubated on ice for 15 minutes. Next, Pacific Blue™ AnnexinV (Invitrogen™, A35122) was added (1:20 dilution) and incubated at room temperature for 15 minutes. Samples were left on ice until flow cytometry analysis.

2.16.2 Acquisition and Data Analysis

All samples were acquired on an ImageStreamX MkII (ISX; Amnis/Luminex). The ISX had 4 lasers (405 nm, 488 nm, 642 nm, and 785 nm (side scatter laser) and 3 objectives (20×, 40×, and 60×). All samples were captured at 60× magnification with the following laser powers:

- 120.00 mW; 405 nm
- 200.00 mW; 488 nm
- 150.00 mW; 642 nm

Samples were collected in the following channels:

- Ch03 for DiI (560-595 nm)
- Ch07 for Annexin V (435-505 nm)
- Ch11 for CD9 (642-745 nm)

Standard, unfiltered sheath fluid (BioSure sheath solution (D-PBS, pH 7.4)) was used for all measurements. For each sample, acquisition was set up to capture all events that were of lower side scatter (SSC) than the speed beads. 10,000 events were captured in the 2K SN (most diluted sample), or samples were captured for 12 minutes, whichever came first. All samples were acquired for the same amount of time within each experiment with the fluidics set to low and sensitivity high.

Data analysis was performed in IDEAS software (version 6.2). As a first step in the analysis, we gated on Intensity_Ch06 (SSC) in order to remove any remaining speed beads in the analysis. To ensure we were analyzing only 1 EV in each image, we created a mask to identify DiI intensity (Intensity(M03,Ch03_DiI, 50-4095)). Using this mask, we developed a spot count feature (Spot Count_Intensity(M03,Ch03_DiI, 50-4095)_4) and gated on images that had no more than 1 DiI spot. This gave us a population of EVs.

From here we wished to quantify brightfield positive vs negative events. For this purpose, we created a mask to identify brightfield images (Dilate(Peak(M01, Ch01_brightfield, Bright, 1.02)1). This identified all brightfield images that had a 'bright' spot. However, we noticed that there were some images unrecognized by the mask that had a 'dark' spot and negative intensity on the brightfield field scaling. To identify these, we created another mask (Dilate(Peak(M01, Ch01_brightfield, Dark, 1.02)1). These populations (Brightfield Bright and Brightfield Dark) were combined into a single population, leaving two distinct populations: those that were DiI positive and had

detectable single in the brightfield channel (brightfield positive) and those that were DiI positive and had no detectable signal in the brightfield channel (brightfield negative).

For analysis of DiI in recipient cells, the wizards for internalization and mean Haralick entropy were used. When applying each wizard, first the channels corresponding to the cells (brightfield, Channel 01) and the internalized probe (DiI labeled EVs, Channel 03) were identified. Next, single cells were gated by applying a plot of area of the brightfield channel (Area_M01) vs aspect ratio of the brightfield channel (Aspect Ratio_M01). Single cells have a high aspect ratio and intermediate area. This analysis was sufficient to calculate the mean Haralick entropy. For the internalization wizard, the internalization positive cells were then gated with a scatter plot of max pixel vs intensity of the probe. As we tracked DiI in the cells, we gated cells with a high max pixel in Channel 03 and high intensity of Channel 03. The gate was confirmed by looking at the individual images to ensure the cells were positive for DiI. Next, the software calculates an internalization score.

2.17 Nanoparticle Tracking Analysis (NTA)

NTA measurements were done with NanoSight LM10 system equipped with a 405nm laser (NanoSight, Amesbury, United Kingdom). EV samples were diluted with 0.1μm-filtered PBS to achieve 20-100 particles/frame. Samples were injected into the sample chamber with sterile syringes until the liquid was seen on the opposite side. The sample was measured for one minute for each replicate and advanced gently to measure the each subsequent replicate. Five replicates were obtained for each sample. The precise temperature was recorded manually to accurately determine particle concentration, and camera level set to 14. The detection level threshold was set to 7 for

analysis. Every sample was captured with the same camera level and detection threshold. 200nm polystyrene beads (Nanosphere, CAT# 3200A) diluted in potassium chloride (KCl) were measured to optimize the instrument prior to data collection. For analysis, all dilutions and volumes were factored in to compare the number of particles. To combine data from experiments, values were normalized to cellular protein content.

2.18 Transmission Electron Microscopy (TEM)

Normalized samples were obtained and supernatants concentrated with Amicon Ultra-15 100K MWCO filters. Freshly prepared samples were fixed with an equal volume of 2× Karnovsky fixative [0.2M Na Cacodylate, 4% Paraformaldehyde and 4% Glutharaldehyde (Ted Pella, inc.)], mixed gently and incubated on ice for 30 minutes or more. Next, 5-10µL of sample was transferred on top of carbon-formvar-coated grids (Ted Pella, inc.) following glow discharge. Alternatively, grids could be transferred on top of drops of sample. The grids were washed gently after 5-10 minutes and transferred on top of 2.5% Uranyl Acetate (EMS inc.) for 10 minutes. The grids were washed gently again and left to dry on a Kimwipe® (Kimberly-Clark®, Texas, United States) in the dark. Imaging was performed using a Jeol JEM-2100 TEM.

2.19 Analysis of Autophagic flux using tandem mCherry-GFP-LC3 (tLC3)

The AAV-tLC3 autophagy reporter (**Figure 11**) was kindly prepared by our collaborator, Chris St. Laurent. To transduce cells, glass coverslips were coated with poly-L-lysine (1:10, Millipore-Sigma) for one hour at room temperature, washed three times with sterile PBS, then allowed to dry under laminar flow. Cells were plated onto coated coverslips in a 24 well plate at a density of 1.5×10^4 cells/well for N2a, 1.5×10^4

cells/well for N2aAPP^{swe}, and 3.0×10^4 cells/well for N2a ATG5KO. The seeding densities were determined to achieve approximately 80% confluence by the end of the experiment for all cell lines. Cells were allowed to attach for 24 hours. Subsequently, cells were transduced with t-LC3 AAV2/2 virus (titer of 8.4×10^{10} vg/mL) at 2000 MOI in serum-free media (OptiMEM:DMEM 1:1, 1% penicillin/streptomycin) for 20 hours when cells were ~30% confluent. The virus was removed and cells washed with N2a growth media, and incubated in fresh N2a growth media for 1 hour (OptiMEM:DMEM 1:1, 1% penicillin/streptomycin, 10% BGS). Aβ was added to N2a cells at 20μM for 24 hours. Bafilomycin was added to another well of N2a cells for 4 hours at 500nM. This higher concentration of bafilomycin has been used previously in the lab for similar experiments (Smith, 2016). Cells were washed and incubated in N2a growth media for 1 hour (OptiMEM:DMEM 1:1, 1% penicillin/streptomycin, 10% BGS) and proceeded to DAPI staining and microscopy.

Coverslips were washed twice with pre-warmed HBSS. Cells were fixed with 4% PFA for 15 minutes, then permeabilized with 0.1% Triton X-100 in PBS for 5 minutes. DAPI was used to stain nuclei (1:3000 in PBS for 15 minutes), and coverslips were mounted onto slides. Cells were visualized with Zeiss Axio Observer Z1 epifluorescence microscope under oil immersion, 63x objective.

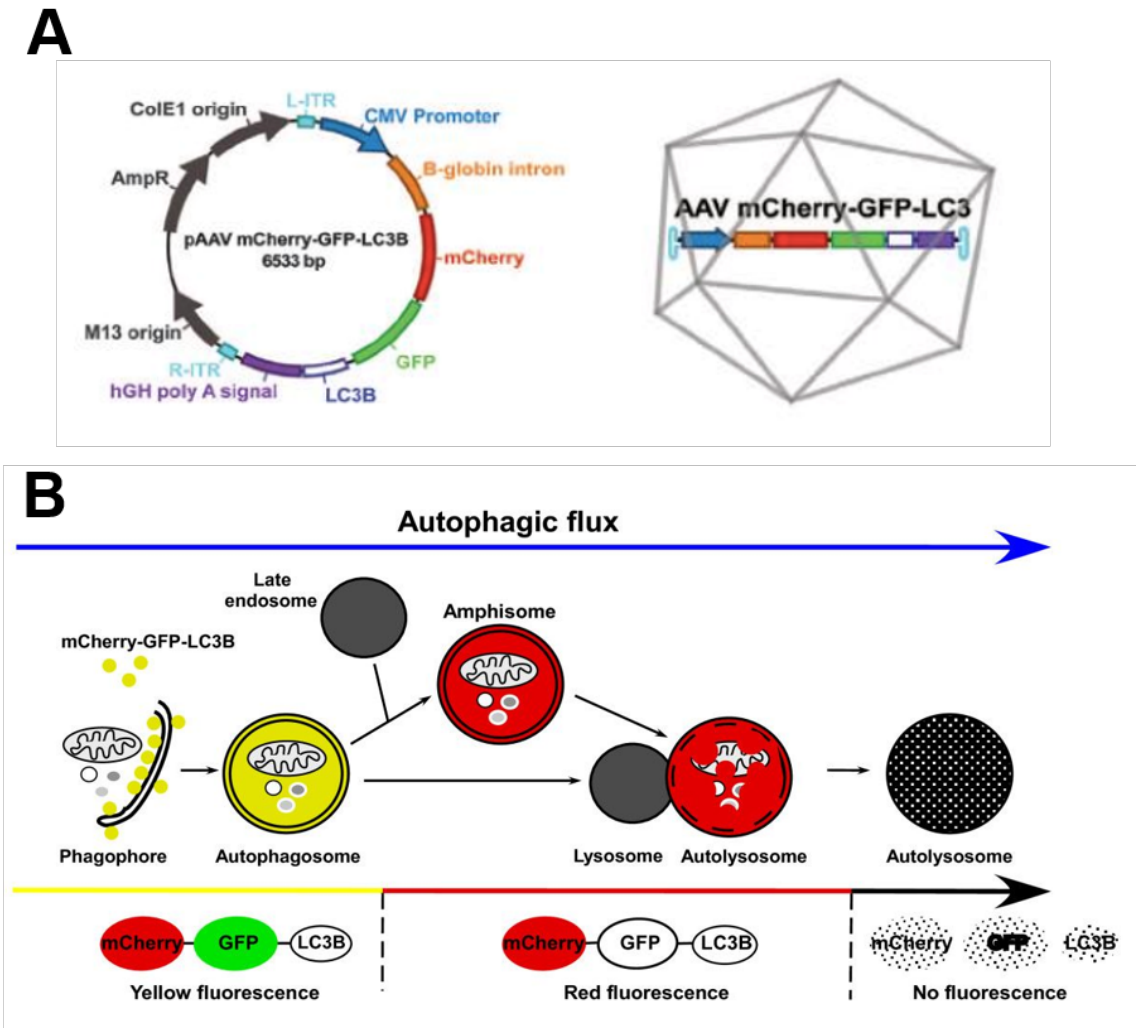

Figure 11. tandem LC3 for measuring autophagic flux in cells (A) Schematic representation of tandem LC3 plasmid and AAV2/2 viral vecor. *Adapted from Castillo, K. et al. Measurement of autophagy flux in the nervous system in vivo. Cell Death Dis 4, e917, doi:10.1038/cddis.2013.421 (2013* **(B)** LC3 conjugated to mCherry and GFP fluorophores to generate a tandem fluorescent probe with pH sensitivity to monitor autophagy in cells. The fluorescence of GFP is quenched in acidic compartments, namely the lysosome and autolysosome. mCherry is pH insensitive. Accumulation of red puncta indicate increased autophagy and normal degradation, whereas accumulation of yellow puncta indicate impaired autophagic flux. *Adapted from Hansen, T. E. & Johansen, T. Following autophagy step by step. BMC Biol* **9**, *39, doi:10.1186/1741-7007-9-39 (2011).*

2.20 Aβ Localization in EVs

To determine the intraluminal or surface localization of Aβ in EVs, we performed a protease protection assay based on a published paper (Danzer et al., 2012). If Aβ is intraluminal, the EV membrane would protect the Aβ from degradation by trypsin unless the membrane permeabilized by detergent saponin. However, surface localized Aβ will not be protected, thus cleaved completely by trypsin alone.

To assess Aβ localization, conditioned media was harvested from a minimum of four $10cm^2$ plates of cells. The conditioned media was subjected to sequential UC as previously described, and the 100K SN was removed following the first 100,000xg centrifugation. The pellet was resuspended in PBS, then divided into separate 2mL centrifuge tubes (Qiagen): 67% into the first tube (tube A), and 33% in the second centrifuge tube (tube B). As tube A will be later divided in half, this unequal separation was necessary to achieve the same amount of material in each group. The tubes were brought to the same volume (1mL) with PBS and centrifuged again at 100,000×g. After the centrifugation, the PBS was aspirated and the pellet from tube A resuspended in 0.25% trypsin-EDTA, and tube B resuspended in TBS with protease inhibitors (untreated). Tube A was then equally divided into two eppendorf tubes. To one of the tubes, saponin was added to a concentration of 0.1% (trypsin/saponin). The other tube was brought to the same volume with PBS (trypsin only). All three groups (untreated, trypsin only and trypsin/saponin) were incubated at 37°C for 30 minutes, then all groups were brought to the same volume with TBS containing protease inhibitors. EVs were sonicated and a dotblot for Aβ was performed.

2.21 Cell-to-cell Transfer

N2aAPP^{swe} cells were plated at a density of 1.5x10^6 cells/10cm^2 plate and labeled with DiI. The next day, half of the plates were treated with bafilomycin (150nM, 4 hours) when the cells were at 50-60% confluency. The culture media was replaced with fresh N2a growth media for one hour. Next, EVs were collected in serum-free media supplemented with N2 for 24 hours. These cells are the donor cells.

N2a unlabeled recipient cells were plated in a 24 well plate at a density of 6.0x10^4 cells/well at the same time that media is replaced in the donor cells.

After 24 hours of EV collection in the donor cells, the normalized 2K SN was obtained as previously described. The 2K SNs were concentrated using the Amicon Ultra-15 100K MWCO filters. Retentates were brought up to a volume of 550uL, and 500uL loaded on top of a qEV column for SEC-based EV separation. The same volume of unconditioned media was concentrated and loaded onto a column as a negative control. Fractions were collected from the column and the DiI peak pooled (Fractions 6-9). A sample of the SEC peak was run on the MarkII Amnis ImageStream and a concentration of particles/mL obtained. With experiments assessing EV uptake, an equal number of EVs were given to unlabeled recipient cells from both untreated and bafilomycin treated donor cells. With experiments assessing EV transfer, the same volume of EVs was given to recipient cells from untreated or bafilomycin treated donor cells.

Recipient cells were incubated with donor EVs for 12 hours, as we found this to be the optimal time to visualize EVs in the recipient cells by IFC in this paradigm. Recipient cells were trypsinized gently and resuspended in PBS (137mM NaCl, 2.7mM KCl, 10mM Na_2HPO_4, 1.8mM KH_2PO_4, pH 7.4). The recipient cells were analyzed by IFC.

After IFC analysis, recipient cells were diluted in an equal volume of PBS with protease inhibitors (Roche) and sonicated. ELISA was performed on recipient cells and donor cell-derived EVs.

2.22 Determination of Protein Prenylation in Cell Lysates

To assess protein prenylation in cells, both GDI extraction and Triton phase separation were performed.

The GDI extraction was performed as previously published (Mohamed et al., 2012). Cells were harvested in GDI capture buffer (75mM potassium acetate, 30mM HEPES, 5mM MgCl2, pH 7.4) with EDTA-free protease inhibitor tablets (Roche) and cells were lysed by sonication. Lysates were cleared of cell debris by centrifugation at 13,000xg for 10 minutes at 4°C and a protein assay was performed. Each sample was separated into 'input' and 'extract' samples, with extracts containing 5x the amount of protein (5µg for input, 25µg for extract). Extract samples were diluted in four volumes of GDI reaction buffer (75mM potassium acetate, 30mM HEPES, 5mM MgCl2, 100µM ATP, 500µM GDP) containing 100µM Rab GDI-GST protein and incubated at 30°C for 20 minutes in a water bath with shaking. Washed Glutathione-Sepharose 4B beads (GE Healthcare) were added to samples and incubated overnight at 4°C with end-over-end rotation. Beads were washed three times to ensure the removal of non-specific binding, then beads boiled in 2× sample buffer (120mM Tris, 50% glycerol, 4% SDS, 10% 2-Mercaptoethanol, 0.2% bromophenol blue, pH 6.8) for 10 minutes to recover prenylated proteins bound to GDI. Extract samples were loaded alongside corresponding input samples. Inputs will contain both prenylated and unprenylated Rabs, whereas the extracts contain a representative sample of the prenylated Rabs. The

prenylated proteins migrate faster than unprenylated proteins, therefore the top and bottom band represent prenylated and unprenylated proteins respectively (Mohamed et al., 2012).

The triton phase separation was performed in reference to a previously described protocol (Bordier, 1981). Cells were harvested in Tris buffer (150mM NaCl, 20mM Tris, pH 7.5) with protease inhibitors, lysates cleared by centrifugation (13,000×g, 10 minutes at 4°C) and a protein assay performed. A small volume (~1µL) of DiI was added to 5% Triton X-114 to 'dye' the detergent and facilitate separation in subsequent steps. The samples were normalized to obtain the same amount of protein and volumes adjusted with Tris buffer. The DiI 'labeled' Triton X-114 was added to normalized cell lysate samples at a final concentration of 2%. Samples were incubated on ice for 30 minutes, then at 37°C for 10 minutes to induce phase separation. Next, samples were centrifuged at 16,000×g for 5 minutes at room temperature. Carefully, the aqueous phase (supernatant) was separated into a new eppendorf tube, leaving the detergent-rich pellet, which was coloured pink from the DiI. Samples were washed once with 2% triton added to the aqueous phase, and Tris buffer to the detergent phase. Samples were incubated at 37°C for 10 minutes, centrifuged again at 16,000×g for 5 minutes, and aqueous and detergent phases separated. The aqueous and detergent phases were pooled from each separation. Immunoblot was performed in the aqueous and detergent phases for Rab7 (1:1000) (Sigma, R8779) diluted in 5% blocking buffer. The detergent phase contained prenylated Rabs and the aqueous unprenylated Rabs. Unprenylated Rabs will run at a higher molecular weight than prenylated Rabs. In parallel, we blotted for heat shock protein 90 (HSP90) (1:1000) (ADI-SPA-846-D, Enzo

Life Sciences) and voltage-dependent anion-selective channel 1 (VDAC1) (1:1000) (MABN504, Millipore Sigma) diluted in 5% BSA to determine the separation efficiency (these proteins should exclusively be in the aqueous and detergent phases respectively).

2.23 Statistics

Statistics were performed in Graphpad PRISM. Paired analyses were performed with paired t-test. With multiple comparisons, one-way ANOVA was applied with Tukey multiple comparisons *post hoc* test. With multiple comparisons comparing to a control group, one-way ANOVA was applied with Dunnet multiple comparisons *post hoc* test. With multiple comparisons comparing multiple variables, two-way ANOVA with Bonferroni *post hoc* test was used. Statistical significance was determined at *$p<0.05$, **$p<0.01$ and ***$p<0.001$.

Chapter 3

Methods for Separation and Analysis of EVs Released by Cultured Cells

3.1 Introduction

Our first goal was to determine the most appropriate EV nomenclature, methods of separation and methods of analysis based on the purpose of our experiments. Inconsistent adoption of EV nomenclature has hampered generalizability of findings across disciplines (Gould and Raposo, 2013). Secreted vesicles have been defined by their cellular origins (Johnstone et al., 1987; Simons and Raposo, 2009), empirically by density, or speed at which they sediment (Thery et al., 2006; Thery et al., 2009), or as vesicles that may have physiological relevance (Trams et al., 1981). We adhere to the International Society for Extracellular Vesicles (ISEV) proposed Minimal Information for Studies of Extracellular Vesicles ("MISEV") guidelines (Thery et al., 2018). The guidelines suggest that "unless authors can establish specific markers of subcellular origin that are reliable within their experimental system(s), authors are urged to consider use of operational terms for EV subtypes that refer to physical characteristics of EVs, such as size ("small EVs" (sEVs) and "medium/large EVs"(m/lEVs))" with ranges defined in each particular case (Thery et al., 2018).

The studies presented here focus on EVs released by cells in culture. We aimed to determine the best conditions for a) cell culture during EV collection (conditioning media), b) EV separation (for subsequent analysis of regulation of EV secretion as well as EV uptake by recipient cells), and c) EV analysis.

The majority of cells are cultured in media supplemented with fetal bovine serum (FBS), which contains significant amounts of EVs (Benz and Moses, 1974; Eitan et al., 2015; Shelke et al., 2014). EVs present in FBS are co-isolated with cell-derived EVs and therefore act as contaminants that may alter the dependability of certain analysis,

as serum-derived EVs are similar to cell-derived EVs. In addition, serum-derived EVs have substantial effects on cultured cells, altering cell phenotype and introducing artefacts in experimental results, such as confounding the RNA profiling of EVs (Shelke et al., 2014; Tosar et al., 2017; Wei et al., 2016). To prevent the effect of serum-derived EVs, two alternatives have been proposed for collecting cell-derived EVs: to use medium prepared with EV depleted-serum or to use serum-free medium. Depletion of EVs from serum is difficult to achieve (Lehrich et al., 2018; Wei et al., 2016). Moreover, depleting EVs from serum may alter cell proliferation and differentiation of cultured cells (Aswad et al., 2016). With respect to culturing cells in serum-free media, this approach will ensure the absence of EVs from sources other than the cells, however the caveat is the potential of altering EV production by switching to a nutrient poor medium during EV collection (Li et al., 2015). More importantly, some cells may not tolerate serum-free media and may undergo apoptosis (Sato et al., 1994). Culturing cells with the addition of supplements (i.e., N2 or B27) may ameliorate the effects of serum-free media. Therefore, identifying the most appropriate medium to collect EVs without compromising cell viability was a critical first step to study EV secretion.

Several methods have been proposed and used to separate EVs from conditioned media, namely UC, iodixanol flotation gradients and SEC, among others (Lobb et al., 2015). Each of these methods has its own benefits and drawbacks; there is no perfect method for all applications and the experimental goal must be considered in deciding which method to employ. The two main goals of our studies focus on the regulation of EV secretion by donor cells and the regulation of EV uptake/internalization by recipient cells. Although separation of EVs from free protein is necessary to delineate the effects

of EVs in isolation when incubated with recipient cells, complete separation of EVs from conditioned media may not be required for analysis of the regulation of EV secretion if EVs can be labeled reliably. With that in mind, we tested the suitability of two methods of EV separation: UC, as it is the most widely utilized method (Konoshenko et al., 2018), and SEC that allows the separation of a more defined EV population (Lobb et al., 2015). For the analysis of the EV samples we considered the yield of vesicles, the elimination of free, non- vesicular proteins and the compatibility of the resulting EV suspension with recipient cells. We analyzed EVs by IFC, NTA and TEM.

3.2 Results

3.2.1 EVs labeling

We require fluorescently labeled EVs in order to apply IFC analysis. In previous work, EVs have been labeled in vitro after separation (Danzer et al., 2012), however this strategy entails the separation of labeled EVs from the free label which presents several complications and subsequent steps. EV floatation up a sucrose gradient was demonstrated as necessary to remove unbound dye from the labeled EV preparation whereas simply washing separated EVs and sedimentation by ultracentrifugation was insufficient (van der Vlist et al., 2012). To avoid the need to separate fluorescent EVs from unbound dye, we opted for labeling the parental cells, which results in the release of fluorescently labeled vesicles. This strategy has been used before with disappointing results when using cytoplasmic dyes, such as calcein and 5,6-carboxy-succinimidyl-fluoresceine ester (CFSE) or expressing fluorescent proteins (van der Vlist et al., 2012). We use the fluorescent lipophilic cationic indocarbocyanine dye DiI. First, we ensured cells and EVs were sufficiently labeled. Microscopy and IFC analysis indicated that

99.9% of cells were labeled with DiI (**Figure 12A-C**), and 95.8% of the EVs were DiI positive (**Figure 13A-B**). The vast majority (98.8%) of DiI positive EVs were detected as single events by IFC (**Figure 13C-D**). Based on these data, EVs were labeled with DiI for all experiments presented here unless specifically indicated.

3.2.2 Selection of Culture Medium for EV Collection

Next, we selected the culture medium that allows collection of EVs without contaminations (e.g. from serum) while preventing cell death. We compared several EV collection media, namely OptiMEM:DMEM (1:1) supplemented with EV-depleted serum (EVd), serum-free OptiMEM:DMEM (1:1) supplemented with B27 (B27), serum-free OptiMEM:DMEM (1:1) supplemented with N2 (N2), or serum-free OptiMEM alone (Opti). The EV collection period was set to 24 hours.

First, we tested if cells undergo apoptosis when cultured in the different media. Analysis of cleaved caspase 3 indicated that cells cultured in any of the media tested did not undergo apoptosis in 24h (**Figure 14A**). Second, we determined changes in autophagy, since the lack of serum in culture media can cause cell autophagy activation if the nutritional requirements of the cells are not fulfilled. Autophagy activation in turn may alter EV secretion. We examined the status of the autophagy reporter LC3II. LC3II is a lipidated protein attached to the autophagosome membrane during the expansion phase of autophagy. When quantifying LC3II, ratios are calculated over actin, or other housekeeping protein as opposed to over LC3I, as the conversion of LC3I and LC3II do not have a direct precursor to product relationship and LC3I is unstable in some cells (Klionsky et al., 2012).

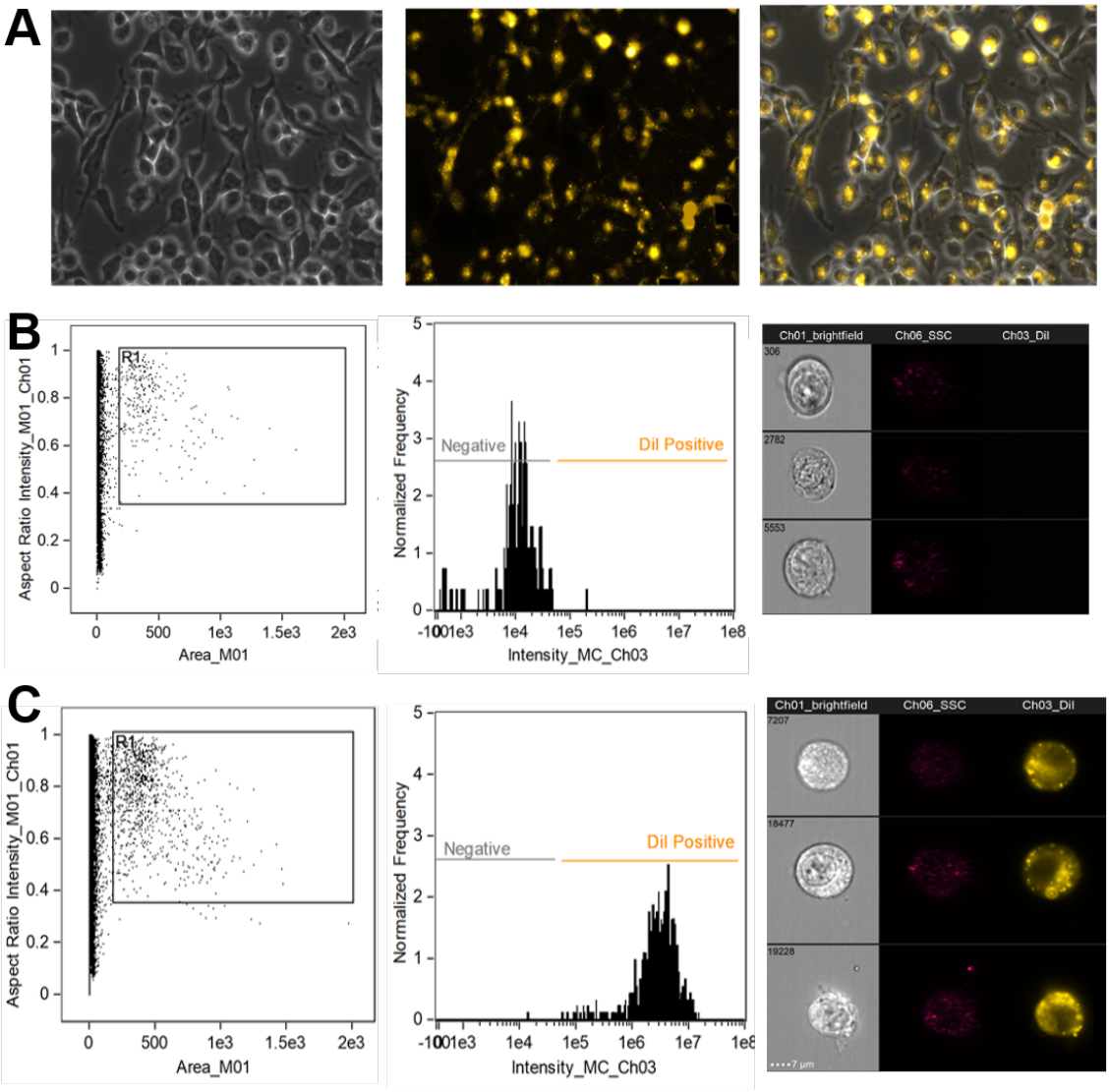

Figure 12. DiI effectively labels cells in culture. N2a cells were labeled with DiI as indicated in the Material and Methods section and examined 48hr after, at the end of the EV collection period. **(A)** Cells were visualized under fluorescence and phase contrast microscopy. **(B, C)** Cells were analyzed by IFC. **(B)** Gating of negative cells to determine background in DiI channel. **(C)** Labeled cells are 99.9% positive for DiI. Representative dotplots and images taken from one experiment, n=3.

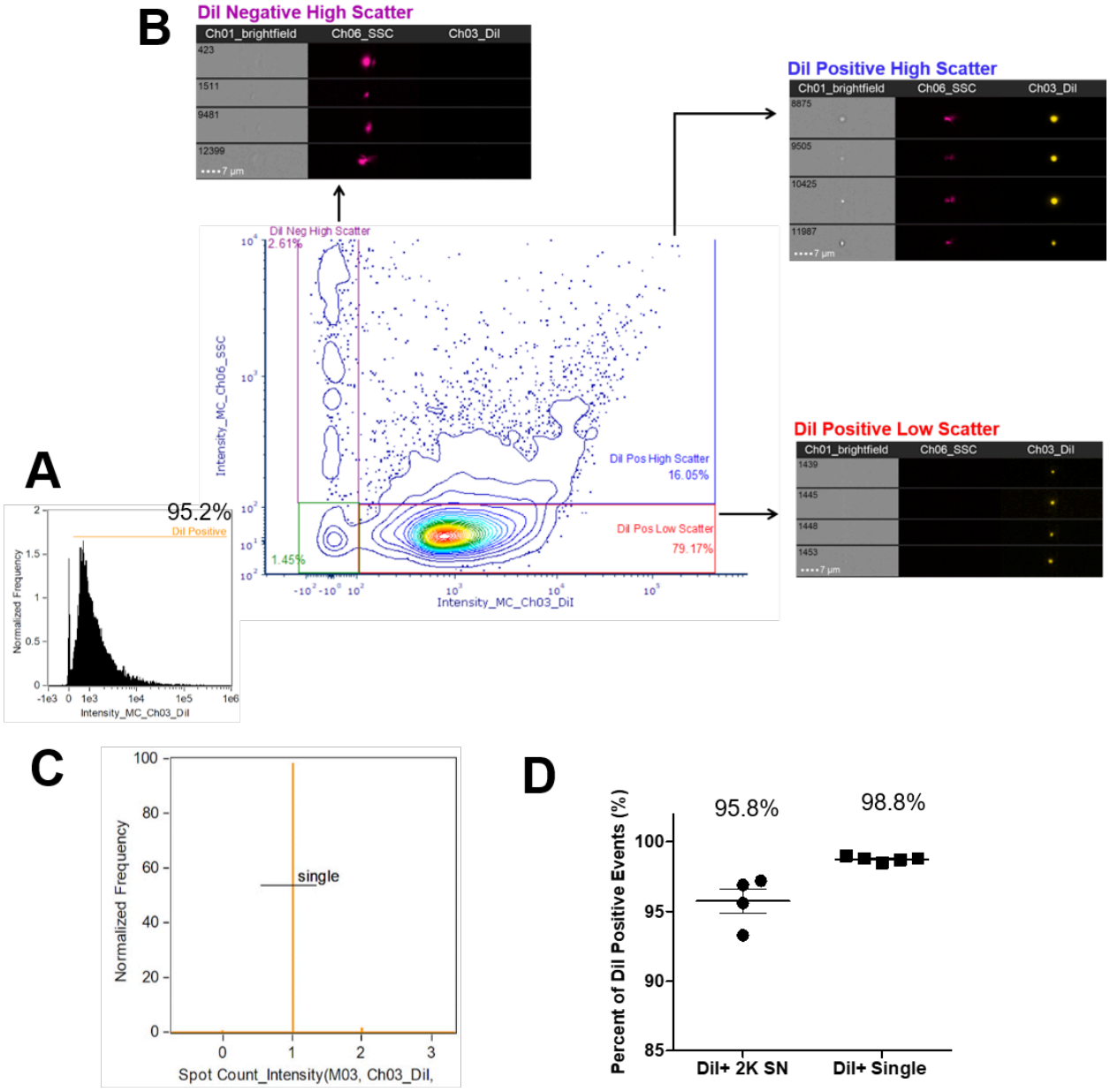

Figure 13. *Figure legend on next page*

Figure 13. The majority of EVs are labeled with DiI and detected as single particles (A) Representative gating of DiI positive events of the supernatant of the 2000xg centrifugation (2K SN). This sample contains EVs. **(B)** Contour plot of a representative 2K SN in N2a untreated cells. Images from each gate represent DiI positive low scatter (red, 79.17% of events), DiI positive high scatter (blue, 16.05% of events) and DiI negative high scatter (purple, 2.61% of events). Events that are negative for DiI and side scatter represent 1.45% of all detected events. **(C)** Determination of single DiI positive events by IFC based on spot count function in the DiI channel. **(D)** Combined experiments to show the percent of DiI positive events in the product of the 2000xg centrifugation (DiI+ 2K SN), which corresponds to DiI positive low scatter and DiI positive high scatter gates in (B) (red and blue), and of the percent of DiI positive EVs that are single events (DiI+ single), corresponding to the graph in (C) for EVs that appear as single events in the spot count for DiI. Mean for each group is listed above the data set. Results are expressed as mean±SEM. n=4-5.

The levels of LC3II were lower in cells cultured in media containing N2 or B27 supplement than those found in cells cultured with EV-depleted serum. Conversely the levels of LC3II present in cells cultured in OptiMEM alone were closer to those in N2a cells treated with the autophagy blocker bafilomycin (**Figure 14B-C**). No gross morphological changes were seen in cells cultured in the different media with the exception of cells in OptiMEM, which had more projections and were more rounded (**Figure 14D**).

We also established if the media formulation affects EV secretion. For that purpose, we followed the protocol depicted in **Figure 15A**. The levels of EVs (as determined by DiI fluorescence) present in concentrated conditioned media (retentate) was similar for the EVd and N2 supplemented media, however conditioning in all other media resulted in a significant reduction of EV secretion (**Figure 15B**). The retentates were then separated using iodixanol density gradients. Analysis of DiI-labeled EVs in fractions collected from the iodixanol gradient showed a similar profile for media without serum (N2, Opti and B27) with the peak in the fraction corresponding to a density of 1.013g/ml. The medium containing EV-depleted serum (EVd) provided a broader peak, with densities between 1.013g/ml and 1.027g/mL (**Figure 15C**). Total EV secretion, as calculated by the area under the curve of DiI fluorescence, followed the same pattern than DiI fluorescence in retentate, that is, it was reduced for OptiMEM and B27 supplemented media whereas N2 medium closely resembled EVd medium (**Figure 15D**).

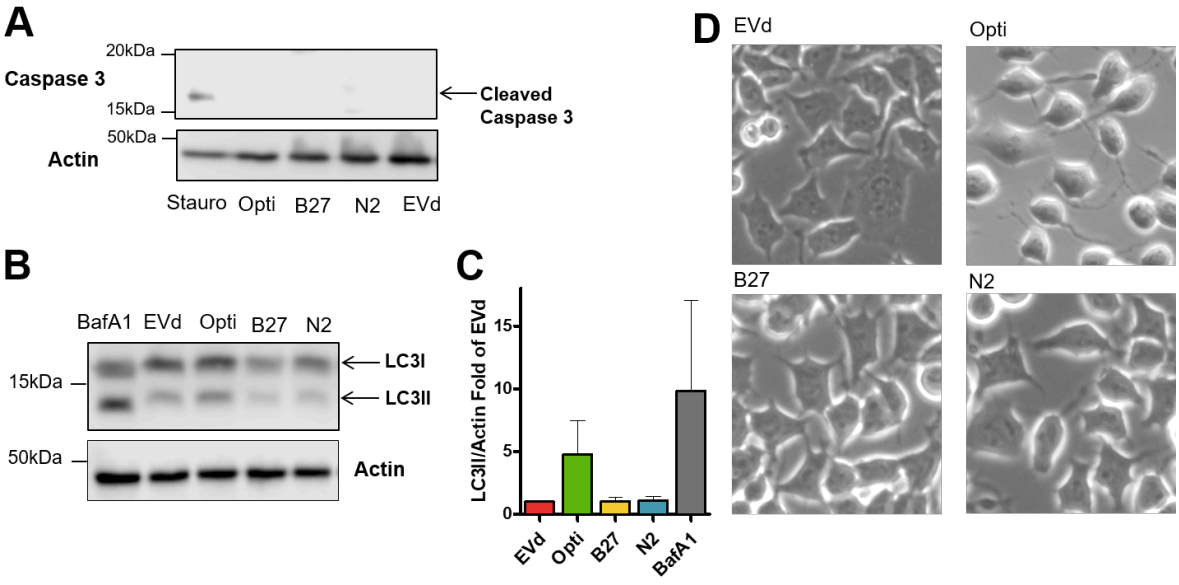

Figure 14. Effect of EV collection media on cell viability. N2a cells were cultured in the following media for 24 hours for EV collection: OptiMEM alone (Opti), OptiMEM:DMEM 1:1 with B27 supplement (B27), OptiMEM:DMEM 1:1 with N2 supplement (N2) or OptiMEM:DMEM 1:1 with 10% EV-depleted serum (EVd). **(A)** caspase 3 cleavage was examined by western blot analysis. Some cells were treated with 10µM Staurosporine (Stauro) for 4 hours as a positive control. **(B)** LC3 was detected by western blot. Some cells were treated with 150nM bafilomycin (BafA1) for 4 hours as a positive control. **(C)** LC3II normalized over actin expressed as fold of EVd, n=2. *Replicate performed by Sarah Samuelson*. **(D)** Cells were visualized by phase contrast microscopy.

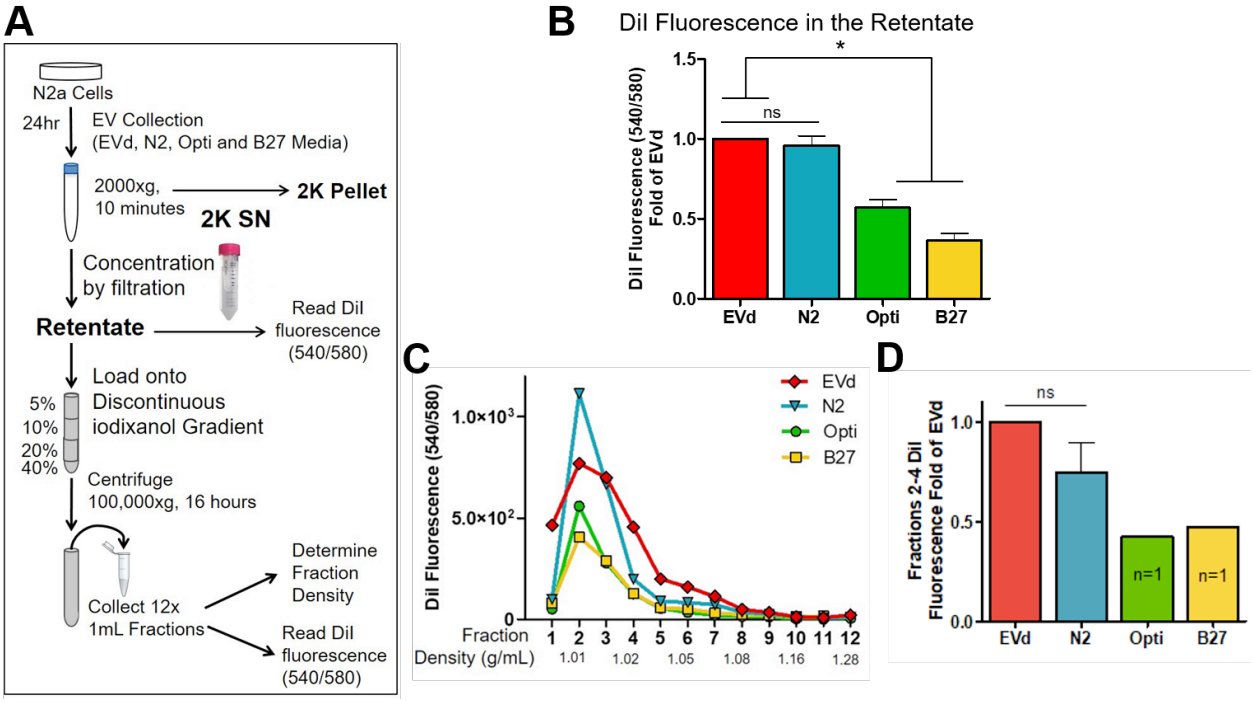

Figure 15. Effect of collection media on EV secretion (A) Scheme of EV separation by iodixanol gradient centrifugation. **(B)** DiI fluorescence was measured in the retentates of each conditioned media. All samples were normalized to the total protein determined in the cell lysates and the results were expressed as fold of DiI fluorescence in EVs collected with media containing EV-depleted serum (EVd). The results represent mean±SEM. n=3. Significance was calculated by one-way ANOVA with Dunnett *post hoc* test compared to EVd. *p<0.05 **(C)** The retentates were separated by iodixanol density gradient centrifugation. Fractions were analyzed by measuring DiI fluorescence (results were normalized to cellular protein content in µg). One representative experiment out of 3 is depicted. **(D)** The total fluorescence of EVs with density between 1.01g/mL and 1.02g/mL (peak) was determined by calculating the area under the curve. Results were expressed as fold of EVd and represent as mean±SEM, n=3. Significance was determined by paired t test for comparing EVd and N2.

The experiments presented above indicated that EVd and N2 media were equally suited to collect EVs produced by N2a cells when taking in consideration cell viability and EV production. Yet, if EV-depleted serum still contains EVs as indicated previously (Momen-Heravi et al., 2012; Shelke et al., 2014) the use of N2 medium would be favoured. Analysis of N2 and EVd unconditioned media (UCM), therefore media that has not been in contact with cells, by density gradient centrifugation demonstrated the presence of the EV marker CD9 in EVd but not in N2 UCM in fractions with densities that correspond to the EVs from conditioned media. The lipid GM1, which associates with lipoproteins (and other serum proteins) (Harpin et al., 1990), was present in EVd but not in N2 UCM (**Figure 16A**). Moreover, we found there were approximately 13-fold more particles in EVd than N2 UCM as enumerated by NTA (**Figure 16B**).

Overall, we determined that media supplemented with N2 is the most appropriate for culturing the cells during the EV collection period as it results in similar EV secretion as EVd, provides EVs with the expected profile by iodixanol density gradient centrifugation, and does not contain EVs before conditioning.

3.2.3 Methods of EV Separation and Analysis

We aimed to select methods for EV separation and analysis best suited to study EV secretion by donor cells and EV effects on recipient cells. For the selection we considered the following outcomes: vesicle quality, yield, successful separation of EVs from free protein and compatibility of the EV preparation (suspension buffer) with recipient cells.

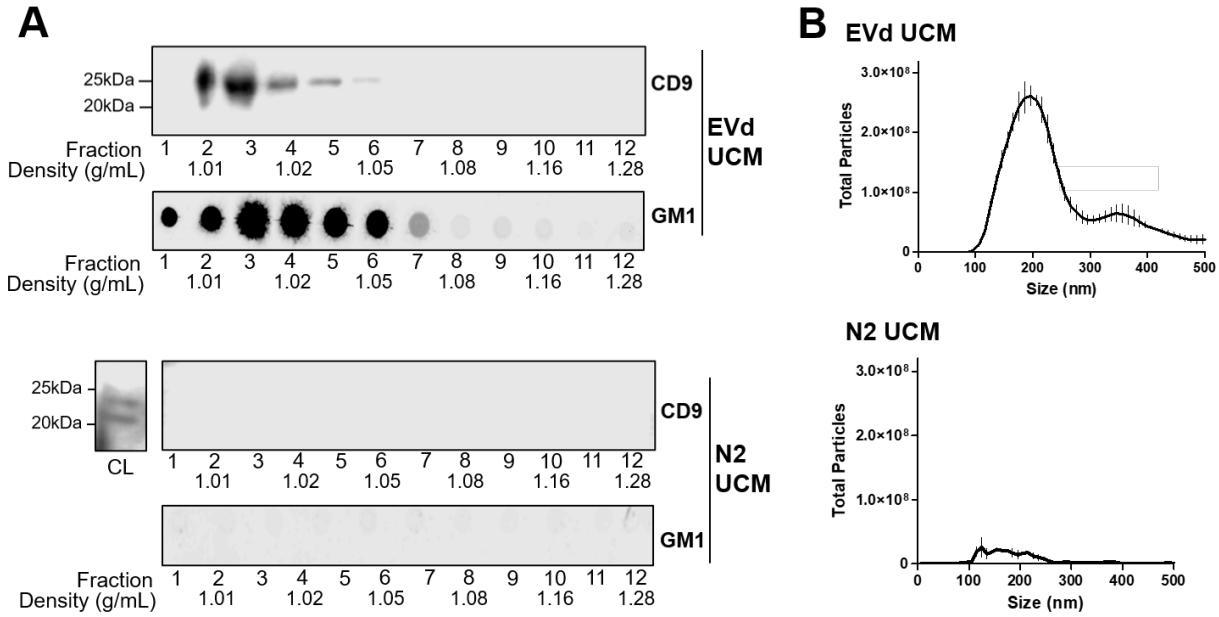

Figure 16. Analysis of unconditioned media (A) UCM of OptiMEM:DMEM (1:1) supplemented with either N2 (N2) or EV-depleted serum (EVd) were separated using iodixanol gradient centrifugation. Fractions were analyzed by Western blot (top panels) with an antibody against the EV marker CD9 and by dotblot to detect GM1 (bottom panels). N2a cell lysates (CL) were blotted as a positive control to confirm the detection of CD9 in the blot. **(B)** UCM of OptiMEM:DMEM (1:1) supplemented with either N2 (N2) or EV depleted serum (EVd) were analyzed by NTA.

We used two widely employed methods of EV separation, namely UC (Thery et al., 2006) and SEC with qEV columns (Greening et al., 2015). EVs separated by these two methods were analyzed by IFC and NTA.

The most common method to separate EVs is by UC, whereby three samples are obtained: the supernatant of the initial centrifugation at 2000xg that has been depleted of cell debris and apoptotic bodies (2K SN), the supernatant from the 100,000xg centrifugation (100K SN) and the 100K Pellet as the final product (**Figure 17A**). TEM of EVs separated in the 100K Pellet demonstrated the characteristic cup-shape morphology of EVs we anticipated employing this technique; an artefact that results from desiccated vesicle collapse (Raposo and Stoorvogel, 2013). More importantly, TEM revealed profound aggregation of EVs by UC, as has been reported (**Figure 17B**) (Fevrier and Raposo, 2004).

All samples, 2K SN, 100K SN and 100K Pellet, were analyzed by IFC and NTA. Both methods demonstrated a substantial loss of EVs in the 100K Pellet compared to the 2K SN (recovery of 9.34 $\pm$2.07% and 4.39 $\pm$1.57% by IFC and NTA respectively). In accordance, a significant portion of EVs remained in 100K SN, indicative of inefficient pelleting upon centrifugation (**Figure 17C**).

Analysis of particle size and concentration by NTA indicated similar proportions of small EVs (<150nm) and large EVs (>150nm) in 2K SN, 100K SN and 100K Pellet (**Figure 18A-D**).

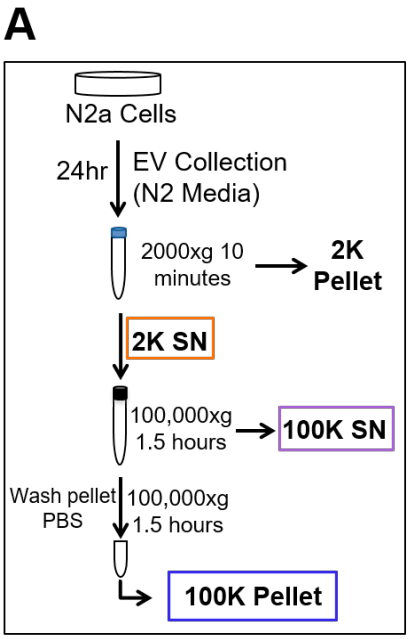

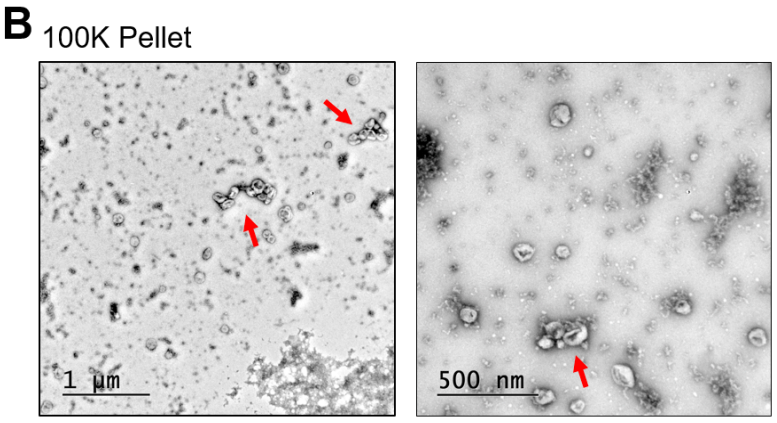

C

	IFC Total particles	IFC Particles Percent of Total	NTA Total particles	NTA Particles Percent of Total
2K SN	$4.95\pm1.14\times10^{6}$	100.00	$1.60\pm0.573\times10^{10}$	100.00
100K SN	$2.18\pm0.573\times10^{6}$ ***	43.29 ± 1.79 ***	$7.42\pm1.76\times10^{9}$ ns	48.05 ± 11.58 ***
100K Pellet	$5.02\pm0.097\times10^{5}$ ***	9.34 ± 2.07 ***	$6.58\pm1.29\times10^{8}$ **	4.39 ± 1.57 ***

Figure 17. Differential ultracentrifugation reduces yield of particles and causes EV aggregation (A) Scheme of classical UC method. **(B)** TEM microphotographs of 100K Pellet at two different magnifications. The red arrows show aggregated EVs. **(C)** Table of the number of particles and percent yield for EVs separated by UC using IFC and NTA. Values were normalized to mass of cellular protein (mg). The experiments were repeated 3 times for NTA and 6 times for IFC. Values are expressed as mean±SEM. Statistics were calculated by one-way ANOVA with Dunnet *post hoc* test compared to 2K SN. *p<0.05, **p<0.01.

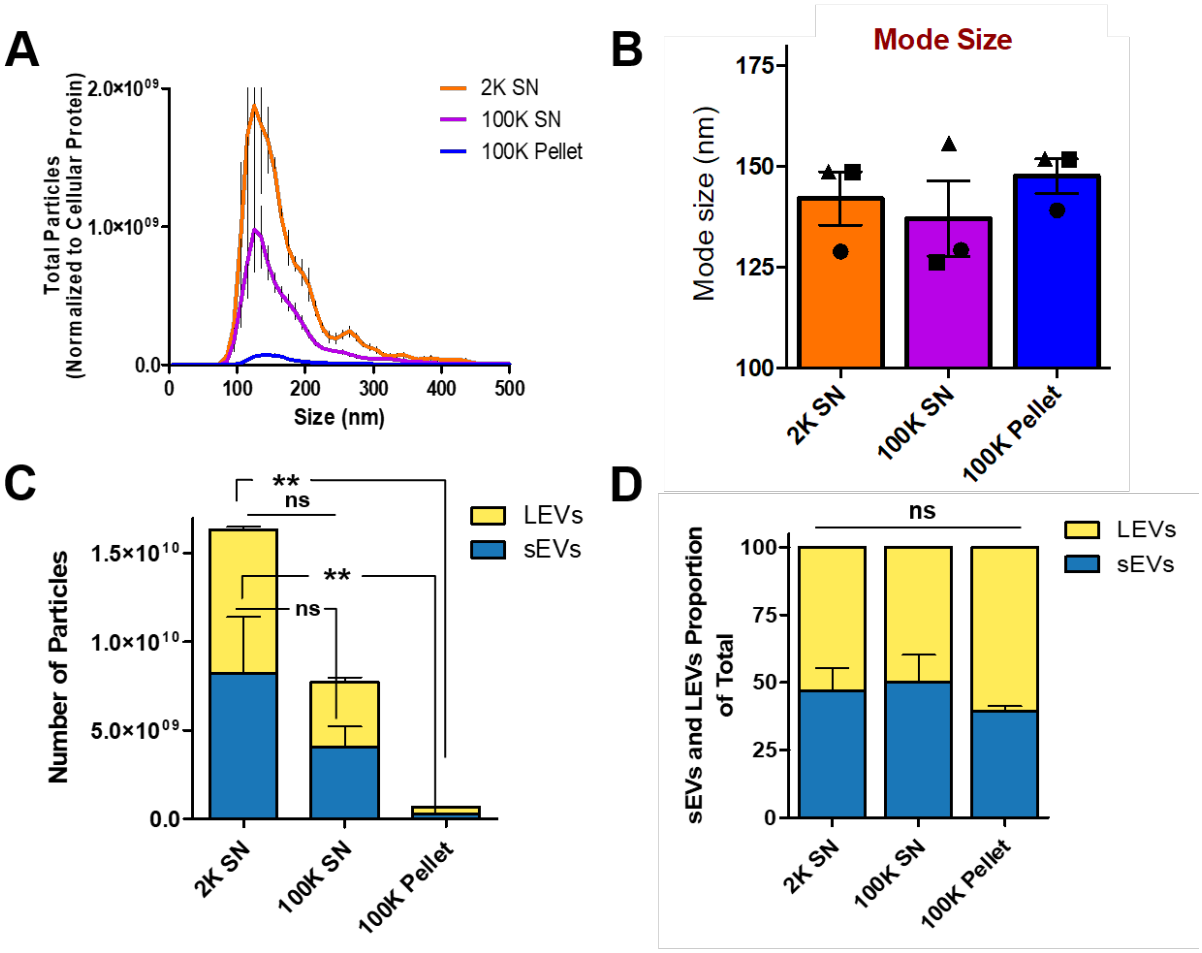

Figure 18. Differential ultracentrifugation reduces the yield of both small and large EVs (A) NTA profile of EVs separated by UC. **(B)** Mode size of the total particles tracked by NTA. **(C)** Total particles were separated into bins denoting small EVs (sEVs, 1-150nm; blue portion) and large EVs (LEVs, 151-500nm; yellow portion). **(D)** The proportion of small and large EVs for each sample was calculated by dividing the number of small or large EVs over the total EVs tracked by NTA within that group. Results are expressed as mean±SEM. n=3. Statistics were calculated by two-way ANOVA with Bonferroni *post hoc* test compared to the 2K SN. *p<0.05, **p<0.01.

We next separated EVs by SEC with qEV columns according to the scheme depicted in **Figure 19A.** TEM of EVs separated in the peak of the qEV column (SEC peak) showed the characteristic cup-shape morphology of EVs and, contrary to EVs separated by UC, there were no apparent signs of EV aggregation (**Figure 19B**). We next analyzed the 2K SN, the retentate, and the SEC peak by IFC and NTA. Both methods demonstrated a significant loss of EVs during the concentration step of the 2K SN. The recovery of EVs in retentate was 25.92 $\pm$1.90% and 51.57$\pm$17.45% as determined by IFC and NTA respectively. Moreover, the recovery of EVs in the qEV peak was only 47.00$\pm$8.62 and 47.41$\pm$17.00 of the retentate, which overall represents 12.21$\pm$1.75 and 18.55$\pm$2.99 of the 2K SN compared by NTA and IFC respectively (**Figure 19C**). Analysis of EV size distributions by NTA indicated that the proportion of small and large EVs are equivalent for each sample, including the SEC peak (**Figure 20A-D**).

We have used IFC to characterize EV populations based on phenotypic makers, such as CD9 and AnnexinV (**Figure 21A-C**). We found that UC results in a significantly different subpopulations of EVs remaining in the 100K SN compared to the 2K SN, however the distribution of labeled markers within the 100K Pellet was not significantly different than the 2K SN. EVs separated in the SEC peak matched the 100K SN in the enrichment of CD9 positive EVs (**Figure 22A-B**). Further, the data suggest that EVs labeled with DiI only and those labeled with DiI and AnnexinV are selectively lost during SEC (**Figure 22C**).

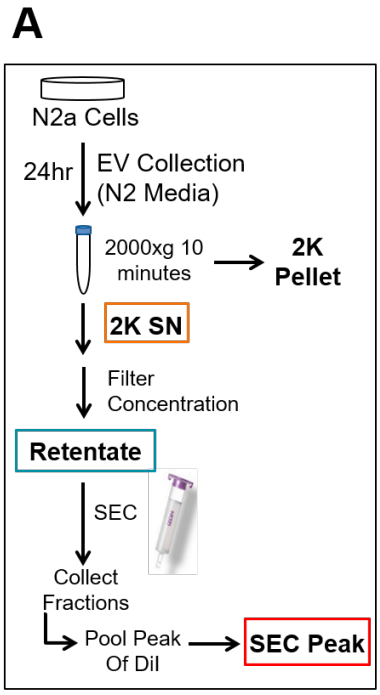

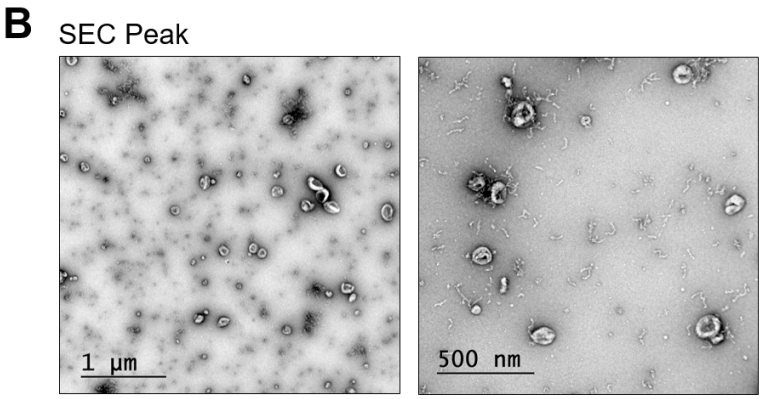

C

	IFC Total particles	IFC Particles Percent of Total	NTA Total particles	NTA Particles Percent of Total
2K SN	$4.95\pm1.14\times10^{6}$	100.00	$1.60\pm0.331\times10^{10}$	100.00
Retentate	$1.24\pm0.219\times10^{6}$ *	25.92±1.90 ***	$9.40\pm5.04\times10^{9}$ ns	51.57±17.45 ***
SEC peak	$5.72\pm0.096\times10^{5}$ ***	12.21±1.75 ***	$2.78\pm0.065\times10^{9}$ *	18.55±2.99 ***

	IFC Particles Percent of Total	NTA Particles Percent of Total
Retentate	100	100
SEC peak	47.00±8.62 **	47.41±17.0 ns

Figure 19. SEC reduces yield of particles yet separates non-aggregated EVs (A) Scheme of SEC method with qEV columns. **(B)** TEM microphotograph of SEC peak at two different magnifications. **(C)** Tables of SEC-separated EVs represented as the total number of particles and yield calculated as the percent of total particles in the 2K SN (top table), OR as a percent of total particles in the retentate (bottom table) using IFC and NTA. Values are normalized to cellular protein (mg). The experiments were repeated 3 times for NTA and for IFC. Values are expressed as mean±SEM. Statistics were calculated by one-way ANOVA with Dunnett *post hoc* test compared 2K SN. *p<0.05,**p<0.01,***p<0.001.

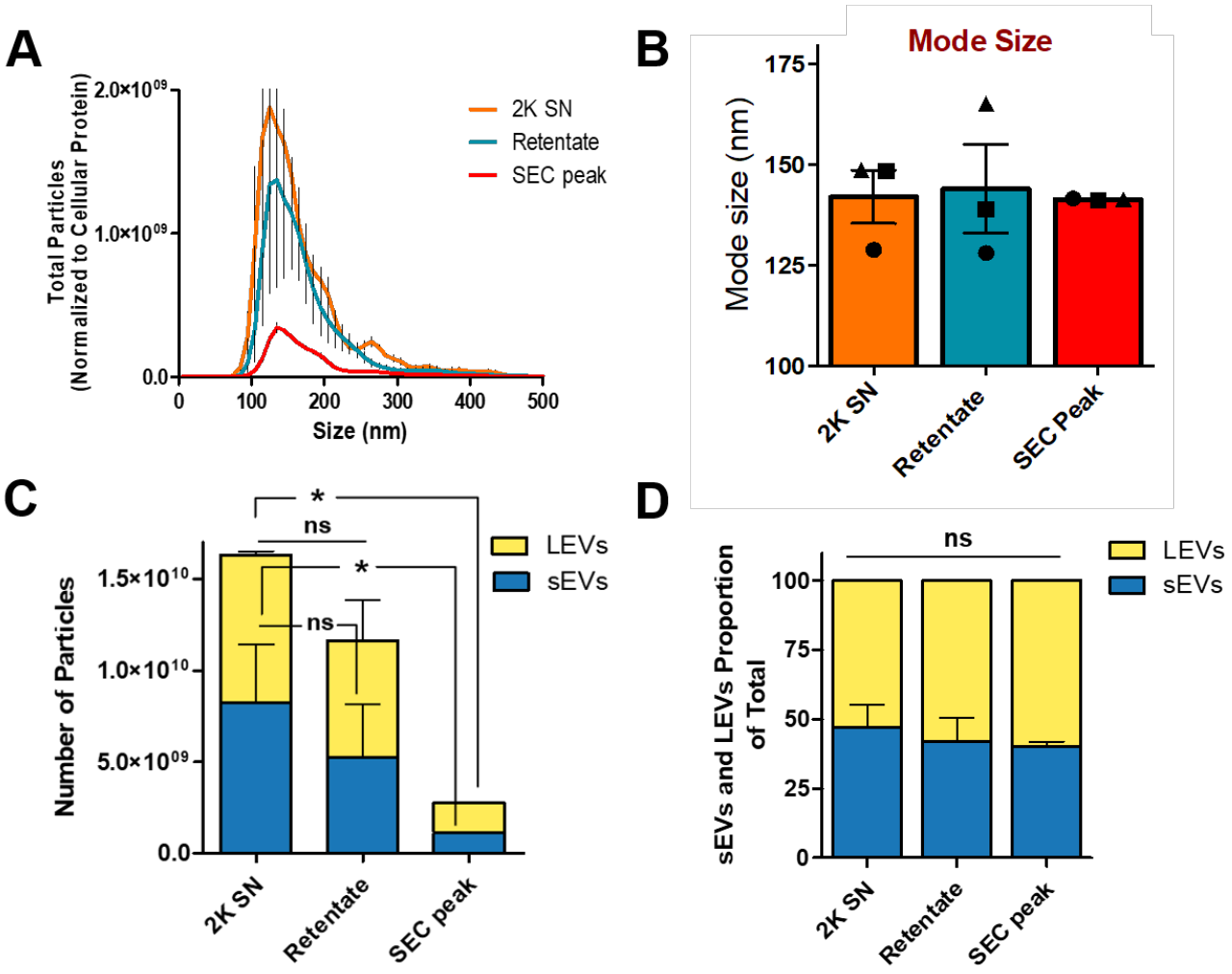

Figure 20. SEC reduces the yield of both small and large EVs (A) NTA profile for EVs separated by SEC**. (B)** Mode size of total particles tracked by NTA. **(C)** Total particles were separated into bins denoting small EVs (sEVs, 1-150nm; blue portion) and large EVs (LEVs, 151-500nm; yellow portion). **(D)** The proportion of small and large EVs for each sample was calculated by dividing either group in the total of particles tracked for each sample. Results are expressed as mean±SEM. n=3. Statistics were calculated by two-way ANOVA with Bonferroni *post hoc* test. *p<0.05, **p<0.01,***p<0.001.

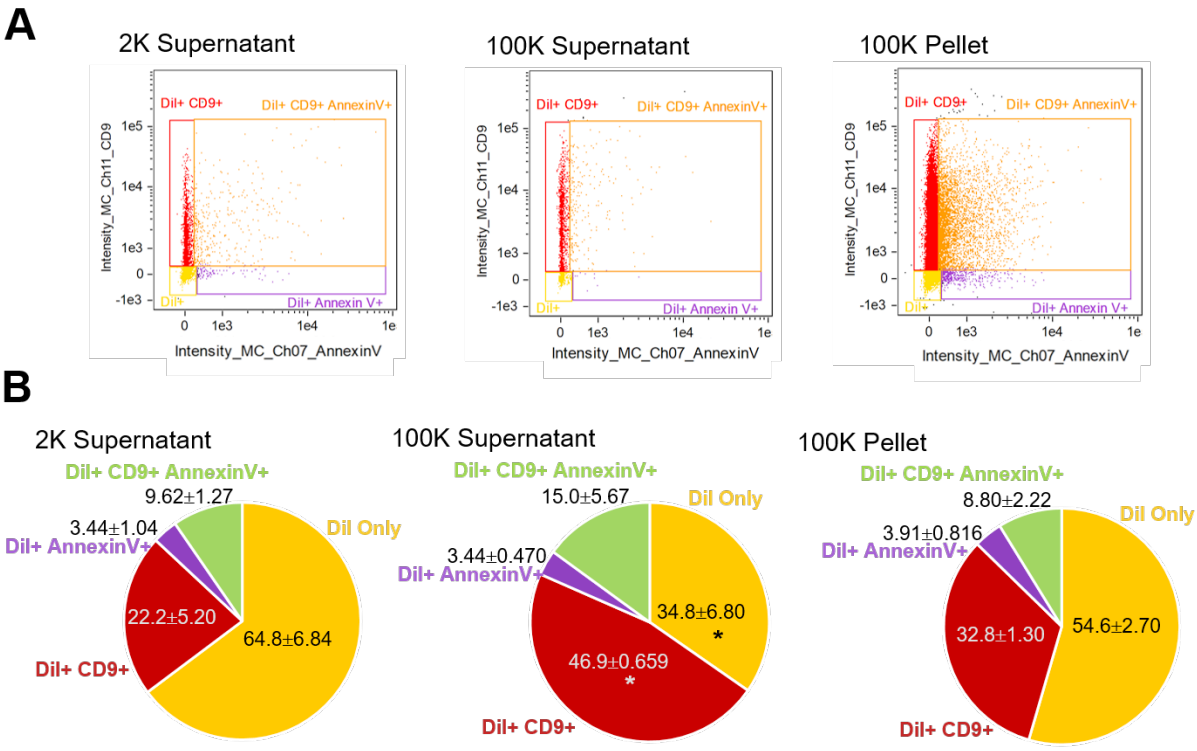

C

	DiI Total	DiI Only	DiI+ CD9+	DiI+ AnnexinV+	DiI+ CD9+ AnnexinV+
2K SN	**100.00**	**100.00**	**100.00**	**100.00**	**100.00**
100K SN	**42.74**±7.69***	**22.36**±1.85***	**75.93**±17.04 ns	**24.75**±9.66***	**57.49**±14.74 *
100K Pellet	**7.11**±2.30 ***	**5.11**±0.76 ***	**10.34**±4.37 **	**4.98**±0.93***	**7.15**±3.10 ***

Figure 21. UC affects EV subtypes separated (A) Representative DotPlots of 2K SN, 100K SN, 100K Pellet obtained by ultracentrifugation of conditioned media from N2a cells. Four different populations were detected: EVs labeled with DiI only (DiI only), EVs labeled with DiI and positive for CD9 (DiI+ CD9+), EVs labeled with DiI and positive for AnnexinV (DiI+ AnnexinV+) and EVs labeled with DiI and positive for CD9 and for AnnexinV (DiI+ CD9+ AnnexinV+). **(B)** Quantification of the proportion of each subtype in the 2K SN, 100K SN and 100K Pellet. Pie charts represent each group as a percent of the total DiI labeled particles detected. Results are expressed as mean±SEM. n=3. Statistics were calculated by one-way ANOVA with Dunnett *post hoc* test compared to 2K SN. *p<0.05. **(C)** Each subtype represented as a percent of the total number of that subtype in the 2K SN. Results expressed as mean±SEM. n=3. Significance was calculated with one-way ANOVA with Dunnett *post hoc* test compared to the 2K SN. *p<0.05, **p<0.01, ***p<0.001.

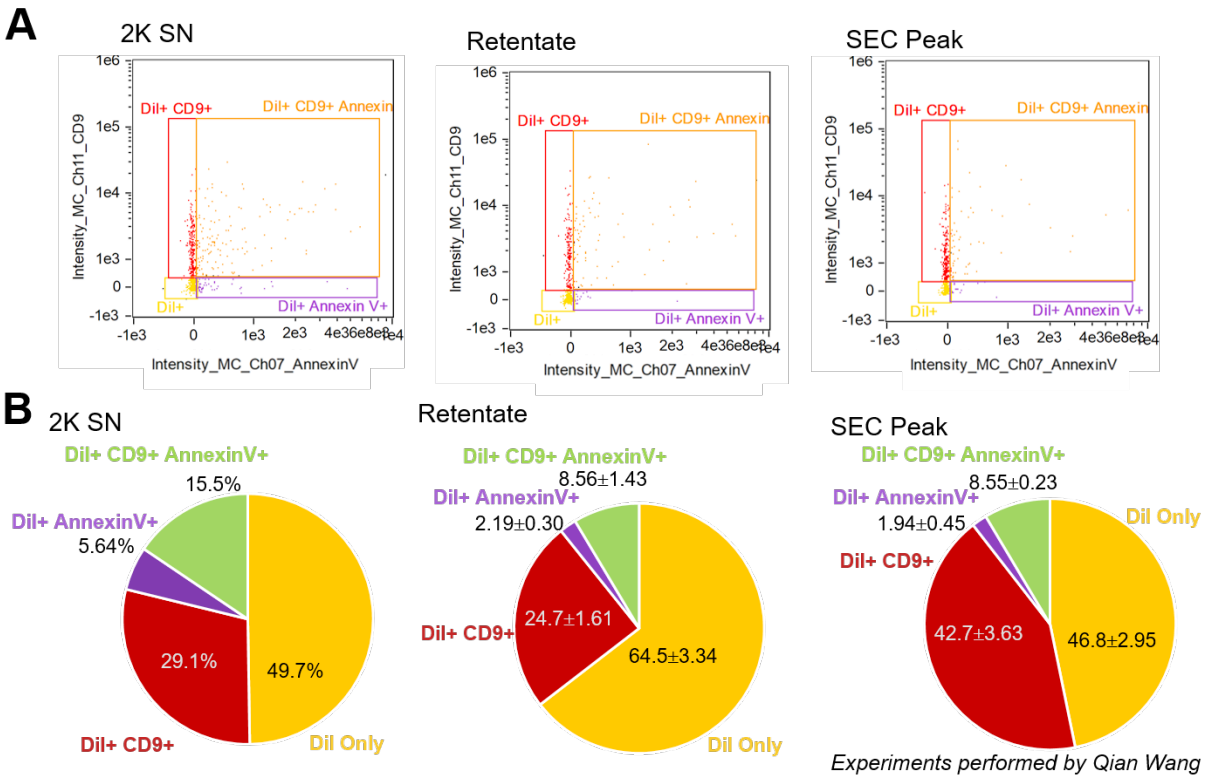

C

	Dil Total	Dil Only	Dil+ CD9+	Dil+ AnnexinV+	Dil+ CD9+ AnnexinV+
Retentate	**100.00**	**100.00**	**100.00**	**100.00**	**100.00**
SEC peak	**60.82**±0.64	**44.51**±4.62	**107.51**±17.04	**52.50**±4.81	**63.93**±9.69

Figure 22. SEC may affect EV subtypes separated (A) Representative DotPlots of the retentate and SEC peak obtained from conditioned media of N2a cells. The 2K SN only corresponds to one experiment. Four different populations were detected: EVs labeled with DiI only (DiI only), EVs labeled with DiI and positive for CD9 (DiI+ CD9+), EVs labeled with DiI and positive for AnnexinV (DiI+ AnnexinV+) and EVs labeled with DiI and positive for CD9 and for AnnexinV (DiI+ CD9+ AnnexinV+). **(B)** Quantification of the proportion of each subtype in the 2K SN, retentate and SEC peak. Pie charts represent each group as a percent of the total DiI labeled particles detected. Results are expressed as mean±SEM. n=1-2. **(C)** Each subtype represented as a percent of the total number of that subtype in the retentate. Results expressed as mean±SEM. n=2.

3.3 Discussion

Separation and analysis of EV released by cultured cells require the use of a suitable EV collection medium and EV separation technique.

Previous reports indicated that the medium used during the EV collection period might alter cell survival as well as the quantity and protein composition of cell-derived EVs (Aswad et al., 2016; Eitan et al., 2015; Li et al., 2015). Cells are usually cultured in the presence of serum, which is needed to promote cell attachment, cell growth, and cell proliferation. However, serum provides EVs and non-EV components that may be detected during EV analysis (Coumans et al., 2017). To mitigate this problem, the use of serum depleted of EVs has been proposed (Coumans et al., 2017; Driedonks et al., 2019; Shelke et al., 2014). In some cases, EV-depleted serum may not fully support cell growth and viability (Aswad et al., 2016; Eitan et al., 2015). Moreover, the ultracentrifugation method employed may not sufficiently deplete EVs from serum (Driedonks et al., 2019; Shelke et al., 2014). Our results confirmed the presence of particles with a density corresponding to EVs, and that contain the EV marker CD9 and the lipid GM1 in UCM prepared with EV-depleted serum but not in serum-free medium.

Some cells that are normally grown with serum can survive without serum for a few days, especially if nutritional supplements are added to the medium. We therefore tested different combinations of media and supplements. All media tested supported survival of N2a cells for 24h, which is the duration of the EV collection period in our experiments.

The switch from serum-containing medium to nutrient-poor medium may induce a cell stress response, most probably in the form of autophagy, which in turn

may increase or decrease EV secretion (Abdulrahman et al., 2018; Fader et al., 2008) or may lead to secretion of EV of different composition and/or intracellular origin (Witwer et al., 2013). We found that autophagy was altered in N2a cells grown in OptiMEM alone, but not in the other media. Although our experiments using LC3II as an autophagy reporter cannot differentiate whether autophagy was increased or autophagic flux was impaired, autophagy alterations in any direction should be avoided during the EV collection period.

The quantity of EVs secreted is also affected by the cell culture medium (Li et al., 2015). Based on measurement of DiI fluorescence and separation by density gradients, N2a cells cultured in medium containing N2 supplement secrete the same amount of EVs than N2a cells cultured with EV-depleted serum. On the other hand, OptiMEM alone and medium supplemented with B27 significantly reduced EV release.

Therefore, taking in consideration cell viability, autophagy activation and quantity of EVs, we determined that medium containing N2 supplement was the most suitable for EV collection during the 24 hour conditioning period.

As recognized in the recent guidelines for studies of EVs, the level of EV purity required depends on the experimental question and EV end use (Thery et al., 2018). Our goal was to identify an EV preparation suitable for: (i) analysis of EV secretion and its regulation, and (ii) studies on EVs uptake by recipient cells. For the analysis of EV secretion we aimed to obtain a virtually "unprocessed" sample to minimize common artefacts associated with most EVs separation techniques, such as aggregation of EVs (UC), co-sedimentation of protein aggregates (UC) and separation of a specific population of EVs based on size (SEC) or density (UC) (Coumans et al., 2017). When

separating EVs for performing experiments of uptake by recipient cells, EVs must be separated from soluble proteins and suspended in a medium that would not affect the survival and growth of recipient cells.

Although iodixanol gradients are useful for characterizing EVs, the preparation does not yield material suitable for feeding cells in culture; this protocol cannot be performed in sterile conditions and the iodixanol is toxic at the concentration of EVs required to incubate with recipient cells.

UC, the most common method of EV separation, demonstrated very low yield. A contributing factor to the low yield is the limitation of pelleting based on the sedimentation path length and EV density (Livshits et al., 2015). The relative position of EVs in a sample, thus the distance particles are required to travel within the sample to effectively pellet, determines the vesicles separated and results in co-sedimentation of small and large EVs (Livshits et al., 2015). Further, density of particles will dictate pelleting by ultracentrifugation, thereby vesicles with less than a threshold density will remain in the 100K SN (Livshits et al., 2015). Our data agree with these concepts. Although it has been previously established that the EV yield is affected by centrifugation (Lamparski et al., 2002; Lobb et al., 2015), to our knowledge analysis of the 100K SN specifically, has not been reported. Our data indicate that ultracentrifugation at 100,000xg induces the artificial aggregation of EVs. It has been described before that EVs can aggregate, fuse and fragment during ultracentrifugation (Erdbrugger and Lannigan, 2016) and that aggregation masks antigens on the membrane surface, thus complicating phenotypic analysis of EVs based on markers (Linares et al., 2015). As a result, incorrect conclusions may be drawn if either antigens

are masked, or if steric hindrance of aggregated EVs prevents their cellular uptake. Further, aggregation and co-sedimentation of free proteins with the EV pellet makes this technique unable to separate EVs from proteins (Lamparski et al., 2002). Although the ultracentrifugation pellet can be re-suspended in a cell compatible buffer, the problem of aggregation may result in the separation of EVs that are no longer physiologically relevant.

EV separation using SEC also suffers of low yield. In this case, concentration of the 2K SN by filtration retains a portion of EVs in the filter and decreases yield (Vergauwen et al., 2017). To ameliorate this loss, filters with different pore sizes can be tested and addition of 2% BSA to reduce hydrophobic interactions between EVs and the cellulose membrane (Yamashita et al., 2016) might be useful. SEC is a better choice than ultracentrifugation, as it does not cause EV aggregation, separates disperse EVs without free protein contamination, and EVs are collected in a cell-compatible buffer.

We used two complementary methods to analyze cell-derived EVs, namely IFC and NTA. Although both methods are used to detect the concentration of particles in a sample, NTA detects particle scatter to determine number and size (Filipe et al., 2010), while IFC detects fluorescently labeled nanoparticles with improved sensitivity than classical flow cytometry triggering on scatter (Erdbrugger and Lannigan, 2016).

We found a significant difference in the total number of particles determined by IFC and NTA, being the number found by NTA is several orders of magnitude larger than the EVs enumerated by IFC. A similar difference has been recently reported (Mastoridis et al., 2018). There are few explanations for the discrepancy between the number of EVs measured by IFC and NTA. First, NTA detects non-EV particles such as

large protein aggregates and dust; tracking them as events (Filipe et al., 2010). IFC detects fluorescence, and relies on the sensitivity of the instrument to the fluorophore signal, thus IFC is more likely to underestimate events.

We report here the labeling of EVs by labeling the parental cells with the hydrophobic lipid DiI. We effectively labeled the majority of cells and EVs as detected by IFC. However, the IFC instrument we used is equipped with a laser to excite the DiI fluorophore which is not optimal. In future experiments, we will use a derivative of DiI called DiD, which has a florescence spectrum more compatible with the lasers available.

Despite the differences in absolute number of particles detected by IFC and NTA, they both indicated very poor EV yield using UC and SEC. Estimation of the total number of EVs by IFC and NTA shows UC to separate significantly fewer EVs, which is in agreement with previous reports (Baranyai et al., 2015; Lobb et al., 2015; Mastoridis et al., 2018). Thus, our data demonstrate that IFC can be used to detect reliably changes in the quantity of EVs secreted by cultured cells.

NTA provides information on the mean size and size distribution of the EV population. We found no significant difference in the mode size (and mean size) of EVs in any of the samples analyzed. We also determined if, despite having similar mode sizes, the size distribution within each sample was different. We defined two subpopulations as “small EVs” with sizes from 1nm to 150nm and “large EVs” with sizes from 151nm to 500nm. There was no significant change in the proportion of small or large EVs with any of the samples separated by UC or SEC. In the past, the size of EVs has been used as one parameter to characterize and classify different EV subtypes,

however there is sufficient evidence that different populations of EVs secreted by different cellular mechanisms may have similar sizes (Mastoridis et al., 2018).

IFC allows vesicle-by-vesicle analysis of large populations (Mastoridis et al., 2018). IFC analysis of EVs released by DiI-labeled N2a cells demonstrated that more than 98% of EVs were detected as single vesicles and only less than 5% of EVs with detectable scatter were unlabeled. Multiparametric characterization of EVs was performed with either a fluorophore-conjugated antibody against the tetraspanin protein CD9, or fluorescent probe AnnexinV, which binds to phosphatidylserine. In the unprocessed 2K SN, the majority of EVs (64.8±6.84%) were negative for CD9 and AnnexinV (DiI only) while most of the remaining EVs were labeled with the CD9 antibody either without AnnexinV (DiI+, CD9+; 22.2±5.20%) or together with AnnexinV (DiI+, CD9+, AnnexinV+; 9.62±1.27%). Only a very small proportion of EVs were labeled with AnnexinV but not CD9 (DiI+, AnnexinV+; 3.44±1.04%). The 100K SN was significantly enriched in CD9+ vesicles, while the proportions of EV subtypes in 100K Pellet were not significantly different from 2K SN. Analysis of the recovery of different EV subtypes during ultracentrifugation suggests that vesicles that do not express CD9 (DiI only and DiI+, AnnexinV+) are lost during the ultracentrifugation procedure. A caveat of these experiments is that we purposely followed the most common ultracentrifugation procedure, which includes washing the 100K Pellet with buffer, followed by a second centrifugation at 100,000x g (Thery et al., 2006). The supernatant of this second centrifugation is not included in the analysis.

The retentate was used for comparison to the SEC peak in preliminary experiments. Subtypes in the retentate were not different from the 2K SN, both

compared to the 2K SN within this experiment and to previous results from UC (DiI only 64.5±3.34%; DiI+,CD9+, 24.7±1.61%; DiI+, AnnexinV+, 2.19±0.30%; and DiI+, CD9+, AnnexinV+8.56±1.43%). The SEC peak follows the same pattern of enrichment for CD9+ EVs seen in the 100K SN (42.7±3.63% CD9+).

Originally, CD9 was characterized as an exosomal marker, and PS exposure, therefore AnnexinV binding, as indicative of microvesicles. CD9 was first recognized in exosomes from dendritic cells (Thery et al., 1999). CD9 was found as highly enriched in exosomes, thus considered by some as an exosomes-specific marker (Bobrie et al., 2012; Thery et al., 2002). However, caution was heeded since many tetraspanins are also distributed in the plasma membrane, thus likely to be incorporated in plasma membrane-derived EVs (i.e., microvesicles) (Andreu and Yanez-Mo, 2014). In fact, it was discovered that both small (defined as less than 100nm) and large EVs (defined as greater than 200nm) contain CD9 (Bobrie et al., 2012). Further, a subpopulation of CD9+ EVs was found secreted directly from the plasma membrane with an early endocytic signature (Kowal et al., 2016).

PS exposure was first described in platelet-derived microparticles (we refer to as microvesicles) that consequently bound AnnexinV (Dachary-Prigent et al., 1993; Thiagarajan and Tait, 1991). Limited data for the lipid composition of exosomes was previously available, however, due to the limited binding of AnnexinV, the exposure of PS was considered very low in exosomes (Heijnen et al., 1999; Thery et al., 2002). However, later reviews considered the surface exposure of PS as a feature of both exosomes and microvesicles (Thery et al., 2009). Importantly, the majority of microvesicles derived from platelets were AnnexinV negative (approximately 80%)

(Connor et al., 2010), suggesting a subset of EVs maintain phospholipid asymmetry, thus do not expose PS, assuming no experimental limitation in AnnexinV detection or binding in this study. Therefore, AnnexinV does not label microvesicles exclusively, and a population of microvesicles likely remain unlabeled with AnnexinV.

For a more thorough characterization of EV subtypes, other EV markers could be used such as CD63 and CD81 (Gorgens et al., 2019; Mastoridis et al., 2018), and, based on recent reports, these markers in combination with CD9 would be reasonable confirmation of *bona fide* exosomes based on proteomic data with EVs separated by UC (Kowal et al., 2016). Nevertheless our data, together with previous findings (Mastoridis et al., 2018) demonstrate the value of IFC in the analysis of EV subtypes. This analysis would be of great importance to understand the differential regulation of secretion of specific EVs subtypes by donor cells, as well as preferential uptake by recipient cells.

3.4 Conclusion

In conclusion, our experiments indicate that the preferred method to study the regulation of EV secretion by cultured cells consists of labeling parental cells before plating, separating the "unprocessed" 2K SN and analyzing EVs by IFC after labeling for EV subtypes. Parental cell labeling does not require the separation of EVs from the free label when done in vitro, which usually involves ultracentrifugation and/or filtration, and presents several complications (Lannigan and Erdbruegger, 2017; van der Vlist et al., 2012). The use of the 2K SN offers the most representative sample of secreted EVs and circumvents unfavourable impacts of EV separation procedures. IFC is a rapid and reliable method to quantify EVs and to identify EVs subtypes. Moreover, it is

noteworthy that IFC is able to quantify different subsets of EVs, while NTA quantifies particles with sizes corresponding to vesicles.

Chapter 4

Effect of Autophagy on EV Secretion and Cell-to-cell Transfer of Aβ

4.1 Introduction

EV-mediated prion-like spreading of Aβ implies that a) Aβ is released in EVs and b) cells take up Aβ-loaded EVs. The idea of prion-like propagation of neurodegenerative-disease relevant proteins has been proposed (Guo and Lee, 2014), and the intercellular transmissibility of Aβ, specifically following intracerebral inoculation of diseased brain extracts or purified Aβ aggregates from AD patients into healthy mice, has been demonstrated (Meyer-Luehmann et al., 2006; Stohr et al., 2012). The role of EVs in the spreading of Aβ was suggested as a potential contributing mechanism of disease (Vingtdeux et al., 2012). The presence of disease-relevant pathological proteins in EVs is an emerging area of research interest. Although investigations were pioneered in prion disease (Fevrier et al., 2004), EVs have been found to contain α-synuclein (Alvarez-Erviti et al., 2011; Danzer et al., 2012), mutant Huntington (mHTT) (Zhang et al., 2016), and Aβ (Rajendran et al., 2006) in models of Parkinson's disease, Huntington's disease and Alzheimer's disease respectively. In AD, the cell-to-cell spreading of Aβ has recently been linked to EVs (Sinha et al., 2018).

Studies using the lysosomal vacuolar ATPase (V-ATPase) inhibitor bafilomycin demonstrated that blocking autophagy increases EV secretion (Abdulrahman et al., 2018; Alvarez-Erviti et al., 2011; Danzer et al., 2012). Again, the majority of the experiments make conclusions based on the analysis of the pellet of ultracentrifugation (100K Pellet) alone. Considering the problems of reproducibility of the centrifugation methods, and the differential pelleting based on EV density, the validity of results is uncertain, specifically if bafilomycin alters EV properties (ie. density, cargo, size, etc.) (Cvjetkovic et al., 2014; Lamparski et al., 2002). Nevertheless the autophagy activator

rapamycin, an inhibitor of the mammalian target of rapamycin (mTOR), has been shown to direct MVBs containing intraluminal vesicles to the lysosome (Fader et al., 2008). In all, the evidence points at an increase of EV secretion when autophagy is blocked, and a decrease in EV secretion when autophagy is activated. The regulation of the exosomal release of prions by autophagy has recently been reported (Abdulrahman et al., 2018), however to our knowledge, the specific connection between autophagy regulation, EV secretion, and the spreading of pathological proteins in AD has yet to be elucidated.

Our laboratory has demonstrated that Aβ blocks autophagy, and Aβ-induced autophagy blockade is a result of inhibition of protein prenylation (Smith, 2016). Preliminary data also showed impaired protein prenylation in N2a cells expressing human Swedish-mutant APP695 (N2aAPP^{swe}) that was moderately restored by exogenous administration of isoprenoid GGPP (**Appendix 3**). These data suggest that cells treated with Aβ or the N2aAPP^{swe} cells will release more EVs, thus potentially enhancing the transmission of Aβ to neighbouring cells.

4.2 Results

4.2.1 Regulation of EV secretion detected by IFC

To investigate if IFC is a suitable technique to quantitatively determine changes in EV secretion, we compared EVs released by cells treated with bafilomycin to cells that remained untreated. Bafilomycin treatment has been reported to increase EV secretion based on the analysis of the 100K Pellet (Alvarez-Erviti et al., 2011; Danzer et al., 2012), however to our knowledge, the 2K SN has not been investigated. EVs were separated by UC in 2K SN, 100K SN and 100K Pellet (**Figure 23A**). Blocking autophagy

with bafilomycin significantly increased the number of EVs in the 2K SN and the 100K Pellet (**Figure 23B-C**). To investigate if inhibition of autophagy causes the increase of a specific EV subtype, EVs were labeled with a fluorophore-conjugated antibody against CD9 as previously described. The total number of CD9+ EVs was not affected by bafilomycin, therefore bafilomycin may cause a preferential secretion of CD9 negative EVs (**Figure 23C**). Bafilomycin did not affect the pelleting efficiency as indicated by the lack of difference between the proportion of EVs present in 100K SN or the 100K Pellet compared to the 2K SN (**Figure 23D**).

In all, the data show that conclusions derived from analysis of 2K SN and the 100K Pellet are analogous. As the UC procedure may bias the separation of EVs based on size or density, we decided to analyze the unprocessed 2K SN by IFC in experiments comparing models of blocked autophagy in subsequent experiments.

4.2.2 Aβ blocks autophagic flux

Our goal was to examine if Aβ-induced inhibition of autophagy contributes to the spreading of Aβ via EVs. We first confirmed that Aβ blocks autophagy. We used five models of blocked autophagy: N2a cells treated with bafilomycin (N2a+BafA1), N2a cells treated with Aβ (N2a+Aβ), N2a cells with a CRISPR/Cas9 knockout of ATG5 (N2a ATG5KO) and the N2aAPP^{swe} (APP^{swe}) cells. The Atg5 protein is essential for the ubiquitin-like conjugation of PE to LC3, therefore lack of this protein will effectively inhibit autophagosome expansion, cargo recognition and autophagosome lysosome fusion (Kaur and Debnath, 2015). N2aAPP^{swe} cells were also tested as a more relevant model of endogenously produced Aβ.

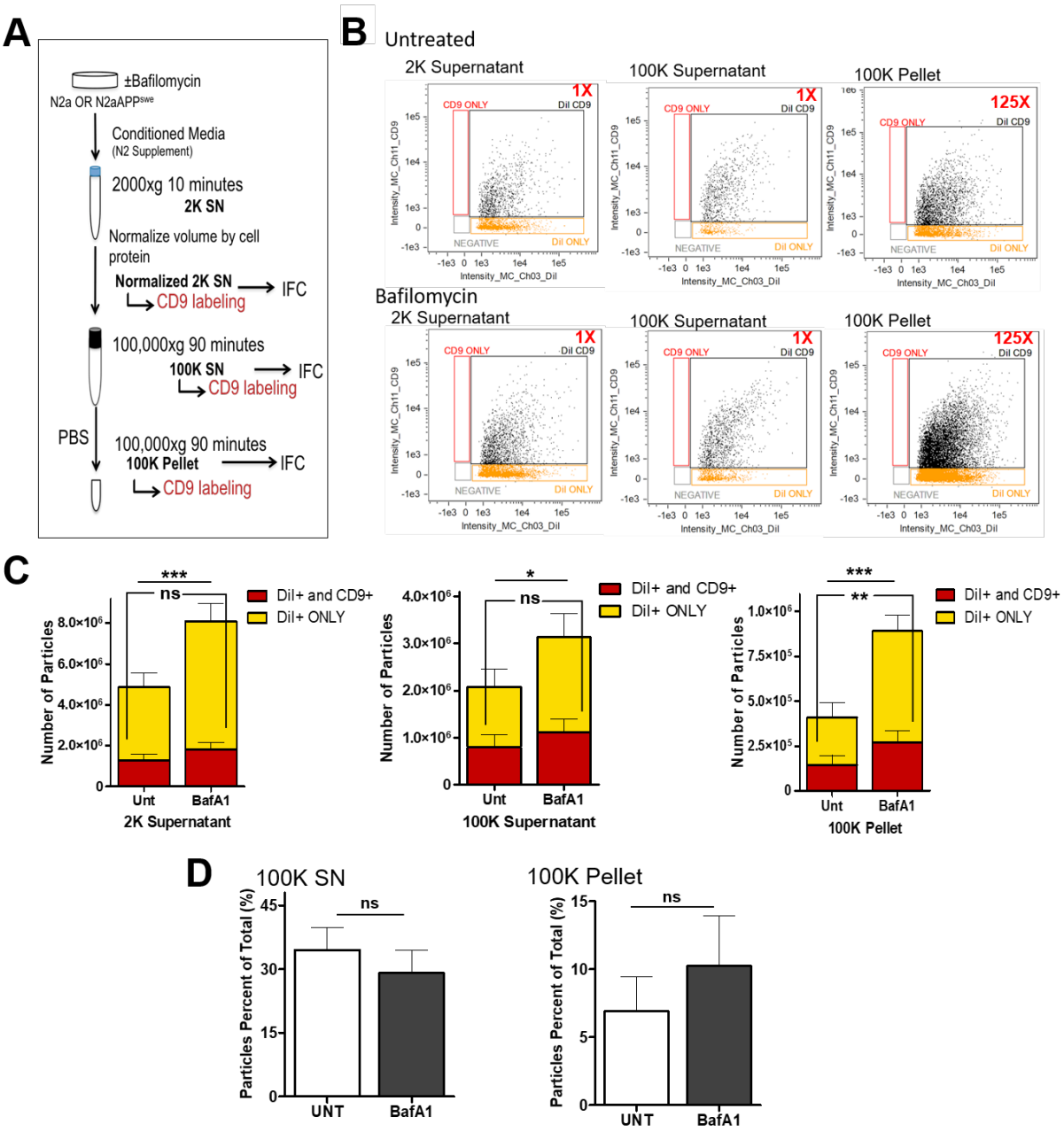

Figure 23. Bafilomycin increases EV secretion (A) Scheme of UC method and IFC samples. The volume of 2K SN was adjusted to normalize all samples based on the protein mass of the parental cells. **(B)** Representative dotplots from N2a untreated and cells treated with bafilomycin (4 hrs,150nM). Factors (red) indicate how concentrated samples are compared to the 2K SN **(C)** Graph of the total number of particles in each group, for DiI positive and DiI and CD9 double positive for samples already normalized to cellular protein. Significance determined by two-way ANOVA with Bonferroni *post hoc* test, *p<0.05, **p<0.01, ***p<0.001. **(D)** No difference in pelleting efficiency as determined by number of particles in each as a percent of the total 2K SN. Results expressed as mean±SEM. n=3. Significance determined by unpaired t test, *p<0.05.

To determine if Aβ affects autophagy, we used LC3II as a reporter. The levels of LC3II were higher in Aβ and bafilomycin treated cells. The levels of LC3II in N2aAPP^{swe} cells were similar to cells treated with Aβ (**Figure 24A-B**). The N2a ATG5KO cell line had virtually no LC3II, thus confirming its lack in lipidation of LC3 (Abdulrahman et al., 2018; Kaur and Debnath, 2015) (**Figure 24A-B**). As the nature of autophagic dysfunction cannot be inferred from immunoblot for LC3 alone, we expressed the tLC3 reporter, whereby LC3 is conjugated to both mCherry and GFP. The tLC3 is a reporter of autophagic flux, because GFP fluorescence is quenched in the acidic environment of the lysosome, therefore cells exhibiting red puncta indicate increased autophagy, whereas cells with yellow puncta indicate accumulation of autophagosomes and a problem in their degradation (Hansen and Johansen, 2011) (**Figure 11**). As autophagy is generally a transient process (Klionsky et al., 2012), diffuse cytosolic staining is expected rather than the punctated pattern with autophagosome generation. We observed diffuse staining in N2a untreated cells. We found the N2aAPP^{swe} cells and treatment with bafilomycin or Aβ accumulated yellow puncta, indicative of impaired autophagic flux. The N2a ATG5KO cell line, although they also have impaired autophagy, are unable to conjugate PE to LC3. This prevents expansion of the autophagosome membrane and impairs membrane localization of LC3 (Kaur and Debnath, 2015), thus the diffuse staining we observed in these cells was expected (**Figure 24C**). As we confirmed alterations in autophagy with Aβ treatment, we aimed to address the implications on EV secretion.

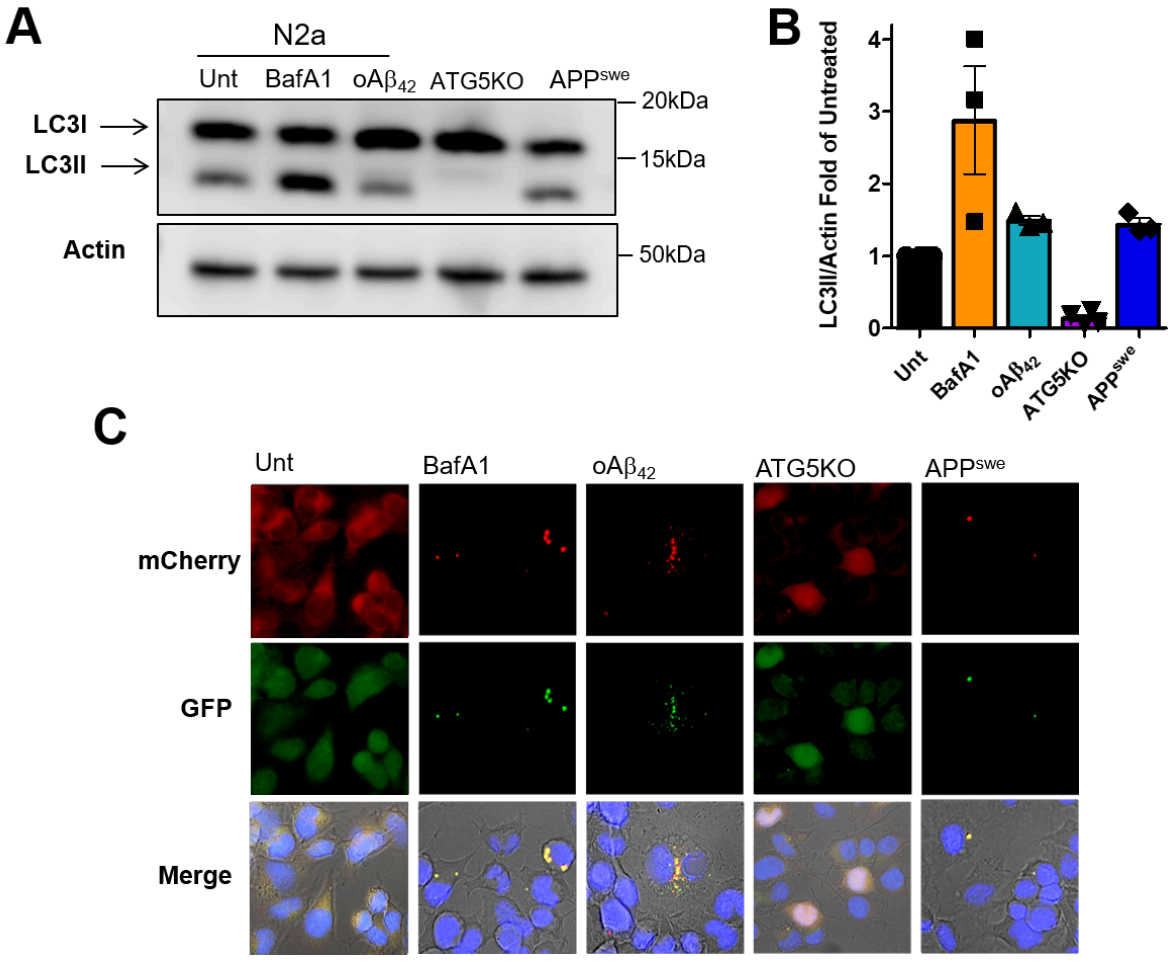

Figure 24. Autophagy is altered in cells treated with bafilomycin or Aβ and in N2aAPP^{swe} and N2a ATG5KO cells. N2a cells were treated with oAβ_{42} at 20μM for 24 hours or bafilomycin at 150nM for 4 hours prior to the EV collection period. N2aAPP^{swe} and N2a ATG5KO cells were plated in parallel but left untreated. After 24 hours (equivalent EV collection period) cells were harvested and LC3 was examined by western blotting **(A)** and quantified in reference to actin **(B).** Data was represented as fold of untreated, n=3. **(C)** Cells transduced with AAV2/2 harboring mCherry-GFP- LC3 were cultured and treated as in (A) and visualized by fluorescence microscopy.

4.2.3 Aβ increases EV secretion

Prior to testing the regulation of EV secretion by autophagy, we confirmed that the three different cell lines used, namely the N2a cells, N2a ATG5KO and the N2aAPP^{swe}, had no significant difference in DiI incorporation and labeling (**Figure 25**).

To determine the effect of blocked autophagy on EV secretion, we performed IFC and NTA. We used bafilomycin-treated cells and the N2a ATG5KO cell line as positive controls for the inhibition of autophagy. We found that all models tested (N2a+BafA1, N2a+Aβ, and N2a ATG5KO) had a corresponding increase in EV secretion measured by DiI fluorescence and number of particles by IFC, with the exception of the N2aAPP^{swe} cells (**Figure 26A-B**). Preliminary experiments with NTA supported this finding (**Figure 26C-D**).

To determine if there are phenotypic differences in EVs secreted by these difference cell types, EVs were labeled in vitro with two markers: CD9 and AnnexinV as described in the Materials and Methods. Cells treated with Aβ produced a higher proportion of EVs negative for AnnexinV and CD9 (DiI only), less DiI and CD9 positive (DiI+ CD9+) more DiI and AnnexinV positive EVs (DiI+ AnnexinV+), less triple positive (DiI+ CD9+ AnnexinV+) compared to untreated cells (**Figure 27A**). However, only significant differences were seen with the AnnexinV positive groups (DiI+ CD9+ AnnexinV+ and DiI+ AnnexinV+). Next, we looked at each CD9 and AnnexinV positive EVs labeling as a percent of the total DiI positive EVs released from each cell type and treatment. We found significantly less CD9 positive EVs in cells treated with Aβ and in the N2a ATG5KO cell line (**Figure 27B**). Further, we found that N2aAPP^{swe} –derived EVs were significantly more CD9 positive than untreated (**Figure 27B**).

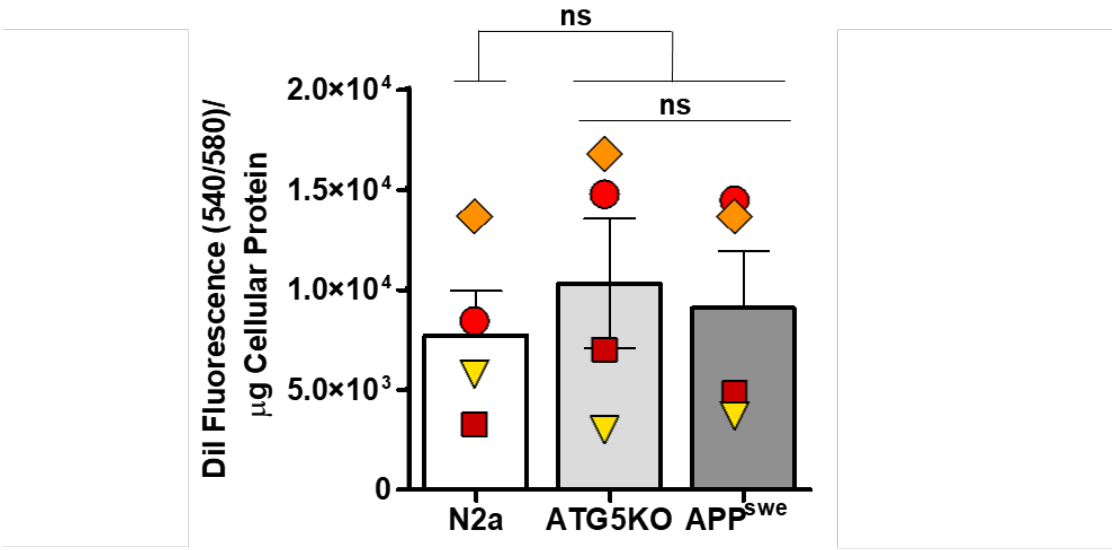

Figure 25. DiI incorporation in N2a, N2a ATG5KO and N2aAPP^{swe} cell lines. Incorporation was calculated as DiI fluorescence over mass of protein (μg). Each experiment is depicted by a different colour/symbol. Results represented as mean±SEM, n=4. Statistics were calculated by one-way ANOVA with Tukey *post hoc* test.

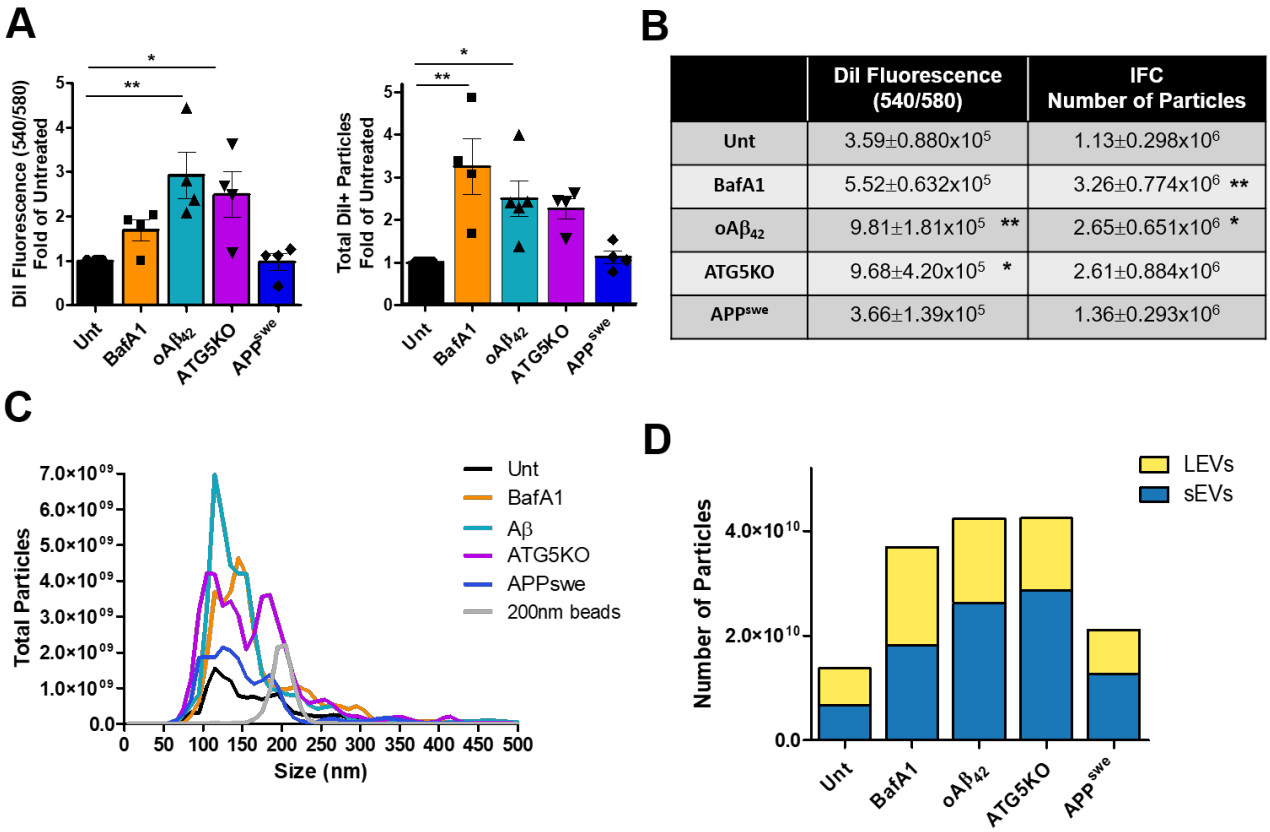

	DiI Fluorescence (540/580)	IFC Number of Particles
Unt	3.59±0.880x10^5	1.13±0.298x10^6
BafA1	5.52±0.632x10^5	3.26±0.774x10^6 **
oAβ$_{42}$	9.81±1.81x10^5 **	2.65±0.651x10^6 *
ATG5KO	9.68±4.20x10^5 *	2.61±0.884x10^6
APP^{swe}	3.66±1.39x10^5	1.36±0.293x10^6

Figure 26. Blocked autophagy increases EV secretion (A) N2a cells were treated with oAβ$_{42}$ at 20μM for 24 hours or bafilomycin at 150nM for 4 hours prior to the EV collection period. N2aAPP^{swe} and N2a ATG5KO cells were plated in parallel, but left untreated. Media were conditioned for 24 hours and collected. The 2K SNs were obtained, normalized to mass of cellular protein for each group, and then subjected to measurements of DiI fluorescence and IFC. Results represented as mean±SEM, n=3. **(B)** Numerical values for DiI fluorescence and total particles. Data represented as mean±SEM, n=3 **(C)** Preliminary NTA profile of the 2K SN of samples. n=1. **(D)** Total number of particles tracked between 1 and 500nm by NTA. Bins were adjusted to group small EVs (sEVs) from 1-150nm, and large EVs (LEVs) from 151-500nm. n=1. Statistics were calculated with one-way ANOVA and Dunnett *post hoc* test compared to untreated cells. *p<0.05, **p<0.01, ***p<0.001.

There was no difference in AnnexinV between groups (**Figure 27C**). Overall, the different profiles of EV subtypes suggest that EV secretion is affected differently in models of AD and/or blocked autophagy. After determining population differences of EVs based on markers, we determined differences in the size of secreted EVs.

Intuitively, larger EVs will elicit an image in the brightfield channel at a microscope objective of 60x, and smaller EVs will not be above the threshold for detection by the transmitted light even at such a high magnification. Therefore, we analyzed brightfield positive and negative EVs as a surrogate measure for EV size by IFC (Gorgens et al., 2019). We defined small EVs as brightfield negative and large EVs as brightfield positive. First, we aimed to determine the approximate size cut-off for detection by brightfield by performing experiments with syringe filters. We analyzed the 2K SN of untreated N2a cells unfiltered, filtered at 0.22μm, and filtered at 0.1μm (**Figure 28A-B**). Although there is no specific size cut off for brightfield positive and negative, we determined that all events from 0.22μm filtered 2K SN were brightfield negative, therefore brightfield positive events are at minimum larger than 220nm (**Figure 28C**). We found no significant difference in the proportion of brightfield positive and negative EVs between treatment groups (**Figure 29A-B**).

Preliminary data with NTA supported that blocking autophagy increases both small (1-150nm) and large (151-500nm) EVs, as there was no significant difference in the proportion of each population (**Figure 29C**).

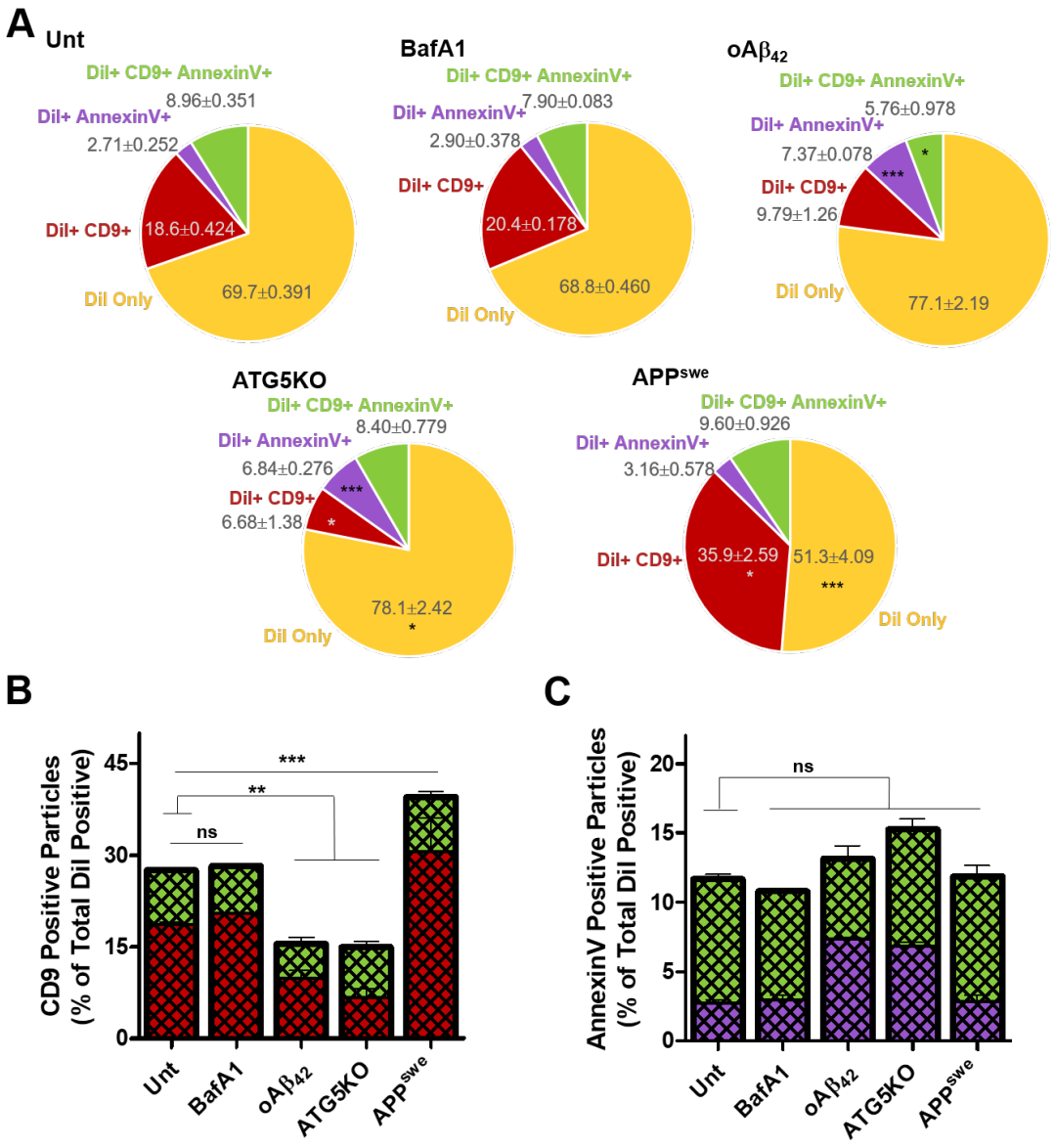

Figure 27. EVs subtype enrichment are cell type and treatment specific (A) N2a cells were treated with oAβ_{42} at 20μM for 24 hours or bafilomycin at 150nM for 4 hours prior to the EV collection period. N2aAPP^{swe} and N2a ATG5KO cells were plated in parallel but left untreated. Media were conditioned for 24 hours and collected. The 2K SNs were obtained, normalized to cellular protein, and subjected to IFC. Pie charts represent each group as a percent of the total DiI labeled particles detected. Data represented as mean±SEM, n=3. **(B)** CD9-positive (red+green from pie chart) and **(C)** AnnexinV-positive (purple+green from pie chart) EVs as a percent of total DiI positive particles. Data represented as mean±SEM, n=3. Statistics were calculated with one-way ANOVA and Dunnett *post hoc* test compared to untreated cells. *p<0.05, **p<0.01, ***p<0.001.

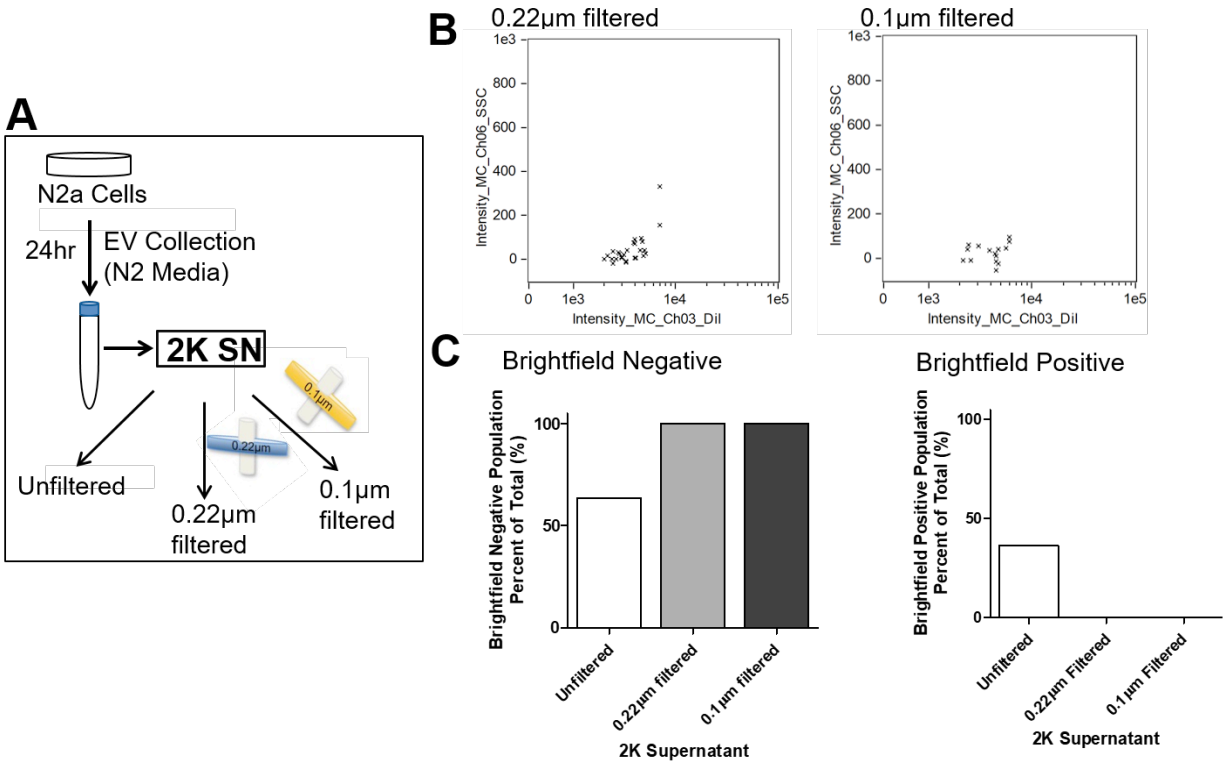

Figure 28. sEVs are detected by IFC and are exclusively brightfield negative (A) Scheme of syringe filtration method of the 2K SN to obtain filtered and unfiltered samples. The 2K SN was obtained and divided into three groups, one of which was passed through 0.22µm filter and the other a 0.1µm filter. The final sample was left unfiltered and considered as total EVs. **(B)** Dotplots of filtered (0.22µm and 0.1µm) samples. **(C)** Graph of brightfield negative events as a proportion of the total detected events in each group.

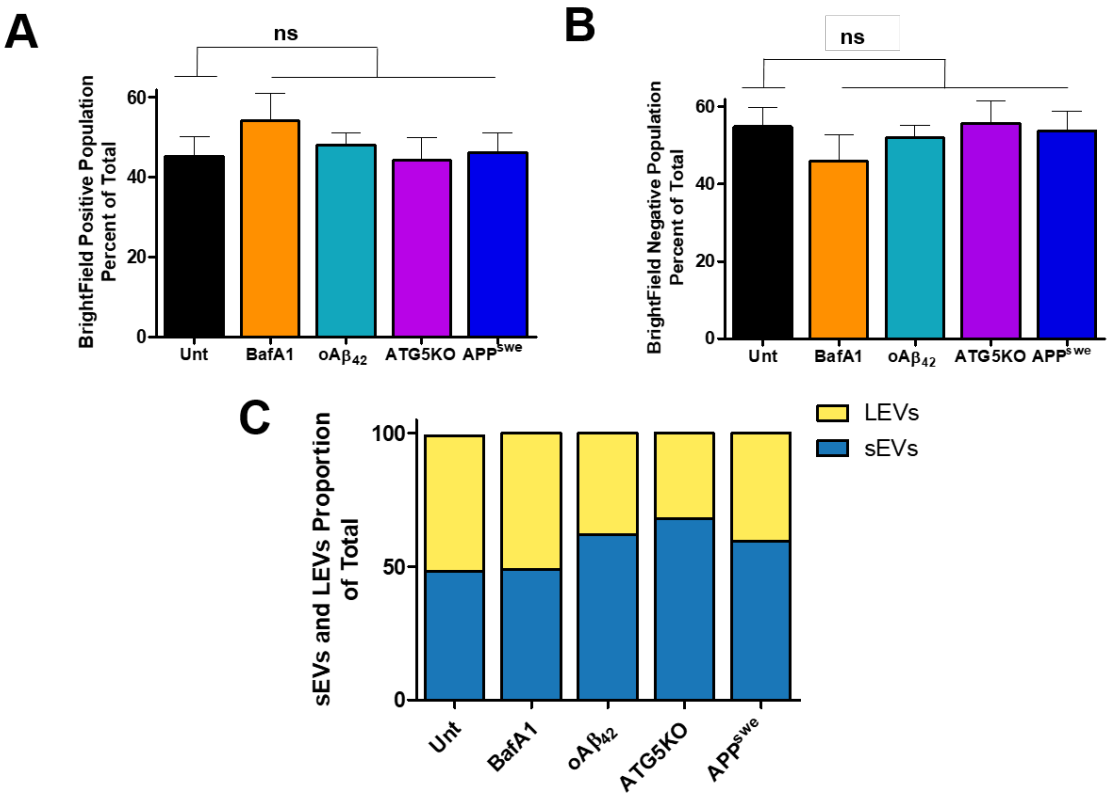

Figure 29. Blocked autophagy increases both small and large EVs (A) N2a cells were treated with oAβ_{42} at 20μM for 24 hours or bafilomycin at 150nM for 4 hours prior to the EV collection period. N2aAPP^{swe} and N2a ATG5KO cells were plated in parallel but left untreated. Media were conditioned for 24 hours and collected. The 2K SNs were obtained, normalized to cellular protein, and subjected to IFC and NTA. **(A)** The proportion of brightfield positive and **(B)** negative events by IFC between experimental models. Data represented as mean±SEM, n=3. Statistics were calculated with one-way ANOVA and Dunnett *post hoc* test compared to untreated cells. *p<0.05, **p<0.01, ***p<0.001. **(C)** Bins were adjusted to group small EVs (sEVs) from 1-150nm, and large EVs (LEVs) from 151-500nm. The proportion of small and large EVs for each sample was calculated by dividing the number of small or large EVs over the total EVs tracked by NTA within that group. n=1.

4.2.4 Aβ is loaded in EVs

To claim EVs are instrumental in Aβ propagation, we first confirmed and examined Aβ in EVs. We found that Aβ is loaded into N2aAPP^{swe} cell-derived EVs as a heterogeneous mixture of species. We found prominent bands at high molecular weights (>100kDa), at 50kDa and at 25kDa (**Figure 30A**). To determine if Aβ was localized on the inside or outside of EVs, we performed an assay exploiting the properties of the protease trypsin, and membrane disrupter saponin as previously described (Danzer et al., 2012) (**Figure 30B**). We found that Aβ is localized on the inside as well as the outside of EVs (**Figure 30C**).

4.2.5 Blocking autophagy increases EV transfer

To determine the intercellular spreading of Aβ, we chose to use the N2aAPP^{swe} line, as they endogenously produce Aβ and this mutation is relevant in familial AD (Thinakaran et al., 1996). We first aimed to assess the secretion of EVs by cultured N2aAPP^{swe} cells treated in the absence or presence of bafilomycin by IFC and measurements of DiI fluorescence. In line with our previous data with the 2K SN, bafilomycin increased the number of SEC-separated EVs (**Figure 31A-B**). Further, EVs were positive for CD9, flotillin-1 and ALIX and absent of ER markers (Calnexin). Calnexin was detected in the pellet of the 2000xg centrifugation and in cell lysates (**Figure 31C**). Blocking autophagy increased the number of recipient cells bearing DiI-positive EVs (**Figure 32A-C**). However, when SEC-separated EVs were normalized to give the same number of particles to recipient cells, the uptake of bafilomycin-treated donor cell-derived vesicles was less than untreated (**Figure 32D**).

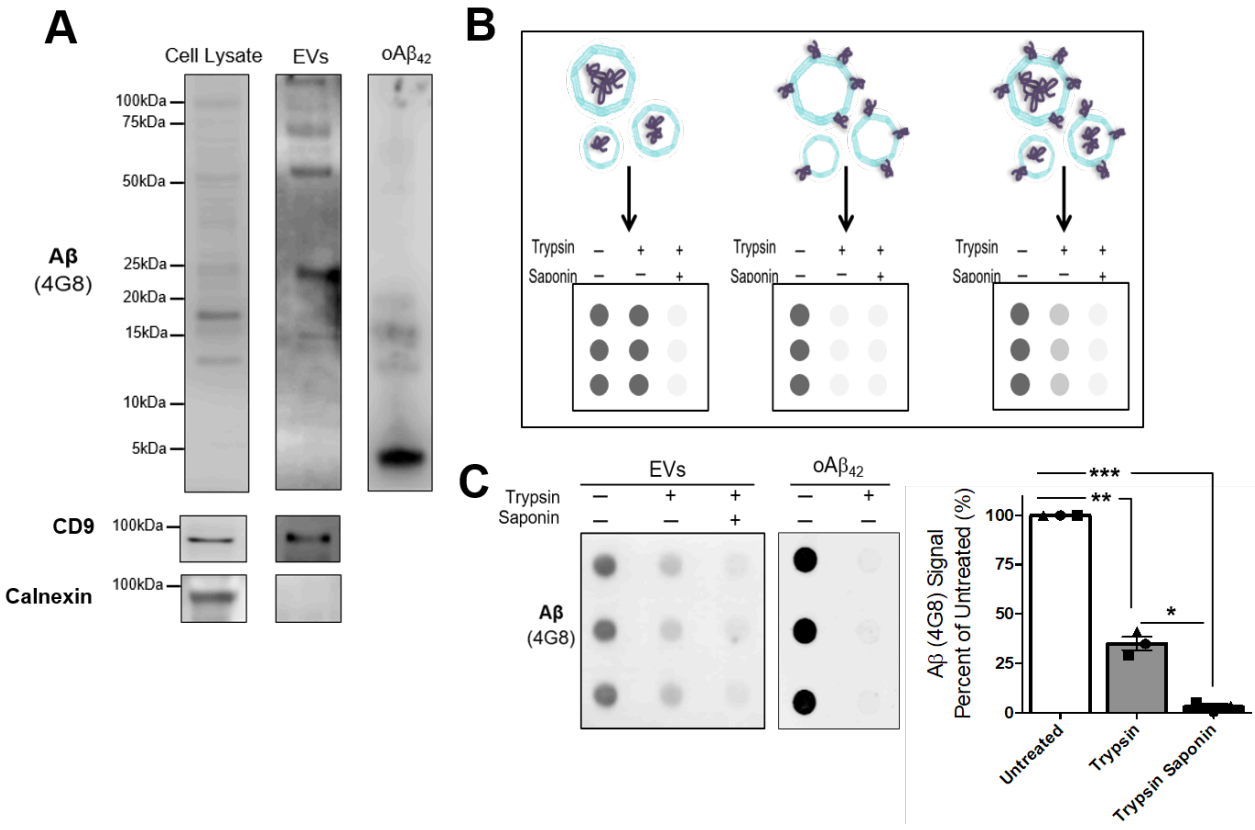

Figure 30. Characterizing Aβ in EVs (A) Western blot for N2aAPP^{swe} derived EVs, cell lysates and oligomeric Aβ_{42} positive control. **(B)** Scheme illustrating theory of trypsin saponin experiment. **(C)** Trypsin saponin experiment in N2aAPP^{swe} EVs. EVs were separated by differential ultracentrifugation and divided into three groups. Each group was incubated with or without 0.25% trypsin and/or 0.1% saponin to permeabilize membranes for 30 minutes at 37 degrees. Dotblot and densitometry analysis of Aβ probed with 4G8 antibody. Data represented as mean±SEM, n=3. Statistics were calculated with one-way ANOVA and Dunnett *post hoc* test compared to untreated cells. *p<0.05, **p<0.01, ***p<0.001.

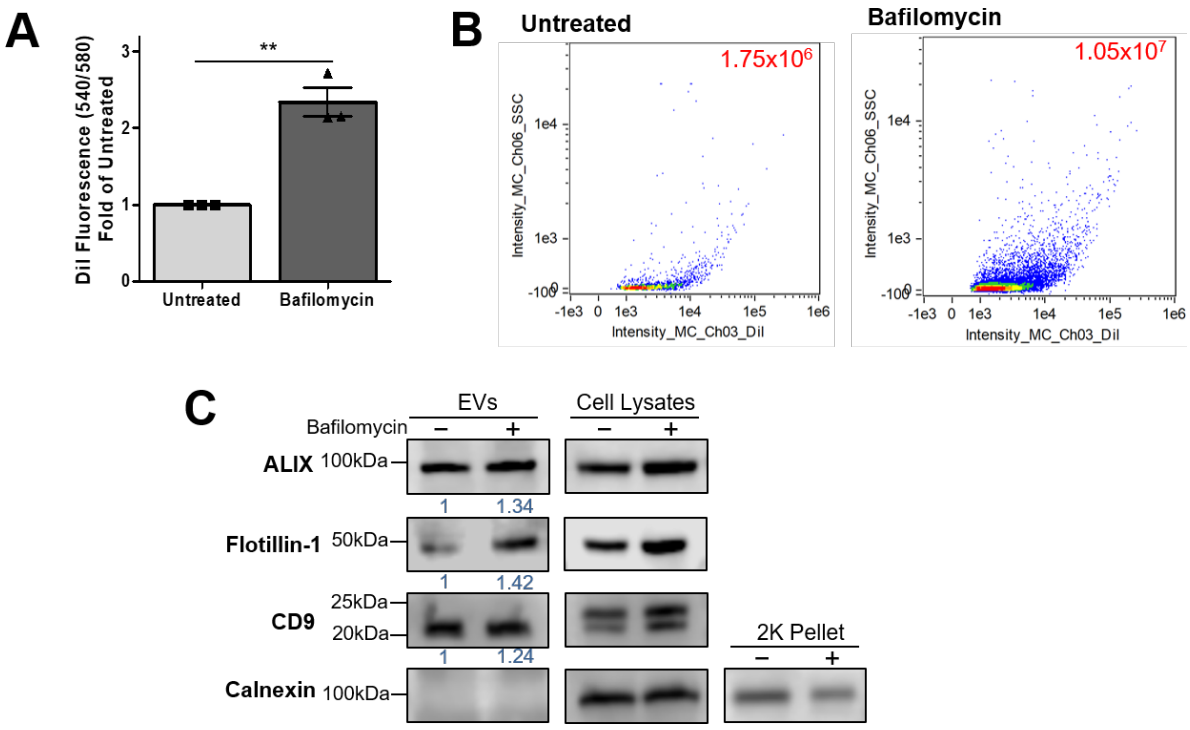

Figure 31. Blocking autophagy in N2aAPP^{swe} donor cells increases EV secretion **(A)** DiI fluorescence as determined by the area under the curve of the SEC peak from donor N2aAPP^{swe} cells treated in the absence or presence of 150nM bafilomycin for 4 hours. Results represented mean±SEM as a fold of untreated, n=3. Statistics were calculated by paired t test, **p<0.01. **(B)** IFC of the pooled SEC peak of DiI. Number of particles for each group indicated in the top right hand corner (red text). **(C)** The SEC peak contains EV markers (ALIX, Flotillin-1 and CD9) and both are absent for ER markers (Calnexin). The 2K Pellets are positive for Calnexin.

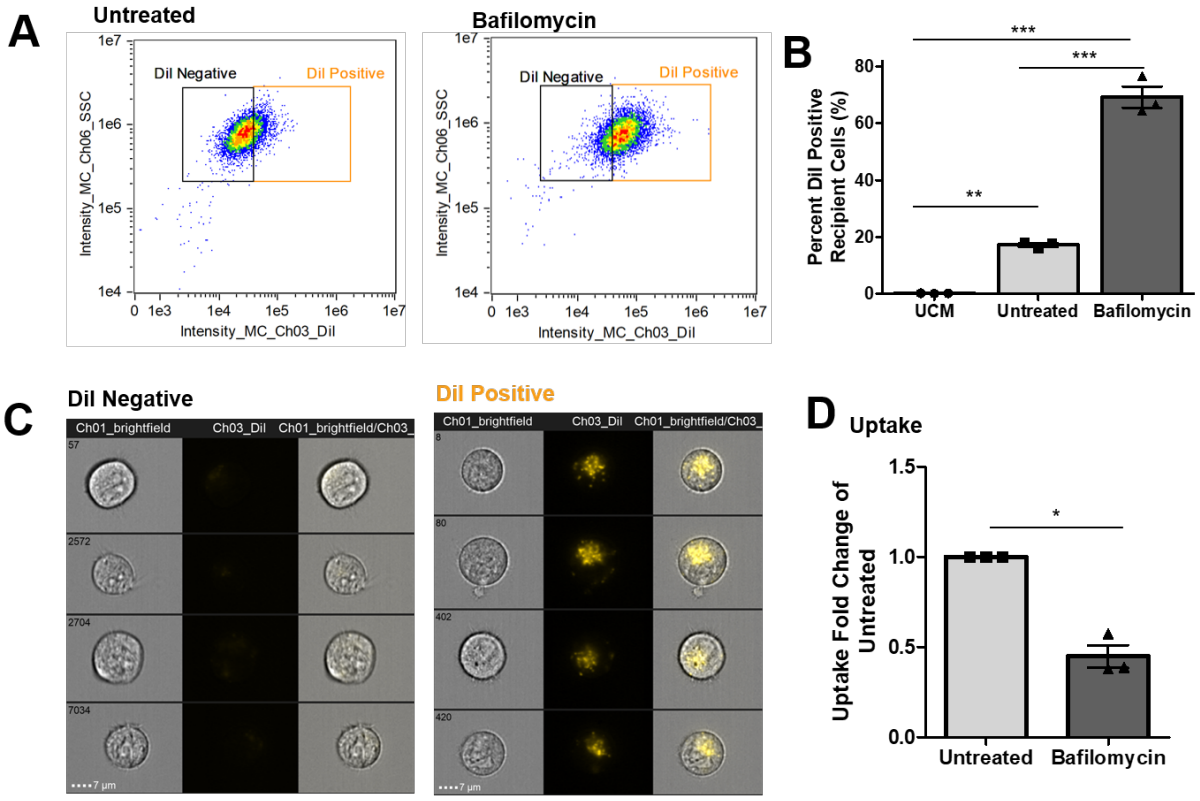

Figure 32. Blocking autophagy in N2aAPP^{swe} donor cells increases EV transfer. N2aAPP^{swe} donor cells were treated in the absence and presence of 150 nM balilomycin, and media conditioned with EVs for 24 hours. The 2K SNs were obtained, EVs separated by SEC, and EVs were incubated with N2a unlabeled recipient cells for 12 hours in serum-free media (OptiMEM:DMEM 1:1, 1% penicillin/streptomycin). A SEC 'peak' obtained from UCM was used as a negative control. After incubation, cells were trypsinized gently, resuspended in PBS and analyzed by IFC **(A)** Dotplot and gating of DiI positive and negative populations of recipient cells following 12 hour incubation of untreated and bafilomycin treated N2aAPP^{swe} donor cell-derived EVs. The retentate volumes were normalized to protein mass in donor cells prior to SEC. **(B)** Quantification of DiI positive recipient cells. Data represented as mean±SEM, n=3. **(C)** Representative cell images captured by IFC of both DiI negative N2a recipient cells, and DiI positive N2a recipient cells. **(D)** For uptake, a proportion of the 2K SNs were normalized to give the same number of EVs to recipient cells. Statistics were calculated with an unpaired t test, *p<0.05, **p<0.01, ***p<0.001.

4.2.6 Blocking autophagy does not increase the cell-to-cell transfer of Aβ

In order to examine the cell-to-cell spread of neurotoxic proteins, we measured human $A\beta_{42}$ in donor cell-derived EVs, as well as in the recipient cells themselves following EV incubation. There was no difference in Aβ loaded into EVs derived from bafilomycin treated donor cells (**Figure 33A**). In accordance, there was no increase the amount of Aβ in recipient cells following incubation with EVs from bafilomycin treated donor cells (**Figure 33B**) and the amount of Aβ per particle was reduced in EVs from bafilomycin treated cells (**Figure 33C**).

4.2.7 EVs are highly internalized by recipient cells

To ensure that DiI-positive EVs are actually taken up by recipient cells rather than DiI transfer between membranes, we calculated the internalization score for each sample. We found that EVs are highly internalized by cells, and that DiI staining is not localized to the membranes of recipient cells overall (**Figure 34A**). However, this post analysis is problematized as DiI is highly internalized by labeled parental cells in general, as the internalization score is greater than zero. To combat this, we performed a measure of entropy in recipient cells given DiI positive EVs and compared this value to DiI-labeled parental cells. We found that labeled parental cells had high entropy and recipient cells had low entropy, indicative of random incorporation of the dye and distinct localizations of DiI intensity respectively (**Figure 34B-E**).

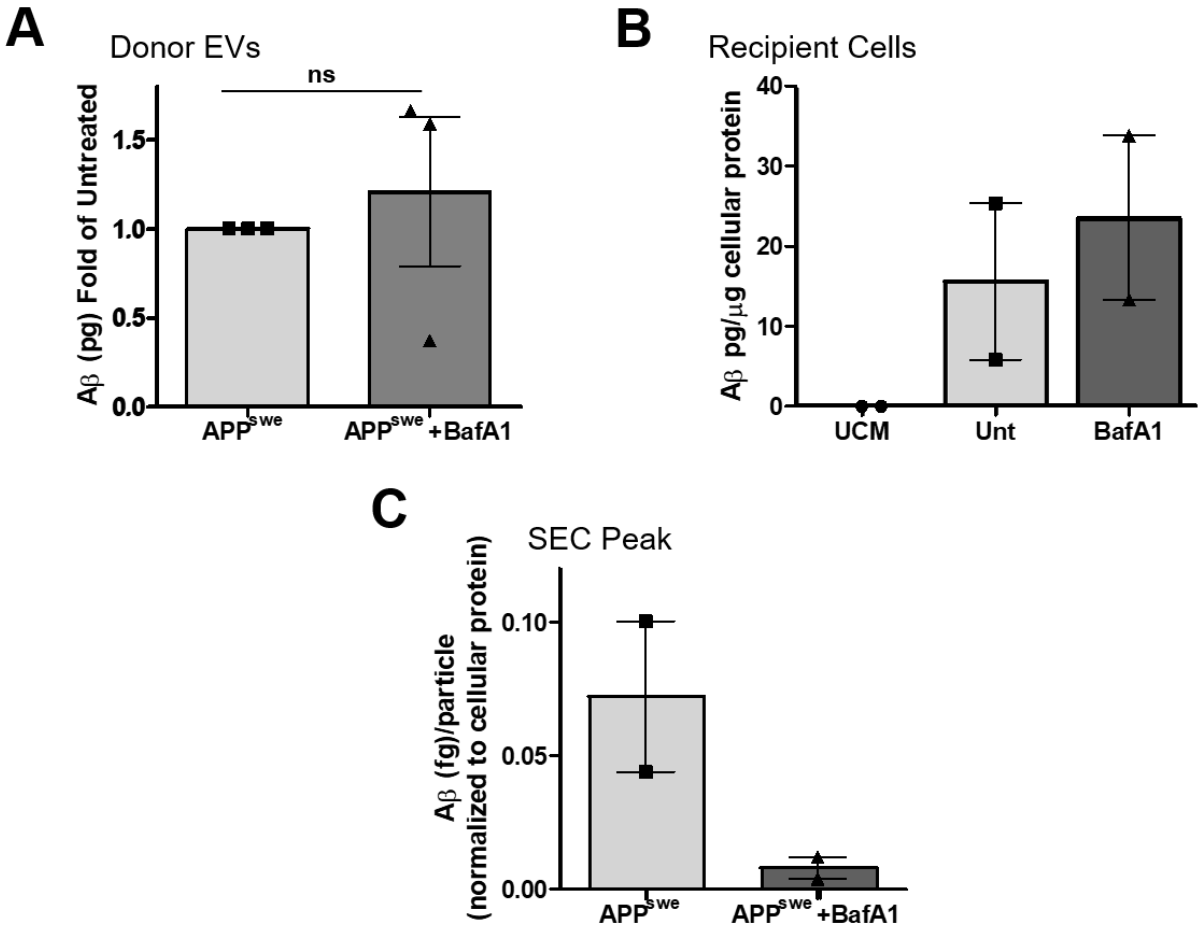

Figure 33. Blocking autophagy does not increase Aβ transfer (A) $A\beta_{42}$ ELISA was performed on an equivalent volume of SEC-separated EVs from untreated and bafilomycin treated N2aAPP^{swe} donor cells. Results represent mean±SEM, n=3. Statistics were calculated with a paired t test. **(B)** $A\beta_{42}$ was measured in recipient cells that were incubated with either EVs from donor untreated N2aAPP^{swe} cells or N2aAPP^{swe} cells treated with bafilomycin (4hr, 150nM). Background values of the UCM SEC 'peak' given to recipient cells were subtracted from the other treatment groups. Values were normalized to the protein content of the recipient cells (mg). Results represent mean±SEM, n=2. **(C)** Calculation of $A\beta_{42}$ by ELISA over the total number of DiI-labeled EVs as detected by IFC to determine $A\beta_{42}$ load per EV. Data represent mean±SEM, n=2.

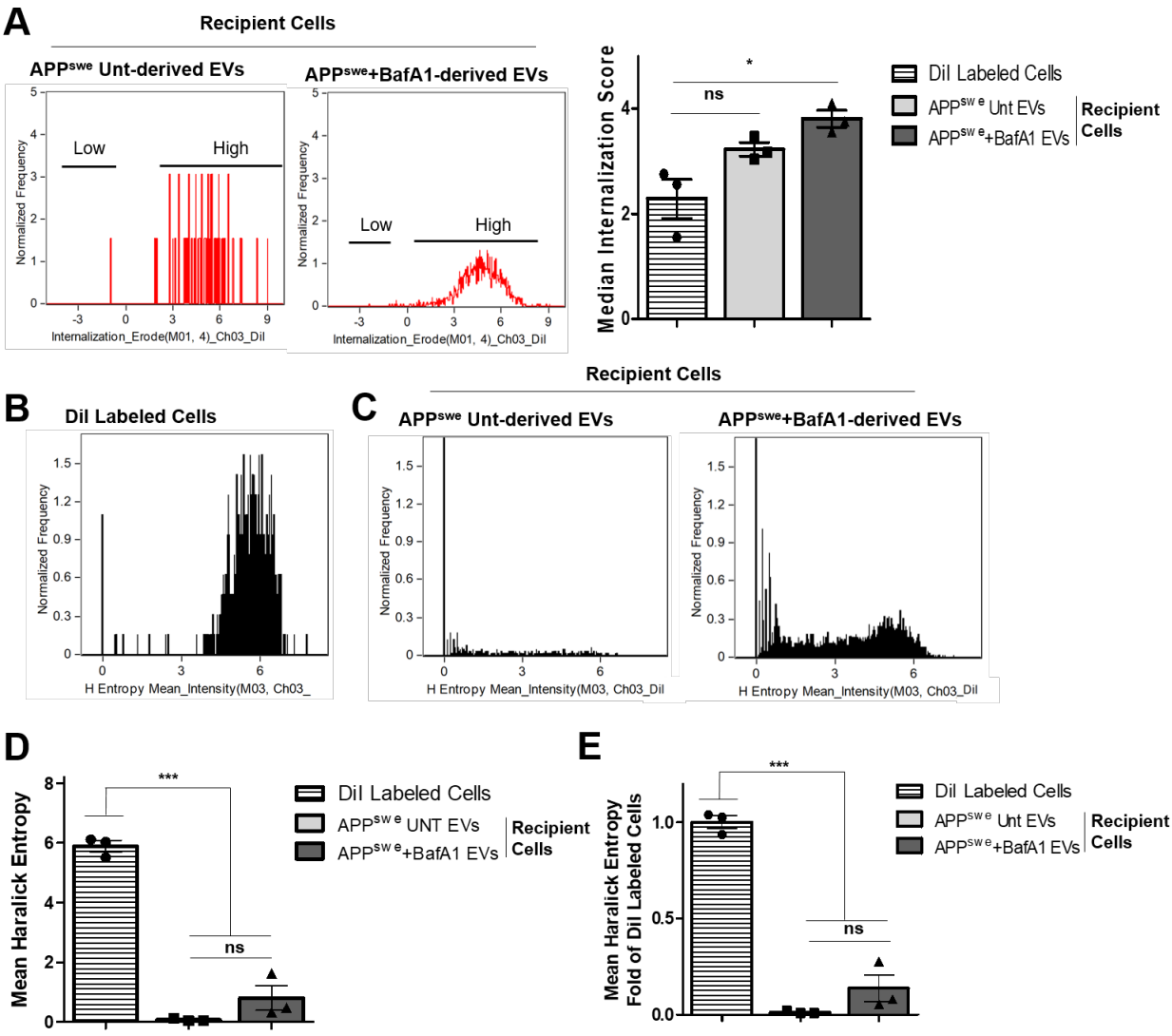

Figure 34. *Figure legend on next page*

Figure 34. DiI internalization by recipient cells is not an artefact of DiI transfer between membranes (A) DiI-positive EVs are highly internalized in recipient cells for both treatment groups. Internalization score below zero denotes low internalization (membrane bound or outside of cell), internalization score of 0 indicates a mix of internalized and membrane bound areas of fluorescence, and internalization score of greater than zero indicates high internalization of fluorescent EVs. The median internalization score from all experiments are represented in a bar graph. Results represent mean±SEM, n=3. DiI labeled cells indicates the internalization score for cells directly labeled with DiI in vitro. Statistics were calculated with one-way ANOVA with Tukey *post hoc* test, ***p<0.001. **(B-C)** Histograms of the mean Haralick entropy for each **(B)** cells directly labeled with DiI, and **(C)** N2aAPP^{swe} untreated donor cells, and N2aAPP^{swe} donor cells treated with bafilomycin (4hr, 150nM). **(D-E)** Quantification of the mean Haralick entropy for cells directly labeled with DiI, N2aAPP^{swe} untreated donor cells, and N2aAPP^{swe} donor cells treated with bafilomycin (4hr, 150nM) represented as **(D)** mean value and **(E)** value as fold change of the cells directly labeled with DiI. Data represented as mean±SEM, n=3. Statistics were calculated by one-way ANOVA with Tukey *post hoc* test, *p<0.05, **p<0.01, ***p<0.001.

4.3 Discussion

The prion-like spreading of Aβ requires Aβ regulate EV secretion, Aβ localizes to EVs and the uptake of Aβ-loaded EVs by recipient cells.

Previous reports indicate that autophagy regulates EV secretion (Abdulrahman et al., 2018; Alvarez-Erviti et al., 2011; Danzer et al., 2012; Fader et al., 2008). As the majority of conclusions in these experiments were drawn from the pellet of ultracentrifugation, we aimed to ensure that an unprocessed sample would also demonstrate this relationship. We established that blocking autophagy increases EV secretion, and the effect was detectable in the unprocessed 2K SN by IFC. We also confirmed the effect in the 100K Pellet by IFC. We found that the increase of EV secretion by blocking autophagy was maintained in 100K Pellet and 2K SN, and no significant difference was determined in the 100K SN, therefore the effect of bafilomycin was not an artefact of increasing pelleting efficiency. Therefore, our results align with previous literature, and we validated the 2K SN and IFC as the preferred sample and method for determining EV secretion.

There is considerable evidence that Aβ alters autophagy in AD (Nixon et al., 2005; Yu et al., 2004). Our goal was to investigate the cellular implications of dysfunctional autophagy on EV secretion. Prior to analyzing EV secretion under conditions of altered autophagy, we first confirmed Aβ blocks autophagy in our cellular model. We found that Aβ causes alterations of autophagy with LC3II as a reporter. To assess the nature of LC3II accumulation, we employed the expression of tLC3 as a measure of autophagic flux (Castillo et al., 2013; Hansen and Johansen, 2011; Smith, 2016). Aβ blocks autophagic flux and causes an accumulation of autophagosomes in the

same manner as treatment with bafilomycin, thus coinciding with previous reports from our lab (Smith, 2016). The N2aAPP^{swe} cell line also had impaired autophagic flux. We confirmed that the N2a ATG5KO model had impaired autophagosome expansion based on the absence of lipidated LC3 and no accumulation of autophagosomes. Therefore, all models had blocked autophagic flux.

Autophagy has been proposed to regulate EV secretion, such that autophagy blockade consequently enhances release (Abdulrahman et al., 2018; Danzer et al., 2012). We demonstrated that all of our models of blocked autophagy increased EV secretion, with the exception of the N2aAPP^{swe} cells. One possible explanation was revealed when we observed that N2aAPP^{swe} cells have less GM1 than N2a wild type cells (**Appendix 2B**). As GM1 was found enriched in endocytic-derived EVs (Rajendran et al., 2006), it is reasonable to interpret that reduced EV secretion by N2aAPP^{swe} cells could be a result of less GM1, thus would negate the effects of Aβ-mediated increase in EV secretion. Our laboratory is actively investigating the regulation of EV secretion by GM1 in collaboration with Dr. Sipione.

GM1 itself has been implicated in AD pathogenesis. GM1 was originally thought to promote AD pathology as a seed for the fibrillogenesis of Aβ (Yanagisawa et al., 1995). However, GM1-loaded EVs may sequester Aβ from the extracellular space and promote its degradation by phagocytic cells, thus providing GM1-containing EVs has been suggested as a protective intervention in AD mice and aged non-human primates to enhance Aβ clearance (Yuyama et al., 2014; Yuyama et al., 2015).

Once we determined the effect of blocking autophagy on EV secretion, we aimed to identify if the quality of secreted EVs were different than untreated cell-derived EVs.

To define EV subtypes, we used CD9 and AnnexinV as markers. N2a cells treated with Aβ had a higher proportion of EVs negative for AnnexinV and CD9 (DiI only), less DiI and CD9 positive (DiI+ CD9+), more DiI and AnnexinV positive EVs (DiI+ AnnexinV+), and less triple positive (DiI+ CD9+ AnnexinV+) than untreated N2a cells.

AnnexinV has been proposed as a potential pan label for EVs upon the finding that both microvesicles and exosomes expose PS (Thery et al., 2009). However, it has been demonstrated that approximately 80% of particles are not stained with AnnexinV even with optimal calcium concentrations and labeling conditions (Connor et al., 2010). In fact, vesicles less than 300nm are more likely to be AnnexinV negative (Lannigan and Erdbruegger, 2017). Therefore, groups have cautioned the use of AnnexinV labeling exclusively to derive conclusions on EVs, as this may lead to misleading results (Ahn et al., 2004).

CD9 is considered a marker for tetraspanin positive EVs (Kowal et al., 2016). Although CD9 has been found in exosomes from endocytic origin, it has been demonstrated that larger, plasma membrane derived EVs also have this transmembrane protein (Kowal et al., 2016; Thery et al., 2002). We found that tetraspanin-positive EVs are significantly reduced upon treatment with Aβ and in the N2a ATG5KO cell line, and increased from the N2aAPP^{swe} cell line. However, as there is uncertainty regarding the cellular origin of CD9-positive EVs (Kowal et al., 2016), we cannot make distinct conclusions on the significance. Therefore, although our findings that Aβ produces qualitatively different EVs are interesting, the cellular implications are yet unknown. Another important classifier of EVs is the size distribution, as size can give a potential indication of intracellular origin.

Although small size is required to define exosomes, small size alone is not sufficient to distinguish between MVB-derived EVs or plasma membrane derived EVs (Tkach et al., 2018). First, we examined size by IFC based on the idea that a size cut-off exists for the detection of a brightfield image. Larger EVs will elicit a brightfield image, thus denoted brightfield positive, and smaller EVs will not and be classified brightfield negative (Gorgens et al., 2019). Based on detection of polystyrene beads of a known size, the limit of detection for brightfield positive particles is 240nm (Gorgens et al., 2019), which coincides with our experiments demonstrating EVs smaller than 220nm are brightfield negative. When determining the proportion of brightfield positive and negative for our experiments, we analyzed single, DiI-positive EVs exclusively. We found no differences between treatment groups in the proportion of brightfield positive and negative EVs. As IFC is not a tool inherently optimized for the determination of size, we employed NTA as a standard method to measure particle size distribution to corroborate these results.

Preliminary data with NTA was secondary confirmation that blocking autophagy increases EV secretion. Further, this effect was for both small and large EVs. Therefore, this data provides support for the lack of difference between the percent of brightfield positive and negative EVs by IFC between treatment groups, indicating that the increase of EV secretion is not specifically for one population of EVs. However, repetition of this experiment is required to confirm these initial observations, and to determine if the size profile obtained by NTA is reproducibly different comparing treatment groups. As we determined that blocking autophagy increases EV secretion of both large and small EVs, we aimed to characterize whether or not pathological proteins implicated in

neurodegeneration, in this case Aβ, are loaded into EVs and contribute to the propagation of pathology from cell-to-cell.

Aβ has been shown to be released in association with exosomes (Rajendran et al., 2006). Exosomes derived from AD brains show enrichment of Aβ oligomers (Sinha et al., 2018). However, to our knowledge, the membranous or intraluminal localization of Aβ has yet to be elucidated in EVs, although this topological analysis for α-synuclein has been performed (Danzer et al., 2012).

Interestingly, the existence of distinct 'strains' of Aβ has been reported, such that alterations in the pattern of amyloidosis in mice depend on the host of which inoculates are derived (Meyer-Luehmann et al., 2006; Watts et al., 2014). Therefore, considering the proposed role of EVs in the prion-like spreading of Aβ (Sinha et al., 2018), analysis of Aβ loaded into EVs could provide insight into the pathogenicity of these vesicles in disease. Further, Aβ exists in many aggregation states of which certain species (oligomers) are markedly more cytotoxic (Ahmed et al., 2010; Guglielmotto et al., 2014; Selkoe, 2008b; Walsh and Selkoe, 2007).

Considering these previous studies, we aimed to characterize both the species of Aβ, as well as its membrane or intravesicular localization in N2aAPP^{swe}-derived EVs. Amyloidogenic processing of APP by β-secretase occurs in early endocytic compartments and the Aβ peptide is found in MVBs and associated with secreted vesicles (Rajendran et al., 2006). As the metabolism of the Swedish APP variant has been highly characterized, this was a useful model to determine if particular species are loaded into EVs (Thinakaran et al., 1996). Of the species loaded into EVs, we found prominent bands at just below 15kDa, 25kDa, just above 50kDa, and other high

molecular weight bands (>75kDa). The membrane bound ~13.5 kDa carboxy-terminal fragment containing Aβ has been previously described as resulting from the β-secretase cleavage of APP in the endocytic pathway (Thinakaran et al., 1996). Further, Thinakaran *et al* alludes to a 56-59kDa fragment generated from γ-secretase cleavage of sAPP, however they suggested that this fragment is subject to rapid degradation, as they did not detect it in their experiments (Thinakaran et al., 1996). For a more disease relevant analysis of Aβ in EVs, oligomer-specific antibodies could be used in parallel, such as the 82E1 clone (Sinha et al., 2018). Although we can only speculate Aβ species based on the molecular weight of detected bands, we largely confirmed the presence of Aβ in our separated EVs.

Further, we analyzed the topology of Aβ on EVs. Localization of Aβ on the surface or within EVs is critical, as it has been demonstrated that Aβ tightly binds ganglioside GM1 and acts as a seed for the fibrillogenesis of Aβ (Yanagisawa, 2005; Yanagisawa and Ihara, 1998; Yanagisawa et al., 1995). Therefore, if Aβ is localized on the outside of EVs, it is probable to be involved in the pathogenesis of AD, either by sequestering extracellular Aβ for clearance (Yuyama et al., 2014; Yuyama et al., 2015) or by promoting brain amyloidosis (Yanagisawa et al., 1995). We found that Aβ is localized both on the membrane of EVs, as well as intraluminal. After confirming the presence of Aβ in EVs from N2aAPP^{swe} cells, we aimed to characterize the prion-like spreading of Aβ under conditions of blocked autophagic flux.

The regulation of autophagy in the lateral, EV-mediated transfer of prions has been reported (Abdulrahman et al., 2018). In line with our hypothesis, blocking autophagy increases the transfer of DiI-labeled EVs to recipient cells. However, under

these conditions, we could not detect an increase in Aβ transferred to recipient cells. Further, we found less Aβ per particle in EVs from bafilomycin treated donor cells, indicating that not all EVs secreted by cells treated with bafilomycin incorporated Aβ to the same extent, or that each vesicle incorporates less. Nevertheless, based on the indication that different modes of autophagy blockade caused an increase of selective EV subtypes, it is possible that the lack of increased cell-to-cell transfer of Aβ was due to bafilomycin itself. Although bafilomycin did not increase the amount of Aβ transferred to recipient cells, we confirmed generally the EV-mediated cell-to-cell transfer of Aβ. However, a potential caveat of this experiment is labeling with a lipophilic markers, as they may transfer non-specifically between cells and complicate conclusions on internalization (Lassailly et al., 2010). To address this concern, we assessed internalization of DiI-labeled EVs in recipient cells.

We determined a high degree of internalization of DiI-labeled EVs in recipient cells. However, as DiI itself is also internalized upon cell membrane labeling (Honig and Hume, 1986), this approach is not sufficient to demonstrate the lack of DiI transfer. Therefore, we calculated the entropy of the intensity of DiI fluorescence within recipient cells.

Entropy is defined as the degree of disorder, whereas greater disorder corresponds with higher entropy. Haralick is credited with defining textural features within images, therefore comparing the spatial intensity of pixels, and identifying if they follow a precise pattern (Haralick et al., 1973). We have used this algorithm to demonstrate that the DiI we see internalized in our recipient cells are in fact associated with EVs as opposed to an artefact of the transfer of lipophilic membrane label.

In the context of our IFC data, entropy is a measure of the high concentration of fluorescent intensity (DiI) within a cell as a function of the randomness of the aforementioned intensity. Therefore, if the dye is associated with EVs exclusively in recipient cells, the entropy will be low as the signal will be punctate, highly intense, and at distinct locations. Contrary, when cells are labeled directly with DiI, the dye moves laterally within the membrane and is internalized (Honig and Hume, 1986), which is inherently random. Therefore, high entropy is expected, as the fluorescence will be associated with equally likely intensity pairings rather than at specific locations. We confirmed the low entropy of DiI in recipient cells, indicative of EV uptake by recipient cells rather than non-specific dye transfer.

4.4 Conclusion

In conclusion, we have demonstrated that Aβ increases EV secretion. We have confirmed that Aβ blocks autophagic flux. We also demonstrated that inhibition of autophagic flux or inhibition of autophagosome formation results in a significant increase in EV secretion. Therefore, it is possible that Aβ enhances its own intercellular transmission by promoting EV release. In the context of neurodegenerative diseases as a whole, EVs may be a contributing mechanism by which the predictable pattern of spreading of pathological proteins occurs (Abdulrahman et al., 2018; Danzer et al., 2012; Sinha et al., 2018). Therefore, there is substantial support for the restoration of autophagic flux as a therapeutic approach with disease modifying value in AD: the accumulation of autophagic vacuoles in AD neurons (Nixon et al., 2005), the generation of Aβ within the endocytic pathway (Koo and Squazzo, 1994), the coordinated regulation of EV secretion and autophagic flux (Abdulrahman et al., 2018; Baixauli et al.,

2014; Fader et al., 2008), and the association of disease relevant Aβ oligomers with exosomes (Sinha et al., 2018). Our laboratory has discovered that Aβ blocks autophagy through inhibition of protein prenylation by reducing the cellular pool of isoprenoids (Mohamed et al., 2018; Smith, 2016). Therefore, restoring prenylation and autophagy may reduce Aβ spreading by reducing EV secretion.

References

Abdulrahman, B.A., D.H. Abdelaziz, and H.M. Schatzl. 2018. Autophagy regulates exosomal release of prions in neuronal cells. *J Biol Chem*. 293:8956-8968.

Aguib, Y., A. Heiseke, S. Gilch, C. Riemer, M. Baier, H.M. Schatzl, and A. Ertmer. 2009. Autophagy induction by trehalose counteracts cellular prion infection. *Autophagy*. 5:361-369.

Aguzzi, A., F. Montrasio, and P.S. Kaeser. 2001. Prions: health scare and biological challenge. *Nature reviews. Molecular cell biology*. 2:118-126.

Ahmed, M., J. Davis, D. Aucoin, T. Sato, S. Ahuja, S. Aimoto, J.I. Elliott, W.E. Van Nostrand, and S.O. Smith. 2010. Structural conversion of neurotoxic amyloid-beta(1-42) oligomers to fibrils. *Nat Struct Mol Biol*. 17:561-567.

Ahn, Y.S., W. Jy, J.J. Jimenez, and L.L. Horstman. 2004. More on: Cellular microparticles: what are they bad or good for? *Journal of Thrombosis and Haemostasis*. 2:1215-1216.

Akers, J.C., D. Gonda, R. Kim, B.S. Carter, and C.C. Chen. 2013. Biogenesis of extracellular vesicles (EV): exosomes, microvesicles, retrovirus-like vesicles, and apoptotic bodies. *J Neurooncol*. 113:1-11.

Allinson, T.M., E.T. Parkin, A.J. Turner, and N.M. Hooper. 2003. ADAMs family members as amyloid precursor protein alpha-secretases. *J Neurosci Res*. 74:342-352.

Alvarez-Erviti, L., Y. Seow, A.H. Schapira, C. Gardiner, I.L. Sargent, M.J. Wood, and J.M. Cooper. 2011. Lysosomal dysfunction increases exosome-mediated alpha-synuclein release and transmission. *Neurobiol Dis*. 42:360-367.

Alzheimer, A., R.A. Stelzmann, H.N. Schnitzlein, and F.R. Murtagh. 1995. An English translation of Alzheimer's 1907 paper, "Uber eine eigenartige Erkankung der Hirnrinde". *Clin Anat*. 8:429-431.

Alzheimer-Society. 2010. Rising Tide: The Impact of Denentia on Canadian Society. . *In* Alzheimer Society of Canada. 1-66.

Anderson, N.G. 1966. An introduction to particle separations in zonal centrifuges. *Natl Cancer Inst Monogr*. 21:9-39.

Andreu, Z., E. Rivas, A. Sanguino-Pascual, A. Lamana, M. Marazuela, I. Gonzalez-Alvaro, F. Sanchez-Madrid, H. de la Fuente, and M. Yanez-Mo. 2016. Comparative analysis of EV isolation procedures for miRNAs detection in serum samples. *Journal of extracellular vesicles*. 5:31655.

Andreu, Z., and M. Yanez-Mo. 2014. Tetraspanins in extracellular vesicle formation and function. *Frontiers in immunology*. 5:442.

Ao, X., L. Zou, and Y. Wu. 2014. Regulation of autophagy by the Rab GTPase network. *Cell death and differentiation*. 21:348-358.

Armstrong, A., N. Mattsson, H. Appelqvist, C. Janefjord, L. Sandin, L. Agholme, B. Olsson, S. Svensson, K. Blennow, H. Zetterberg, and K. Kagedal. 2014. Lysosomal network proteins as potential novel CSF biomarkers for Alzheimer's disease. *Neuromolecular Med*. 16:150-160.

Aswad, H., A. Jalabert, and S. Rome. 2016. Depleting extracellular vesicles from fetal bovine serum alters proliferation and differentiation of skeletal muscle cells in vitro. *BMC Biotechnol*. 16:32.

Baixauli, F., C. Lopez-Otin, and M. Mittelbrunn. 2014. Exosomes and autophagy: coordinated mechanisms for the maintenance of cellular fitness. *Front Immunol*. 5:403.

Baranyai, T., K. Herczeg, Z. Onodi, I. Voszka, K. Modos, N. Marton, G. Nagy, I. Mager, M.J. Wood, S. El Andaloussi, Z. Palinkas, V. Kumar, P. Nagy, A. Kittel, E.I. Buzas, P. Ferdinandy, and Z. Giricz. 2015. Isolation of Exosomes from Blood Plasma: Qualitative and Quantitative Comparison of Ultracentrifugation and Size Exclusion Chromatography Methods. *PloS one*. 10:e0145686.

Barker, W.W., C.A. Luis, A. Kashuba, M. Luis, D.G. Harwood, D. Loewenstein, C. Waters, P. Jimison, E. Shepherd, S. Sevush, N. Graff-Radford, D. Newland, M. Todd, B. Miller, M. Gold, K. Heilman, L. Doty, I. Goodman, B. Robinson, G. Pearl, D. Dickson, and R. Duara. 2002. Relative frequencies of Alzheimer disease, Lewy body, vascular and frontotemporal dementia, and hippocampal sclerosis in the State of Florida Brain Bank. *Alzheimer Dis Assoc Disord*. 16:203-212.

Basso, M., and V. Bonetto. 2016. Extracellular Vesicles and a Novel Form of Communication in the Brain. *Front Neurosci*. 10:127.

Bateman, R.J., P.S. Aisen, B. De Strooper, N.C. Fox, C.A. Lemere, J.M. Ringman, S. Salloway, R.A. Sperling, M. Windisch, and C. Xiong. 2011. Autosomal-dominant Alzheimer's disease: a review and proposal for the prevention of Alzheimer's disease. *Alzheimers Res Ther*. 3:1.

Beal, M.F. 2005. Oxidative damage as an early marker of Alzheimer's disease and mild cognitive impairment. *Neurobiol Aging*. 26:585-586.

Bellingham, S.A., B.B. Guo, B.M. Coleman, and A.F. Hill. 2012. Exosomes: vehicles for the transfer of toxic proteins associated with neurodegenerative diseases? *Front Physiol*. 3:124.

Bento, C.F., C. Puri, K. Moreau, and D.C. Rubinsztein. 2013. The role of membrane-trafficking small GTPases in the regulation of autophagy. *J Cell Sci*. 126:1059-1069.

Benz, E.W., Jr., and H.L. Moses. 1974. Small, virus-like particles detected in bovine sera by electron microscopy. *J Natl Cancer Inst*. 52:1931-1934.

Bertram, L., and R.E. Tanzi. 2004. The current status of Alzheimer's disease genetics: what do we tell the patients? *Pharmacol Res*. 50:385-396.

Blennow, K., M.J. de Leon, and H. Zetterberg. 2006. Alzheimer's disease. *Lancet*. 368:387-403.

Bloch, K. 1965. The biological synthesis of cholesterol. *Science*. 150:19-28.

Blume, T., C. Focke, F. Peters, M. Deussing, N.L. Albert, S. Lindner, F.J. Gildehaus, B. von Ungern-Sternberg, L. Ozmen, K. Baumann, P. Bartenstein, A. Rominger, J. Herms, and M. Brendel. 2018. Microglial response to increasing amyloid load saturates with aging: a longitudinal dual tracer in vivo muPET-study. *J Neuroinflammation*. 15:307.

Bobrie, A., M. Colombo, S. Krumeich, G. Raposo, and C. Thery. 2012. Diverse subpopulations of vesicles secreted by different intracellular mechanisms are present in exosome preparations obtained by differential ultracentrifugation. *Journal of extracellular vesicles*. 1.

Boellaard, J.W., W. Schlote, and J. Tateishi. 1989. Neuronal autophagy in experimental Creutzfeldt-Jakob's disease. *Acta Neuropathol*. 78:410-418.

Boland, B., A. Kumar, S. Lee, F.M. Platt, J. Wegiel, W.H. Yu, and R.A. Nixon. 2008. Autophagy induction and autophagosome clearance in neurons: relationship to autophagic pathology in Alzheimer's disease. *The Journal of neuroscience : the official journal of the Society for Neuroscience*. 28:6926-6937.

Bordier, C. 1981. Phase separation of integral membrane proteins in Triton X-114 solution. *The Journal of biological chemistry*. 256:1604-1607.

Bove, J., M. Martinez-Vicente, and M. Vila. 2011. Fighting neurodegeneration with rapamycin: mechanistic insights. *Nat Rev Neurosci*. 12:437-452.

Braak, H., and E. Braak. 1991. Neuropathological stageing of Alzheimer-related changes. *Acta Neuropathol*. 82:239-259.

Brakke, M.K. 1953. Zonal separations by density-gradient centrifugation. *Arch Biochem Biophys*. 45:275-290.

Bucci, C., P. Thomsen, P. Nicoziani, J. McCarthy, and B. van Deurs. 2000. Rab7: a key to lysosome biogenesis. *Mol Biol Cell*. 11:467-480.

Buckholtz, N.S., L.M. Ryan, S. Petanceska, and L.M. Refolo. 2012. NIA commentary: translational issues in Alzheimer's disease drug development. *Neuropsychopharmacology*. 37:284-286.

Budnik, V., C. Ruiz-Canada, and F. Wendler. 2016. Extracellular vesicles round off communication in the nervous system. *Nat Rev Neurosci*. 17:160-172.

Caccamo, A., S. Majumder, A. Richardson, R. Strong, and S. Oddo. 2010. Molecular interplay between mammalian target of rapamycin (mTOR), amyloid-beta, and Tau: effects on cognitive impairments. *The Journal of biological chemistry*. 285:13107-13120.

Cantalupo, G., P. Alifano, V. Roberti, C.B. Bruni, and C. Bucci. 2001. Rab-interacting lysosomal protein (RILP): the Rab7 effector required for transport to lysosomes. *EMBO J*. 20:683-693.

Casey, P.J., and M.C. Seabra. 1996. Protein prenyltransferases. *The Journal of biological chemistry*. 271:5289-5292.

Castillo, K., V. Valenzuela, S. Matus, M. Nassif, M. Onate, Y. Fuentealba, G. Encina, T. Irrazabal, G. Parsons, F.A. Court, B.L. Schneider, D. Armentano, and C. Hetz. 2013. Measurement of autophagy flux in the nervous system in vivo. *Cell Death Dis*. 4:e917.

Chettimada, S., D.R. Lorenz, V. Misra, S.T. Dillon, R.K. Reeves, C. Manickam, S. Morgello, G.D. Kirk, S.H. Mehta, and D. Gabuzda. 2018. Exosome markers associated with immune activation and oxidative stress in HIV patients on antiretroviral therapy. *Sci Rep*. 8:7227.

Chishti, M.A., D.S. Yang, C. Janus, A.L. Phinney, P. Horne, J. Pearson, R. Strome, N. Zuker, J. Loukides, J. French, S. Turner, G. Lozza, M. Grilli, S. Kunicki, C. Morissette, J. Paquette, F. Gervais, C. Bergeron, P.E. Fraser, G.A. Carlson, P.S. George-Hyslop, and D. Westaway. 2001. Early-onset amyloid deposition and cognitive deficits in transgenic mice expressing a double mutant form of amyloid precursor protein 695. *The Journal of biological chemistry*. 276:21562-21570.

Chua, C.E., B.Q. Gan, and B.L. Tang. 2011. Involvement of members of the Rab family and related small GTPases in autophagosome formation and maturation. *Cell Mol Life Sci*. 68:3349-3358.

Citron, M., T. Oltersdorf, C. Haass, L. McConlogue, A.Y. Hung, P. Seubert, C. Vigo-Pelfrey, I. Lieberburg, and D.J. Selkoe. 1992. Mutation of the beta-amyloid precursor protein in familial Alzheimer's disease increases beta-protein production. *Nature*. 360:672-674.

Clayton, K.A., A.A. Van Enoo, and T. Ikezu. 2017. Alzheimer's Disease: The Role of Microglia in Brain Homeostasis and Proteopathy. *Front Neurosci*. 11:680.

Cocucci, E., G. Racchetti, and J. Meldolesi. 2009. Shedding microvesicles: artefacts no more. *Trends Cell Biol*. 19:43-51.

Colombo, M., G. Raposo, and C. Thery. 2014. Biogenesis, secretion, and intercellular interactions of exosomes and other extracellular vesicles. *Annual review of cell and developmental biology*. 30:255-289.

Connor, D.E., T. Exner, D.D. Ma, and J.E. Joseph. 2010. The majority of circulating platelet-derived microparticles fail to bind annexin V, lack phospholipid-dependent procoagulant activity and demonstrate greater expression of glycoprotein Ib. *Thromb Haemost*. 103:1044-1052.

Coumans, F.A.W., A.R. Brisson, E.I. Buzas, F. Dignat-George, E.E.E. Drees, S. El-Andaloussi, C. Emanueli, A. Gasecka, A. Hendrix, A.F. Hill, R. Lacroix, Y. Lee, T.G. van Leeuwen, N. Mackman, I. Mager, J.P. Nolan, E. van der Pol, D.M. Pegtel, S. Sahoo, P.R.M. Siljander, G. Sturk, O. de Wever, and R. Nieuwland. 2017. Methodological Guidelines to Study Extracellular Vesicles. *Circ Res*. 120:1632-1648.

Cvjetkovic, A., J. Lotvall, and C. Lasser. 2014. The influence of rotor type and centrifugation time on the yield and purity of extracellular vesicles. *Journal of extracellular vesicles*. 3.

Dachary-Prigent, J., J.M. Freyssinet, J.M. Pasquet, J.C. Carron, and A.T. Nurden. 1993. Annexin V as a probe of aminophospholipid exposure and platelet membrane vesiculation: a flow cytometry study showing a role for free sulfhydryl groups. *Blood*. 81:2554-2565.

Dacharyprigent, J., J.M. Freyssinet, J.M. Pasquet, J.C. Carron, and A.T. Nurden. 1993. Annexin-V as a Probe of Aminophospholipid Exposure and Platelet Membrane Vesiculation - a Flow-Cytometry Study Showing a Role for Free Sulfhydryl-Groups. *Blood*. 81:2554-2565.

Dahlgren, K.N., A.M. Manelli, W.B. Stine, Jr., L.K. Baker, G.A. Krafft, and M.J. LaDu. 2002. Oligomeric and fibrillar species of amyloid-beta peptides differentially affect neuronal viability. *The Journal of biological chemistry*. 277:32046-32053.

Danzer, K.M., L.R. Kranich, W.P. Ruf, O. Cagsal-Getkin, A.R. Winslow, L. Zhu, C.R. Vanderburg, and P.J. McLean. 2012. Exosomal cell-to-cell transmission of alpha synuclein oligomers. *Mol Neurodegener*. 7:42.

Desnoyers, L., J.S. Anant, and M.C. Seabra. 1996. Geranylgeranylation of Rab proteins. *Biochem Soc Trans*. 24:699-703.

Driedonks, T.A.P., M.K. Nijen Twilhaar, and E.N.M. Nolte-'t Hoen. 2019. Technical approaches to reduce interference of Fetal calf serum derived RNA in the analysis of extracellular vesicle RNA from cultured cells. *Journal of extracellular vesicles*. 8:1552059.

Eisele, Y.S., and C. Duyckaerts. 2016. Propagation of A beta pathology: hypotheses, discoveries, and yet unresolved questions from experimental and human brain studies. *Acta neuropathologica*. 131:5-25.
Eitan, E., C. Suire, S. Zhang, and M.P. Mattson. 2016. Impact of lysosome status on extracellular vesicle content and release. *Ageing Res Rev*. 32:65-74.
Eitan, E., S. Zhang, K.W. Witwer, and M.P. Mattson. 2015. Extracellular vesicle-depleted fetal bovine and human sera have reduced capacity to support cell growth. *Journal of extracellular vesicles*. 4:26373.
Emmanouilidou, E., K. Melachroinou, T. Roumeliotis, S.D. Garbis, M. Ntzouni, L.H. Margaritis, L. Stefanis, and K. Vekrellis. 2010. Cell-produced alpha-synuclein is secreted in a calcium-dependent manner by exosomes and impacts neuronal survival. *The Journal of neuroscience : the official journal of the Society for Neuroscience*. 30:6838-6851.
Erdbrugger, U., and J. Lannigan. 2016. Analytical challenges of extracellular vesicle detection: A comparison of different techniques. *Cytometry A*. 89:123-134.
Erdbrugger, U., C.K. Rudy, M.E. Etter, K.A. Dryden, M. Yeager, A.L. Klibanov, and J. Lannigan. 2014. Imaging flow cytometry elucidates limitations of microparticle analysis by conventional flow cytometry. *Cytometry A*. 85:756-770.
Fadeel, B., and D. Xue. 2009. The ins and outs of phospholipid asymmetry in the plasma membrane: roles in health and disease. *Crit Rev Biochem Mol Biol*. 44:264-277.
Fader, C.M., and M.I. Colombo. 2009. Autophagy and multivesicular bodies: two closely related partners. *Cell death and differentiation*. 16:70-78.
Fader, C.M., D. Sanchez, M. Furlan, and M.I. Colombo. 2008. Induction of autophagy promotes fusion of multivesicular bodies with autophagic vacuoles in k562 cells. *Traffic*. 9:230-250.
Feng, Y., B. Press, and A. Wandinger-Ness. 1995. Rab 7: an important regulator of late endocytic membrane traffic. *J Cell Biol*. 131:1435-1452.
Fevrier, B., and G. Raposo. 2004. Exosomes: endosomal-derived vesicles shipping extracellular messages. *Curr Opin Cell Biol*. 16:415-421.
Fevrier, B., D. Vilette, F. Archer, D. Loew, W. Faigle, M. Vidal, H. Laude, and G. Raposo. 2004. Cells release prions in association with exosomes. *Proceedings of the National Academy of Sciences of the United States of America*. 101:9683-9688.
Filipe, V., A. Hawe, and W. Jiskoot. 2010. Critical evaluation of Nanoparticle Tracking Analysis (NTA) by NanoSight for the measurement of nanoparticles and protein aggregates. *Pharm Res*. 27:796-810.
Fitzner, D., M. Schnaars, D. van Rossum, G. Krishnamoorthy, P. Dibaj, M. Bakhti, T. Regen, U.K. Hanisch, and M. Simons. 2011. Selective transfer of exosomes from oligodendrocytes to microglia by macropinocytosis. *J Cell Sci*. 124:447-458.
Frisken, B.J. 2001. Revisiting the method of cumulants for the analysis of dynamic light-scattering data. *Appl Opt*. 40:4087-4091.
Furukawa, K., B.L. Sopher, R.E. Rydel, J.G. Begley, D.G. Pham, G.M. Martin, M. Fox, and M.P. Mattson. 1996. Increased activity-regulating and neuroprotective efficacy of alpha-secretase-derived secreted amyloid precursor protein conferred by a C-terminal heparin-binding domain. *J Neurochem*. 67:1882-1896.
Gamez-Valero, A., M. Monguio-Tortajada, L. Carreras-Planella, M. Franquesa, K. Beyer, and F.E. Borras. 2016. Size-Exclusion Chromatography-based isolation minimally

alters Extracellular Vesicles' characteristics compared to precipitating agents. *Sci Rep*. 6:33641.
Gaugler, J., B. James, T. Johnson, A. Marin, J. Weuve, and A.s. Assoc. 2019. 2019 Alzheimer's disease facts and figures. *Alzheimers & Dementia*. 15:321-387.
Ghidoni, R., L. Benussi, and G. Binetti. 2008. Exosomes: the Trojan horses of neurodegeneration. *Med Hypotheses*. 70:1226-1227.
Ginsberg, S.D., E.J. Mufson, M.J. Alldred, S.E. Counts, J. Wuu, R.A. Nixon, and S. Che. 2011. Upregulation of select rab GTPases in cholinergic basal forebrain neurons in mild cognitive impairment and Alzheimer's disease. *J Chem Neuroanat*. 42:102-110.
Ginsberg, S.D., E.J. Mufson, S.E. Counts, J. Wuu, M.J. Alldred, R.A. Nixon, and S. Che. 2010. Regional selectivity of rab5 and rab7 protein upregulation in mild cognitive impairment and Alzheimer's disease. *J Alzheimers Dis*. 22:631-639.
Gorgens, A., M. Bremer, R. Ferrer-Tur, F. Murke, T. Tertel, P.A. Horn, S. Thalman, J.A. Welsh, C. Probst, C. Guerin, C.M. Boulanger, J.C. Jones, H. Hanenber, U. Erdbrugger, J. Lannigan, F.L. Ricklefs, S. El-Andaloussi, and B. Giebel. 2019. Optimisation of imaging flow cytometry for the analysis of single extracellular vesicles by using fluorescence-tagged vesicles as biological reference material. *Journal of extracellular vesicles*. 8.
Gould, S.J., and G. Raposo. 2013. As we wait: coping with an imperfect nomenclature for extracellular vesicles. *Journal of extracellular vesicles*. 2.
Green, D.R., and B. Levine. 2014. To Be or Not to Be? How Selective Autophagy and Cell Death Govern Cell Fate. *Cell*. 157:65-75.
Greening, D.W., R. Xu, H. Ji, B.J. Tauro, and R.J. Simpson. 2015. A protocol for exosome isolation and characterization: evaluation of ultracentrifugation, density-gradient separation, and immunoaffinity capture methods. *Methods Mol Biol*. 1295:179-209.
Guglielmotto, M., D. Monteleone, A. Piras, V. Valsecchi, M. Tropiano, S. Ariano, M. Fornaro, A. Vercelli, J. Puyal, O. Arancio, M. Tabaton, and E. Tamagno. 2014. Abeta1-42 monomers or oligomers have different effects on autophagy and apoptosis. *Autophagy*. 10:1827-1843.
Guo, J.L., and V.M. Lee. 2014. Cell-to-cell transmission of pathogenic proteins in neurodegenerative diseases. *Nature medicine*. 20:130-138.
Gutierrez, M.G., D.B. Munafo, W. Beron, and M.I. Colombo. 2004. Rab7 is required for the normal progression of the autophagic pathway in mammalian cells. *Journal of Cell Science*. 117:2687-2697.
Haass, C., C.A. Lemere, A. Capell, M. Citron, P. Seubert, D. Schenk, L. Lannfelt, and D.J. Selkoe. 1995. The Swedish mutation causes early-onset Alzheimer's disease by beta-secretase cleavage within the secretory pathway. *Nature medicine*. 1:1291-1296.
Hallbeck, M., S. Nath, and J. Marcusson. 2013. Neuron-to-neuron transmission of neurodegenerative pathology. *The Neuroscientist : a review journal bringing neurobiology, neurology and psychiatry*. 19:560-566.
Hansen, T.E., and T. Johansen. 2011. Following autophagy step by step. *BMC Biol*. 9:39.
Hara, T., K. Nakamura, M. Matsui, A. Yamamoto, Y. Nakahara, R. Suzuki-Migishima, M. Yokoyama, K. Mishima, I. Saito, H. Okano, and N. Mizushima. 2006. Suppression

of basal autophagy in neural cells causes neurodegenerative disease in mice. *Nature*. 441:885-889.
Haralick, R.M., K. Shanmugam, and I. Dinstein. 1973. Textural Features for Image Classification. *Ieee T Syst Man Cyb*. Smc3:610-621.
Harpin, M.L., A.B. Younes-Chennoufi, J.M. Boutry, C. Goujet-Zalc, J.J. Hauw, E. Yavin, and N. Baumann. 1990. Fetal calf serum gangliosides: quantitation and immunodetection of minor ones with R24 and A2B5 monoclonal antibodies. *In Vitro Cell Dev Biol*. 26:217-219.
Hasegawa, M., T. Nonaka, and M. Masuda-Suzukake. 2017. Prion-like mechanisms and potential therapeutic targets in neurodegenerative disorders. *Pharmacol Ther*. 172:22-33.
Heijnen, H.F., A.E. Schiel, R. Fijnheer, H.J. Geuze, and J.J. Sixma. 1999. Activated platelets release two types of membrane vesicles: microvesicles by surface shedding and exosomes derived from exocytosis of multivesicular bodies and alpha-granules. *Blood*. 94:3791-3799.
Heiseke, A., Y. Aguib, C. Riemer, M. Baier, and H.M. Schatzl. 2009. Lithium induces clearance of protease resistant prion protein in prion-infected cells by induction of autophagy. *J Neurochem*. 109:25-34.
Heiseke, A., Y. Aguib, and H.M. Schatzl. 2010. Autophagy, prion infection and their mutual interactions. *Curr Issues Mol Biol*. 12:87-97.
Heneka, M.T., M.J. Carson, J. El Khoury, G.E. Landreth, F. Brosseron, D.L. Feinstein, A.H. Jacobs, T. Wyss-Coray, J. Vitorica, R.M. Ransohoff, K. Herrup, S.A. Frautschy, B. Finsen, G.C. Brown, A. Verkhratsky, K. Yamanaka, J. Koistinaho, E. Latz, A. Halle, G.C. Petzold, T. Town, D. Morgan, M.L. Shinohara, V.H. Perry, C. Holmes, N.G. Bazan, D.J. Brooks, S. Hunot, B. Joseph, N. Deigendesch, O. Garaschuk, E. Boddeke, C.A. Dinarello, J.C. Breitner, G.M. Cole, D.T. Golenbock, and M.P. Kummer. 2015. Neuroinflammation in Alzheimer's disease. *Lancet Neurol*. 14:388-405.
Henne, W.M., N.J. Buchkovich, and S.D. Emr. 2011. The ESCRT pathway. *Dev Cell*. 21:77-91.
Hessvik, N.P., and A. Llorente. 2018. Current knowledge on exosome biogenesis and release. *Cell Mol Life Sci*. 75:193-208.
Hessvik, N.P., A. Overbye, A. Brech, M.L. Torgersen, I.S. Jakobsen, K. Sandvig, and A. Llorente. 2016. PIKfyve inhibition increases exosome release and induces secretory autophagy. *Cell Mol Life Sci*. 73:4717-4737.
Holtzman, D.M., J.C. Morris, and A.M. Goate. 2011. Alzheimer's disease: the challenge of the second century. *Sci Transl Med*. 3:77sr71.
Honig, M.G., and R.I. Hume. 1986. Fluorescent carbocyanine dyes allow living neurons of identified origin to be studied in long-term cultures. *J Cell Biol*. 103:171-187.
Hornick, N.I., J. Huan, B. Doron, N.A. Goloviznina, J. Lapidus, B.H. Chang, and P. Kurre. 2015. Serum Exosome MicroRNA as a Minimally-Invasive Early Biomarker of AML. *Sci Rep*. 5:11295.
Huotari, J., and A. Helenius. 2011. Endosome maturation. *EMBO J*. 30:3481-3500.
Hyttinen, J.M., M. Niittykoski, A. Salminen, and K. Kaarniranta. 2013. Maturation of autophagosomes and endosomes: a key role for Rab7. *Biochimica et biophysica acta*. 1833:503-510.

Jager, S., C. Bucci, I. Tanida, T. Ueno, E. Kominami, P. Saftig, and E.L. Eskelinen. 2004. Role for Rab7 in maturation of late autophagic vacuoles. *Journal of Cell Science*. 117:4837-4848.

Johansson, M., N. Rocha, W. Zwart, I. Jordens, L. Janssen, C. Kuijl, V.M. Olkkonen, and J. Neefjes. 2007. Activation of endosomal dynein motors by stepwise assembly of Rab7-RILP-p150(Glued), ORP1L, and the receptor beta III spectrin. *Journal of Cell Biology*. 176:459-471.

Johnstone, R.M., M. Adam, J.R. Hammond, L. Orr, and C. Turbide. 1987. Vesicle formation during reticulocyte maturation. Association of plasma membrane activities with released vesicles (exosomes). *The Journal of biological chemistry*. 262:9412-9420.

Joshi, P., L. Benussi, R. Furlan, R. Ghidoni, and C. Verderio. 2015. Extracellular vesicles in Alzheimer's disease: friends or foes? Focus on abeta-vesicle interaction. *Int J Mol Sci*. 16:4800-4813.

Joshi, P., E. Turola, A. Ruiz, A. Bergami, D.D. Libera, L. Benussi, P. Giussani, G. Magnani, G. Comi, G. Legname, R. Ghidoni, R. Furlan, M. Matteoli, and C. Verderio. 2014. Microglia convert aggregated amyloid-beta into neurotoxic forms through the shedding of microvesicles. *Cell death and differentiation*. 21:582-593.

Kang, J., H.G. Lemaire, A. Unterbeck, J.M. Salbaum, C.L. Masters, K.H. Grzeschik, G. Multhaup, K. Beyreuther, and B. Muller-Hill. 1987. The precursor of Alzheimer's disease amyloid A4 protein resembles a cell-surface receptor. *Nature*. 325:733-736.

Kaur, J., and J. Debnath. 2015. Autophagy at the crossroads of catabolism and anabolism. *Nature reviews. Molecular cell biology*. 16:461-472.

Kennedy, A.M., S. Newman, A. McCaddon, J. Ball, P. Roques, M. Mullan, J. Hardy, M.C. Chartier-Harlin, R.S. Frackowiak, E.K. Warrington, and et al. 1993. Familial Alzheimer's disease. A pedigree with a mis-sense mutation in the amyloid precursor protein gene (amyloid precursor protein 717 valine-->glycine). *Brain : a journal of neurology*. 116 (Pt 2):309-324.

Kimura, S., T. Noda, and T. Yoshimori. 2007. Dissection of the autophagosome maturation process by a novel reporter protein, tandem fluorescent-tagged LC3. *Autophagy*. 3:452-460.

Klein, A.M., N.W. Kowall, and R.J. Ferrante. 1999. Neurotoxicity and oxidative damage of beta amyloid 1-42 versus beta amyloid 1-40 in the mouse cerebral cortex. *Ann N Y Acad Sci*. 893:314-320.

Klionsky, D.J. 2005. The molecular machinery of autophagy: unanswered questions. *Journal of Cell Science*. 118:7-18.

Klionsky, D.J., F.C. Abdalla, H. Abeliovich, R.T. Abraham, A. Acevedo-Arozena, K. Adeli, L. Agholme, M. Agnello, P. Agostinis, J.A. Aguirre-Ghiso, H.J. Ahn, O. Ait-Mohamed, S. Ait-Si-Ali, T. Akematsu, S. Akira, H.M. Al-Younes, M.A. Al-Zeer, M.L. Albert, R.L. Albin, J. Alegre-Abarrategui, M.F. Aleo, M. Alirezaei, A. Almasan, M. Almonte-Becerril, A. Amano, R. Amaravadi, S. Amarnath, A.O. Amer, N. Andrieu-Abadie, V. Anantharam, D.K. Ann, S. Anoopkumar-Dukie, H. Aoki, N. Apostolova, G. Arancia, J.P. Aris, K. Asanuma, N.Y.O. Asare, H. Ashida, V. Askanas, D.S. Askew, P. Auberger, M. Baba, S.K. Backues, E.H. Baehrecke, B.A. Bahr, X.Y. Bai, Y. Bailly, R. Baiocchi, G. Baldini, W. Balduini, A. Ballabio, B.A. Bamber, E.T.W. Bampton, G. Banhegyi, C.R.

Bartholomew, D.C. Bassham, R.C. Bast, H. Batoko, B.H. Bay, I. Beau, D.M. Bechet, T.J. Begley, C. Behl, C. Behrends, S. Bekri, B. Bellaire, L.J. Bendall, L. Benetti, L. Berliocchi, H. Bernardi, F. Bernassola, S. Besteiro, I. Bhatia-Kissova, X.N. Bi, M. Biard-Piechaczyk, J.S. Blum, L.H. Boise, P. Bonaldo, D.L. Boone, B.C. Bornhauser, K.R. Bortoluci, I. Bossis, F. Bost, J.P. Bourquin, P. Boya, M. Boyer-Guittaut, P.V. Bozhkov, N.R. Brady, C. Brancolini, A. Brech, J.E. Brenman, A. Brennand, E.H. Bresnick, P. Brest, D. Bridges, M.L. Bristol, P.S. Brookes, E.J. Brown, J.H. Brumell, et al. 2012. Guidelines for the use and interpretation of assays for monitoring autophagy. *Autophagy*. 8:445-544.

Kokubo, H., T.C. Saido, N. Iwata, J.B. Helms, R. Shinohara, and H. Yamaguchi. 2005. Part of membrane-bound Abeta exists in rafts within senile plaques in Tg2576 mouse brain. *Neurobiol Aging*. 26:409-418.

Komatsu, M., S. Waguri, T. Chiba, S. Murata, J. Iwata, I. Tanida, T. Ueno, M. Koike, Y. Uchiyama, E. Kominami, and K. Tanaka. 2006. Loss of autophagy in the central nervous system causes neurodegeneration in mice. *Nature*. 441:880-884.

Konoshenko, M.Y., E.A. Lekchnov, A.V. Vlassov, and P.P. Laktionov. 2018. Isolation of Extracellular Vesicles: General Methodologies and Latest Trends. *Biomed Res Int*. 2018:8545347.

Koo, E.H., and S.L. Squazzo. 1994. Evidence that production and release of amyloid beta-protein involves the endocytic pathway. *The Journal of biological chemistry*. 269:17386-17389.

Korolchuk, V.I., S. Saiki, M. Lichtenberg, F.H. Siddiqi, E.A. Roberts, S. Imarisio, L. Jahreiss, S. Sarkar, M. Futter, F.M. Menzies, C.J. O'Kane, V. Deretic, and D.C. Rubinsztein. 2011. Lysosomal positioning coordinates cellular nutrient responses. *Nat Cell Biol*. 13:453-460.

Kowal, J., G. Arras, M. Colombo, M. Jouve, J.P. Morath, B. Primdal-Bengtson, F. Dingli, D. Loew, M. Tkach, and C. Thery. 2016. Proteomic comparison defines novel markers to characterize heterogeneous populations of extracellular vesicle subtypes. *Proceedings of the National Academy of Sciences of the United States of America*. 113:E968-977.

Kowal, J., M. Tkach, and C. Thery. 2014. Biogenesis and secretion of exosomes. *Current opinion in cell biology*. 29:116-125.

Kreutzberg, G.W. 1996. Microglia: a sensor for pathological events in the CNS. *Trends Neurosci*. 19:312-318.

LaFerla, F.M., K.N. Green, and S. Oddo. 2007. Intracellular amyloid-beta in Alzheimer's disease. *Nat Rev Neurosci*. 8:499-509.

Lamparski, H.G., A. Metha-Damani, J.Y. Yao, S. Patel, D.H. Hsu, C. Ruegg, and J.B. Le Pecq. 2002. Production and characterization of clinical grade exosomes derived from dendritic cells. *J Immunol Methods*. 270:211-226.

Lane, R.E., D. Korbie, M.M. Hill, and M. Trau. 2018. Extracellular vesicles as circulating cancer biomarkers: opportunities and challenges. *Clin Transl Med*. 7.

Lannigan, J., and U. Erdbruegger. 2017. Imaging flow cytometry for the characterization of extracellular vesicles. *Methods*. 112:55-67.

Lassailly, F., E. Griessinger, and D. Bonnet. 2010. "Microenvironmental contaminations" induced by fluorescent lipophilic dyes used for noninvasive in vitro and in vivo cell tracking. *Blood*. 115:5347-5354.

Lee, H.J., E.D. Cho, K.W. Lee, J.H. Kim, S.G. Cho, and S.J. Lee. 2013. Autophagic failure promotes the exocytosis and intercellular transfer of alpha-synuclein. *Exp Mol Med*. 45:e22.

Lee, S., Y. Sato, and R.A. Nixon. 2011. Lysosomal proteolysis inhibition selectively disrupts axonal transport of degradative organelles and causes an Alzheimer's-like axonal dystrophy. *The Journal of neuroscience : the official journal of the Society for Neuroscience*. 31:7817-7830.

Lee, T.L., Y.C. Lin, K. Mochitate, and F. Grinnell. 1993. Stress-relaxation of fibroblasts in collagen matrices triggers ectocytosis of plasma membrane vesicles containing actin, annexins II and VI, and beta 1 integrin receptors. *J Cell Sci*. 105 (Pt 1):167-177.

Lehrich, B.M., Y.X. Liang, P. Khosravi, H.J. Federoff, and M.S. Fiandaca. 2018. Fetal Bovine Serum-Derived Extracellular Vesicles Persist within Vesicle-Depleted Culture Media. *International Journal of Molecular Sciences*. 19.

Li, J., Y. Lee, H.J. Johansson, I. Mager, P. Vader, J.Z. Nordin, O.P. Wiklander, J. Lehtio, M.J. Wood, and S.E. Andaloussi. 2015. Serum-free culture alters the quantity and protein composition of neuroblastoma-derived extracellular vesicles. *Journal of extracellular vesicles*. 4:26883.

Linares, R., S. Tan, C. Gounou, N. Arraud, and A.R. Brisson. 2015. High-speed centrifugation induces aggregation of extracellular vesicles. *Journal of extracellular vesicles*. 4:29509.

Livshits, M.A., E. Khomyakova, E.G. Evtushenko, V.N. Lazarev, N.A. Kulemin, S.E. Semina, E.V. Generozov, and V.M. Govorun. 2015. Isolation of exosomes by differential centrifugation: Theoretical analysis of a commonly used protocol. *Sci Rep*. 5:17319.

Lobb, R.J., M. Becker, S.W. Wen, C.S. Wong, A.P. Wiegmans, A. Leimgruber, and A. Moller. 2015. Optimized exosome isolation protocol for cell culture supernatant and human plasma. *Journal of extracellular vesicles*. 4:27031.

Lotvall, J., A.F. Hill, F. Hochberg, E.I. Buzas, D. Di Vizio, C. Gardiner, Y.S. Gho, I.V. Kurochkin, S. Mathivanan, P. Quesenberry, S. Sahoo, H. Tahara, M.H. Wauben, K.W. Witwer, and C. Thery. 2014. Minimal experimental requirements for definition of extracellular vesicles and their functions: a position statement from the International Society for Extracellular Vesicles. *Journal of extracellular vesicles*. 3:26913.

Mastoridis, S., G.M. Bertolino, G. Whitehouse, F. Dazzi, A. Sanchez-Fueyo, and M. Martinez-Llordella. 2018. Multiparametric Analysis of Circulating Exosomes and Other Small Extracellular Vesicles by Advanced Imaging Flow Cytometry. *Frontiers in immunology*. 9:1583.

McCullough, J., R.D. Fisher, F.G. Whitby, W.I. Sundquist, and C.P. Hill. 2008. ALIX-CHMP4 interactions in the human ESCRT pathway. *Proceedings of the National Academy of Sciences of the United States of America*. 105:7687-7691.

McLean, C.A., R.A. Cherny, F.W. Fraser, S.J. Fuller, M.J. Smith, K. Beyreuther, A.I. Bush, and C.L. Masters. 1999. Soluble pool of Abeta amyloid as a determinant of severity of neurodegeneration in Alzheimer's disease. *Annals of neurology*. 46:860-866.

McTaggart, S.J. 2006. Isoprenylated proteins. *Cell Mol Life Sci*. 63:255-267.

Melo, S.A., L.B. Luecke, C. Kahlert, A.F. Fernandez, S.T. Gammon, J. Kaye, V.S. LeBleu, E.A. Mittendorf, J. Weitz, N. Rahbari, C. Reissfelder, C. Pilarsky, M.F. Fraga, D. Piwnica-Worms, and R. Kalluri. 2015. Glypican-1 identifies cancer exosomes and detects early pancreatic cancer. *Nature*. 523:177-182.

Meyer-Luehmann, M., J. Coomaraswamy, T. Bolmont, S. Kaeser, C. Schaefer, E. Kilger, A. Neuenschwander, D. Abramowski, P. Frey, A.L. Jaton, J.M. Vigouret, P. Paganetti, D.M. Walsh, P.M. Mathews, J. Ghiso, M. Staufenbiel, L.C. Walker, and M. Jucker. 2006. Exogenous induction of cerebral beta-amyloidogenesis is governed by agent and host. *Science*. 313:1781-1784.

Meziane, H., J.C. Dodart, C. Mathis, S. Little, J. Clemens, S.M. Paul, and A. Ungerer. 1998. Memory-enhancing effects of secreted forms of the beta-amyloid precursor protein in normal and amnestic mice. *Proceedings of the National Academy of Sciences of the United States of America*. 95:12683-12688.

Milne, J.L., M.J. Borgnia, A. Bartesaghi, E.E. Tran, L.A. Earl, D.M. Schauder, J. Lengyel, J. Pierson, A. Patwardhan, and S. Subramaniam. 2013. Cryo-electron microscopy--a primer for the non-microscopist. *FEBS J*. 280:28-45.

Mizuno-Yamasaki, E., F. Rivera-Molina, and P. Novick. 2012. GTPase Networks in Membrane Traffic. *Annual Review of Biochemistry, Vol 81*. 81:637-659.

Mohamed, A., L. Saavedra, A. Di Pardo, S. Sipione, and E. Posse de Chaves. 2012. beta-amyloid inhibits protein prenylation and induces cholesterol sequestration by impairing SREBP-2 cleavage. *The Journal of neuroscience : the official journal of the Society for Neuroscience*. 32:6490-6500.

Mohamed, A., A. Viveiros, K. Williams, and E. Posse de Chaves. 2018. Abeta inhibits SREBP-2 activation through Akt inhibition. *J Lipid Res*. 59:1-13.

Momen-Heravi, F., L. Balaj, S. Alian, A.J. Trachtenberg, F.H. Hochberg, J. Skog, and W.P. Kuo. 2012. Impact of biofluid viscosity on size and sedimentation efficiency of the isolated microvesicles. *Front Physiol*. 3:162.

Morel, O., L. Jesel, J.M. Freyssinet, and F. Toti. 2011. Cellular mechanisms underlying the formation of circulating microparticles. *Arterioscler Thromb Vasc Biol*. 31:15-26.

Muralidharan-Chari, V., J. Clancy, C. Plou, M. Romao, P. Chavrier, G. Raposo, and C. D'Souza-Schorey. 2009. ARF6-regulated shedding of tumor cell-derived plasma membrane microvesicles. *Curr Biol*. 19:1875-1885.

Nath, S., L. Agholme, F.R. Kurudenkandy, B. Granseth, J. Marcusson, and M. Hallbeck. 2012. Spreading of neurodegenerative pathology via neuron-to-neuron transmission of beta-amyloid. *The Journal of neuroscience : the official journal of the Society for Neuroscience*. 32:8767-8777.

Ng, E.L., and B.L. Tang. 2008. Rab GTPases and their roles in brain neurons and glia. *Brain Res Rev*. 58:236-246.

Nickel, W., and C. Rabouille. 2018. Unconventional protein secretion: Diversity and consensus. *Semin Cell Dev Biol*. 83:1-2.

Nielsen, E., F. Severin, J.M. Backer, A.A. Hyman, and M. Zerial. 1999. Rab5 regulates motility of early endosomes on microtubules. *Nat Cell Biol*. 1:376-382.

Nixon, R.A. 2007. Autophagy, amyloidogenesis and Alzheimer disease. *J Cell Sci*. 120:4081-4091.

Nixon, R.A. 2013. The role of autophagy in neurodegenerative disease. *Nature medicine*. 19:983-997.

Nixon, R.A., J. Wegiel, A. Kumar, W.H. Yu, C. Peterhoff, A. Cataldo, and A.M. Cuervo. 2005. Extensive involvement of autophagy in Alzheimer disease: an immuno-electron microscopy study. *J Neuropathol Exp Neurol*. 64:113-122.
Nixon, R.A., and D.S. Yang. 2011. Autophagy failure in Alzheimer's disease--locating the primary defect. *Neurobiol Dis*. 43:38-45.
Nixon, R.A., and D.S. Yang. 2012. Autophagy and neuronal cell death in neurological disorders. *Cold Spring Harb Perspect Biol*. 4.
O'Brien, R.J., and P.C. Wong. 2011. Amyloid precursor protein processing and Alzheimer's disease. *Annu Rev Neurosci*. 34:185-204.
Ortyn, W.E., B.E. Hall, T.C. George, K. Frost, D.A. Basiji, D.J. Perry, C.A. Zimmerman, D. Coder, and P.J. Morrissey. 2006. Sensitivity measurement and compensation in spectral imaging. *Cytometry A*. 69:852-862.
Palade, G. 1975. Intracellular aspects of the process of protein synthesis. *Science*. 189:347-358.
Pan, B.T., K. Teng, C. Wu, M. Adam, and R.M. Johnstone. 1985. Electron microscopic evidence for externalization of the transferrin receptor in vesicular form in sheep reticulocytes. *J Cell Biol*. 101:942-948.
Panda, T., T. Basak, G. Saraswathi, and T. Theodore. 2011. Kinetic Mechanisms of Cholesterol Synthesis: A Review. *Ind Eng Chem Res*. 50:12847-12864.
Paravastu, A.K., I. Qahwash, R.D. Leapman, S.C. Meredith, and R. Tycko. 2009. Seeded growth of beta-amyloid fibrils from Alzheimer's brain-derived fibrils produces a distinct fibril structure. *Proceedings of the National Academy of Sciences of the United States of America*. 106:7443-7448.
Pereira-Leal, J.B., and M.C. Seabra. 2000. The mammalian Rab family of small GTPases: definition of family and subfamily sequence motifs suggests a mechanism for functional specificity in the Ras superfamily. *J Mol Biol*. 301:1077-1087.
Petkova, A.T., R.D. Leapman, Z. Guo, W.M. Yau, M.P. Mattson, and R. Tycko. 2005. Self-propagating, molecular-level polymorphism in Alzheimer's beta-amyloid fibrils. *Science*. 307:262-265.
Poehler, A.M., W. Xiang, P. Spitzer, V.E. May, H. Meixner, E. Rockenstein, O. Chutna, T.F. Outeiro, J. Winkler, E. Masliah, and J. Klucken. 2014. Autophagy modulates SNCA/alpha-synuclein release, thereby generating a hostile microenvironment. *Autophagy*. 10:2171-2192.
Press, B., Y. Feng, B. Hoflack, and A. Wandinger-Ness. 1998. Mutant Rab7 causes the accumulation of cathepsin D and cation-independent mannose 6-phosphate receptor in an early endocytic compartment. *Journal of Cell Biology*. 140:1075-1089.
Prusiner, S.B. 1998. Prions. *Proceedings of the National Academy of Sciences of the United States of America*. 95:13363-13383.
Rabouille, C. 2017. Pathways of Unconventional Protein Secretion. *Trends Cell Biol*. 27:230-240.
Rabouille, C., V. Malhotra, and W. Nickel. 2012. Diversity in unconventional protein secretion. *J Cell Sci*. 125:5251-5255.
Rajendran, L., M. Honsho, T.R. Zahn, P. Keller, K.D. Geiger, P. Verkade, and K. Simons. 2006. Alzheimer's disease beta-amyloid peptides are released in association

with exosomes. *Proceedings of the National Academy of Sciences of the United States of America*. 103:11172-11177.
Rana, S., S. Yue, D. Stadel, and M. Zoller. 2012. Toward tailored exosomes: the exosomal tetraspanin web contributes to target cell selection. *Int J Biochem Cell Biol*. 44:1574-1584.
Raposo, G., and W. Stoorvogel. 2013. Extracellular vesicles: exosomes, microvesicles, and friends. *J Cell Biol*. 200:373-383.
Ruiz-Riquelme, A., H.H.C. Lau, E. Stuart, A.N. Goczi, Z. Wang, G. Schmitt-Ulms, and J.C. Watts. 2018. Prion-like propagation of beta-amyloid aggregates in the absence of APP overexpression. *Acta Neuropathol Commun*. 6:26.
Sato, N., K. Hotta, S. Waguri, T. Nitatori, K. Tohyama, Y. Tsujimoto, and Y. Uchiyama. 1994. Neuronal differentiation of PC12 cells as a result of prevention of cell death by bcl-2. *J Neurobiol*. 25:1227-1234.
Saxena, S., C. Bucci, J. Weis, and A. Kruttgen. 2005. The small GTPase Rab7 controls the endosomal trafficking and neuritogenic signaling of the nerve growth factor receptor TrkA. *Journal of Neuroscience*. 25:10930-10940.
Schagger, H. 2006. Tricine-SDS-PAGE. *Nat Protoc*. 1:16-22.
Schatz, G., and B. Dobberstein. 1996. Common principles of protein translocation across membranes. *Science*. 271:1519-1526.
Selkoe, D.J. 2001. Alzheimer's disease: genes, proteins, and therapy. *Physiol Rev*. 81:741-766.
Selkoe, D.J. 2008a. Biochemistry and molecular biology of amyloid beta-protein and the mechanism of Alzheimer's disease. *Handb Clin Neurol*. 89:245-260.
Selkoe, D.J. 2008b. Soluble oligomers of the amyloid beta-protein impair synaptic plasticity and behavior. *Behavioural brain research*. 192:106-113.
Shao, H., H. Im, C.M. Castro, X. Breakefield, R. Weissleder, and H. Lee. 2018. New Technologies for Analysis of Extracellular Vesicles. *Chem Rev*. 118:1917-1950.
Shelke, G.V., C. Lasser, Y.S. Gho, and J. Lotvall. 2014. Importance of exosome depletion protocols to eliminate functional and RNA-containing extracellular vesicles from fetal bovine serum. *J Extracell Vesicles*. 3.
Simons, M., and G. Raposo. 2009. Exosomes--vesicular carriers for intercellular communication. *Current opinion in cell biology*. 21:575-581.
Sinha, M.S., A. Ansell-Schultz, L. Civitelli, C. Hildesjo, M. Larsson, L. Lannfelt, M. Ingelsson, and M. Hallbeck. 2018. Alzheimer's disease pathology propagation by exosomes containing toxic amyloid-beta oligomers. *Acta Neuropathologica*. 136:41-56.
Smith, K.T. 2016. Amyloid-beta Causes Autophagy Dysfunction by Inhibiting Protein Prenylation. *In* Center for Neuroscience Vol. MSc. University of Alberta.
Spilman, P., N. Podlutskaya, M.J. Hart, J. Debnath, O. Gorostiza, D. Bredesen, A. Richardson, R. Strong, and V. Galvan. 2010. Inhibition of mTOR by rapamycin abolishes cognitive deficits and reduces amyloid-beta levels in a mouse model of Alzheimer's disease. *PloS one*. 5:e9979.
St George-Hyslop, P.H., R.E. Tanzi, R.J. Polinsky, J.L. Haines, L. Nee, P.C. Watkins, R.H. Myers, R.G. Feldman, D. Pollen, D. Drachman, and et al. 1987. The genetic defect causing familial Alzheimer's disease maps on chromosome 21. *Science*. 235:885-890.

Stein, J.M., and J.P. Luzio. 1991. Ectocytosis caused by sublytic autologous complement attack on human neutrophils. The sorting of endogenous plasma-membrane proteins and lipids into shed vesicles. *The Biochemical journal*. 274 (Pt 2):381-386.

Stohr, J., J.C. Watts, Z.L. Mensinger, A. Oehler, S.K. Grillo, S.J. DeArmond, S.B. Prusiner, and K. Giles. 2012. Purified and synthetic Alzheimer's amyloid beta (Abeta) prions. *Proceedings of the National Academy of Sciences of the United States of America*. 109:11025-11030.

Stuffers, S., C. Sem Wegner, H. Stenmark, and A. Brech. 2009. Multivesicular endosome biogenesis in the absence of ESCRTs. *Traffic*. 10:925-937.

Takahashi, R.H., T.A. Milner, F. Li, E.E. Nam, M.A. Edgar, H. Yamaguchi, M.F. Beal, H. Xu, P. Greengard, and G.K. Gouras. 2002. Intraneuronal Alzheimer abeta42 accumulates in multivesicular bodies and is associated with synaptic pathology. *The American journal of pathology*. 161:1869-1879.

Takai, Y., T. Sasaki, and T. Matozaki. 2001. Small GTP-binding proteins. *Physiol Rev*. 81:153-208.

Tauro, B.J., R.A. Mathias, D.W. Greening, S.K. Gopal, H. Ji, E.A. Kapp, B.M. Coleman, A.F. Hill, U. Kusebauch, J.L. Hallows, D. Shteynberg, R.L. Moritz, H.J. Zhu, and R.J. Simpson. 2013. Oncogenic H-ras reprograms Madin-Darby canine kidney (MDCK) cell-derived exosomal proteins following epithelial-mesenchymal transition. *Mol Cell Proteomics*. 12:2148-2159.

Taylor, D.D., and S. Shah. 2015. Methods of isolating extracellular vesicles impact down-stream analyses of their cargoes. *Methods*. 87:3-10.

Thal, D.R., U. Rub, M. Orantes, and H. Braak. 2002. Phases of A beta-deposition in the human brain and its relevance for the development of AD. *Neurology*. 58:1791-1800.

Thery, C., S. Amigorena, G. Raposo, and A. Clayton. 2006. Isolation and characterization of exosomes from cell culture supernatants and biological fluids. *Curr Protoc Cell Biol*. Chapter 3:Unit 3 22.

Thery, C., M. Ostrowski, and E. Segura. 2009. Membrane vesicles as conveyors of immune responses. *Nat Rev Immunol*. 9:581-593.

Thery, C., A. Regnault, J. Garin, J. Wolfers, L. Zitvogel, P. Ricciardi-Castagnoli, G. Raposo, and S. Amigorena. 1999. Molecular characterization of dendritic cell-derived exosomes. Selective accumulation of the heat shock protein hsc73. *J Cell Biol*. 147:599-610.

Thery, C., K.W. Witwer, E. Aikawa, M.J. Alcaraz, J.D. Anderson, R. Andriantsitohaina, A. Antoniou, T. Arab, F. Archer, G.K. Atkin-Smith, D.C. Ayre, J.M. Bach, D. Bachurski, H. Baharvand, L. Balaj, S. Baldacchino, N.N. Bauer, A.A. Baxter, M. Bebawy, C. Beckham, A. Bedina Zavec, A. Benmoussa, A.C. Berardi, P. Bergese, E. Bielska, C. Blenkiron, S. Bobis-Wozowicz, E. Boilard, W. Boireau, A. Bongiovanni, F.E. Borras, S. Bosch, C.M. Boulanger, X. Breakefield, A.M. Breglio, M.A. Brennan, D.R. Brigstock, A. Brisson, M.L. Broekman, J.F. Bromberg, P. Bryl-Gorecka, S. Buch, A.H. Buck, D. Burger, S. Busatto, D. Buschmann, B. Bussolati, E.I. Buzas, J.B. Byrd, G. Camussi, D.R. Carter, S. Caruso, L.W. Chamley, Y.T. Chang, C. Chen, S. Chen, L. Cheng, A.R. Chin, A. Clayton, S.P. Clerici, A. Cocks, E. Cocucci, R.J. Coffey, A. Cordeiro-da-Silva, Y. Couch, F.A. Coumans, B. Coyle, R. Crescitelli, M.F. Criado, C.

D'Souza-Schorey, S. Das, A. Datta Chaudhuri, P. de Candia, E.F. De Santana, O. De Wever, H.A. Del Portillo, T. Demaret, S. Deville, A. Devitt, B. Dhondt, D. Di Vizio, L.C. Dieterich, V. Dolo, A.P. Dominguez Rubio, M. Dominici, M.R. Dourado, T.A. Driedonks, F.V. Duarte, H.M. Duncan, R.M. Eichenberger, K. Ekstrom, S. El Andaloussi, C. Elie-Caille, U. Erdbrugger, J.M. Falcon-Perez, F. Fatima, J.E. Fish, M. Flores-Bellver, A. Forsonits, A. Frelet-Barrand, et al. 2018. Minimal information for studies of extracellular vesicles 2018 (MISEV2018): a position statement of the International Society for Extracellular Vesicles and update of the MISEV2014 guidelines. *Journal of extracellular vesicles*. 7:1535750.

Thery, C., L. Zitvogel, and S. Amigorena. 2002. Exosomes: composition, biogenesis and function. *Nat Rev Immunol*. 2:569-579.

Thiagarajan, P., and J.F. Tait. 1991. Collagen-induced exposure of anionic phospholipid in platelets and platelet-derived microparticles. *The Journal of biological chemistry*. 266:24302-24307.

Thinakaran, G., and E.H. Koo. 2008. Amyloid precursor protein trafficking, processing, and function. *The Journal of biological chemistry*. 283:29615-29619.

Thinakaran, G., D.B. Teplow, R. Siman, B. Greenberg, and S.S. Sisodia. 1996. Metabolism of the "Swedish" amyloid precursor protein variant in neuro2a (N2a) cells. Evidence that cleavage at the "beta-secretase" site occurs in the golgi apparatus. *The Journal of biological chemistry*. 271:9390-9397.

Tkach, M., J. Kowal, and C. Thery. 2018. Why the need and how to approach the functional diversity of extracellular vesicles. *Philos Trans R Soc Lond B Biol Sci*. 373.

Torres, L.L., N.B. Quaglio, G.T. de Souza, R.T. Garcia, L.M. Dati, W.L. Moreira, A.P. Loureiro, J.N. de Souza-Talarico, J. Smid, C.S. Porto, C.M. Bottino, R. Nitrini, S.B. Barros, R. Camarini, and T. Marcourakis. 2011. Peripheral oxidative stress biomarkers in mild cognitive impairment and Alzheimer's disease. *J Alzheimers Dis*. 26:59-68.

Tosar, J.P., A. Cayota, E. Eitan, M.K. Halushka, and K.W. Witwer. 2017. Ribonucleic artefacts: are some extracellular RNA discoveries driven by cell culture medium components? *Journal of extracellular vesicles*. 6:1272832.

Trajkovic, K., C. Hsu, S. Chiantia, L. Rajendran, D. Wenzel, F. Wieland, P. Schwille, B. Brugger, and M. Simons. 2008. Ceramide triggers budding of exosome vesicles into multivesicular endosomes. *Science*. 319:1244-1247.

Trams, E.G., C.J. Lauter, N. Salem, Jr., and U. Heine. 1981. Exfoliation of membrane ecto-enzymes in the form of micro-vesicles. *Biochimica et biophysica acta*. 645:63-70.

Usman, W.M., T.C. Pham, Y.Y. Kwok, L.T. Vu, V. Ma, B. Peng, Y.S. Chan, L. Wei, S.M. Chin, A. Azad, A.B. He, A.Y.H. Leung, M. Yang, N. Shyh-Chang, W.C. Cho, J. Shi, and M.T.N. Le. 2018. Efficient RNA drug delivery using red blood cell extracellular vesicles. *Nat Commun*. 9:2359.

Vader, P., E.A. Mol, G. Pasterkamp, and R.M. Schiffelers. 2016. Extracellular vesicles for drug delivery. *Adv Drug Deliv Rev*. 106:148-156.

van der Vlist, E.J., E.N. Nolte-'t Hoen, W. Stoorvogel, G.J. Arkesteijn, and M.H. Wauben. 2012. Fluorescent labeling of nano-sized vesicles released by cells and subsequent quantitative and qualitative analysis by high-resolution flow cytometry. *Nat Protoc*. 7:1311-1326.

Vanlandingham, P.A., and B.P. Ceresa. 2009. Rab7 Regulates Late Endocytic Trafficking Downstream of Multivesicular Body Biogenesis and Cargo Sequestration. *Journal of Biological Chemistry*. 284:12110-12124.
VanWijk, M.J., E. VanBavel, A. Sturk, and R. Nieuwland. 2003. Microparticles in cardiovascular diseases. *Cardiovasc Res*. 59:277-287.
Vella, L.J., R.A. Sharples, V.A. Lawson, C.L. Masters, R. Cappai, and A.F. Hill. 2007. Packaging of prions into exosomes is associated with a novel pathway of PrP processing. *J Pathol*. 211:582-590.
Vergauwen, G., B. Dhondt, J. Van Deun, E. De Smedt, G. Berx, E. Timmerman, K. Gevaert, I. Miinalainen, V. Cocquyt, G. Braems, R. Van den Broecke, H. Denys, O. De Wever, and A. Hendrix. 2017. Confounding factors of ultrafiltration and protein analysis in extracellular vesicle research. *Sci Rep*. 7:2704.
Vingtdeux, V., N. Sergeant, and L. Buee. 2012. Potential contribution of exosomes to the prion-like propagation of lesions in Alzheimer's disease. *Front Physiol*. 3:229.
Vysotskii, V.V., O.Y. Uryupina, A.V. Gusel'nikova, and V.I. Roldugin. 2009. On the feasibility of determining nanoparticle concentration by the dynamic light scattering method. *Colloid J+*. 71:739-744.
Vysotsky, V.V., O.Y. Uryupina, V.I. Roldughin, and Y.A. Plachev. 2009. Formation of silver nanoparticles in aqueous carboxymethyl cellulose solutions and the evolution of their sizes. *Colloid J+*. 71:156-162.
Walsh, D.M., and D.J. Selkoe. 2007. A beta oligomers - a decade of discovery. *J Neurochem*. 101:1172-1184.
Wang, T.L., Z. Ming, X.C. Wu, and W.J. Hong. 2011. Rab7: Role of its protein interaction cascades in endo-lysosomal traffic. *Cell Signal*. 23:516-521.
Watts, J.C., C. Condello, J. Stohr, A. Oehler, J. Lee, S.J. DeArmond, L. Lannfelt, M. Ingelsson, K. Giles, and S.B. Prusiner. 2014. Serial propagation of distinct strains of Abeta prions from Alzheimer's disease patients. *Proceedings of the National Academy of Sciences of the United States of America*. 111:10323-10328.
Wei, Z., A.O. Batagov, D.R. Carter, and A.M. Krichevsky. 2016. Fetal Bovine Serum RNA Interferes with the Cell Culture derived Extracellular RNA. *Sci Rep*. 6:31175.
Wells, G.A., A.C. Scott, C.T. Johnson, R.F. Gunning, R.D. Hancock, M. Jeffrey, M. Dawson, and R. Bradley. 1987. A novel progressive spongiform encephalopathy in cattle. *Vet Rec*. 121:419-420.
Witwer, K.W., E.I. Buzas, L.T. Bemis, A. Bora, C. Lasser, J. Lotvall, E.N. Nolte-'t Hoen, M.G. Piper, S. Sivaraman, J. Skog, C. Thery, M.H. Wauben, and F. Hochberg. 2013. Standardization of sample collection, isolation and analysis methods in extracellular vesicle research. *Journal of extracellular vesicles*. 2.
Wolf, P. 1967. The nature and significance of platelet products in human plasma. *Br J Haematol*. 13:269-288.
Yamashita, T., Y. Takahashi, M. Nishikawa, and Y. Takakura. 2016. Effect of exosome isolation methods on physicochemical properties of exosomes and clearance of exosomes from the blood circulation. *Eur J Pharm Biopharm*. 98:1-8.
Yanagisawa, K. 2005. GM1 ganglioside and the seeding of amyloid in Alzheimer's disease: endogenous seed for Alzheimer amyloid. *The Neuroscientist : a review journal bringing neurobiology, neurology and psychiatry*. 11:250-260.

Yanagisawa, K., and Y. Ihara. 1998. GM1 ganglioside-bound amyloid beta-protein in Alzheimer's disease brain. *Neurobiol Aging*. 19:S65-67.

Yanagisawa, K., A. Odaka, N. Suzuki, and Y. Ihara. 1995. GM1 ganglioside-bound amyloid beta-protein (A beta): a possible form of preamyloid in Alzheimer's disease. *Nature medicine*. 1:1062-1066.

Yang, Y., L.Q. Feng, and X.X. Zheng. 2011. Microtubule and kinesin/dynein-dependent, bi-directional transport of autolysosomes in neurites of PC12 cells. *Int J Biochem Cell Biol*. 43:1147-1156.

Yang, Z., and D.J. Klionsky. 2010. Mammalian autophagy: core molecular machinery and signaling regulation. *Current opinion in cell biology*. 22:124-131.

Yao, H., D. Zhao, S.H. Khan, and L. Yang. 2013. Role of autophagy in prion protein-induced neurodegenerative diseases. *Acta Biochim Biophys Sin (Shanghai)*. 45:494-502.

Yim, Y.I., B.C. Park, R. Yadavalli, X.H. Zhao, E. Eisenberg, and L.E. Greene. 2015. The multivesicular body is the major internal site of prion conversion. *Journal of Cell Science*. 128:1434-1443.

Yu, W.H., A.M. Cuervo, A. Kumar, C.M. Peterhoff, S.D. Schmidt, J.H. Lee, P.S. Mohan, M. Mercken, M.R. Farmery, L.O. Tjernberg, Y. Jiang, K. Duff, Y. Uchiyama, J. Naslund, P.M. Mathews, A.M. Cataldo, and R.A. Nixon. 2005. Macroautophagy--a novel Beta-amyloid peptide-generating pathway activated in Alzheimer's disease. *J Cell Biol*. 171:87-98.

Yu, W.H., A. Kumar, C. Peterhoff, L. Shapiro Kulnane, Y. Uchiyama, B.T. Lamb, A.M. Cuervo, and R.A. Nixon. 2004. Autophagic vacuoles are enriched in amyloid precursor protein-secretase activities: implications for beta-amyloid peptide over-production and localization in Alzheimer's disease. *Int J Biochem Cell Biol*. 36:2531-2540.

Yuana, Y., R.I. Koning, M.E. Kuil, P.C. Rensen, A.J. Koster, R.M. Bertina, and S. Osanto. 2013. Cryo-electron microscopy of extracellular vesicles in fresh plasma. *Journal of extracellular vesicles*. 2.

Yuyama, K., and Y. Igarashi. 2017. Exosomes as Carriers of Alzheimer's Amyloid-beta. *Front Neurosci-Switz*. 11.

Yuyama, K., H. Sun, S. Mitsutake, and Y. Igarashi. 2012. Sphingolipid-modulated exosome secretion promotes clearance of amyloid-beta by microglia. *J Biol Chem*. 287:10977-10989.

Yuyama, K., H. Sun, S. Sakai, S. Mitsutake, M. Okada, H. Tahara, J. Furukawa, N. Fujitani, Y. Shinohara, and Y. Igarashi. 2014. Decreased amyloid-beta pathologies by intracerebral loading of glycosphingolipid-enriched exosomes in Alzheimer model mice. *The Journal of biological chemistry*. 289:24488-24498.

Yuyama, K., H. Sun, S. Usuki, S. Sakai, H. Hanamatsu, T. Mioka, N. Kimura, M. Okada, H. Tahara, J. Furukawa, N. Fujitani, Y. Shinohara, and Y. Igarashi. 2015. A potential function for neuronal exosomes: sequestering intracerebral amyloid-beta peptide. *FEBS Lett*. 589:84-88.

Zhang, M., and R. Schekman. 2013. Cell biology. Unconventional secretion, unconventional solutions. *Science*. 340:559-561.

Zhang, S., J. Salemi, H. Hou, Y. Zhu, T. Mori, B. Giunta, D. Obregon, and J. Tan. 2010. Rapamycin promotes beta-amyloid production via ADAM-10 inhibition. *Biochem Biophys Res Commun*. 398:337-341.

Zhang, X., E.R. Abels, J.S. Redzic, J. Margulis, S. Finkbeiner, and X.O. Breakefield. 2016. Potential Transfer of Polyglutamine and CAG-Repeat RNA in Extracellular Vesicles in Huntington's Disease: Background and Evaluation in Cell Culture. *Cell Mol Neurobiol*. 36:459-470.

Zhou, J., S.H. Tan, V. Nicolas, C. Bauvy, N.D. Yang, J. Zhang, Y. Xue, P. Codogno, and H.M. Shen. 2013. Activation of lysosomal function in the course of autophagy via mTORC1 suppression and autophagosome-lysosome fusion. *Cell Res*. 23:508-523.

Appendices

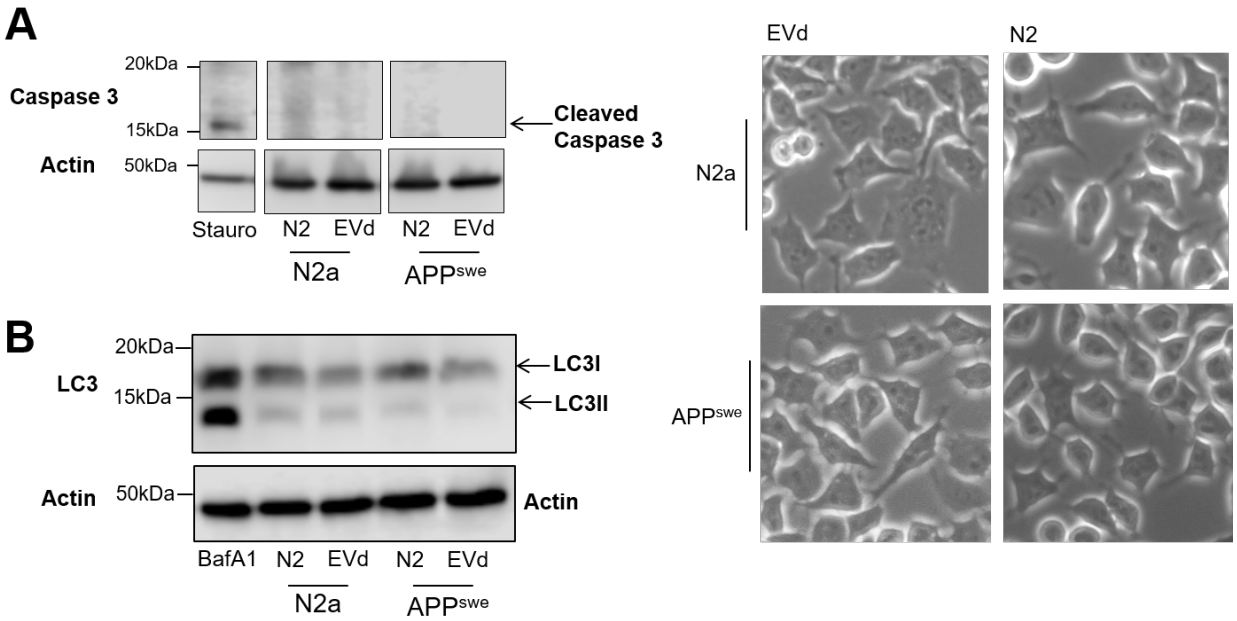

Appendix 1. Effect of EV collection media on cell viability. EVs were collected from N2a or N2aAPP^{swe} cells in the following media for 24 hours: OptiMEM alone (Opti), OptiMEM:DMEM 1:1 with B27 (B27), OptiMEM:DMEM 1:1 with N2 (N2) or OptiMEM:DMEM 1:1 with 10% EV-depleted serum (EVd). **(A)** Caspase 3 cleavage was examined by western blot analysis. Some cells were treated with 10μM Staurosporine (Stauro) for 4 hours as a positive control. **(B)** LC3 was detected by western blot. Some cells were treated with 150nM bafilomycin (BafA1) for 4 hours as a positive control. **(C)** Cells were visualized by phase contrast microscopy.

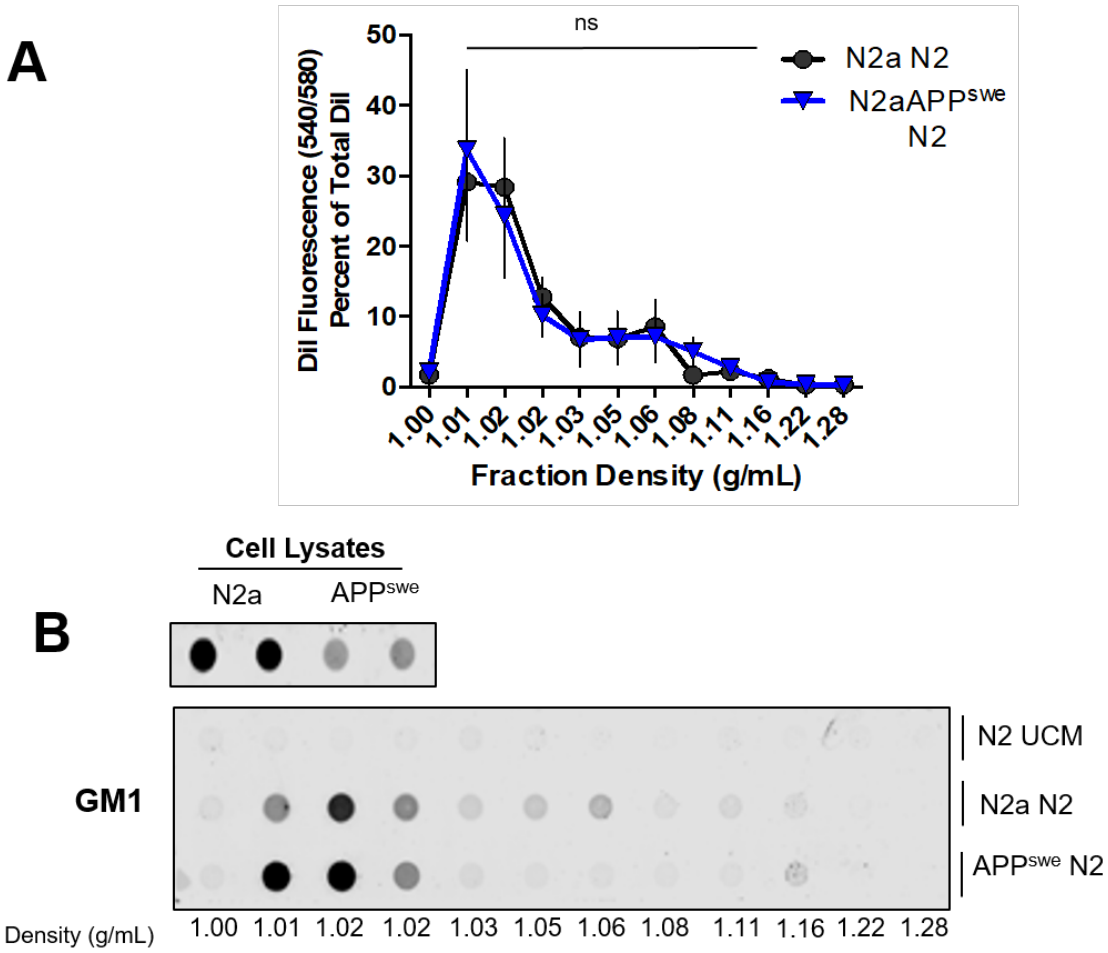

Appendix 2. N2a and N2aAPP^{swe} cells produce similar EVs (A) EVs from cultured cells were collected in media containing N2 supplement for 24 hours, subjected to a 2000xg centrifugation, and then protein concentrated. Retentates were normalized to cellular protein, loaded onto an iodixanol gradient and twelve fractions were collected. DiI fluorescence in each fraction was measured and plotted as a percent of total DiI in the gradient for each of N2a and N2aAPP^{swe} cells. Data represents the mean±SEM, n=3. Significance was determined by one-way ANOVA with Tukey *post hoc* test. **(B)** Fractions and 5ug of corresponding cell lysates were subject to dotblot for GM1. N2 UCM was used as a negative control.

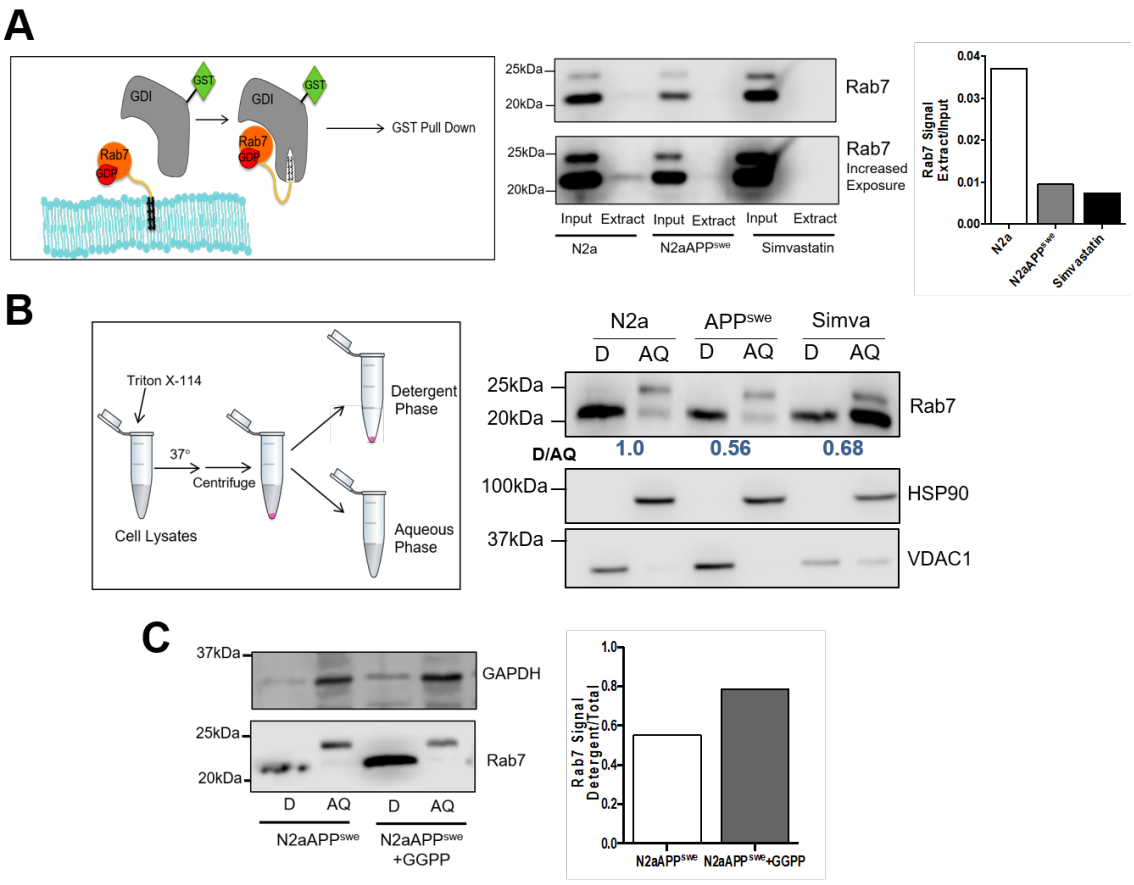

Appendix 3. N2aAPP^{swe} cells have a defect in protein prenylation (A) Rab prenylation was assessed by GDI capture assay. Equal amounts of protein for each N2a and N2aAPP^{swe} were loaded into inputs and five times the amount of protein of cell lysates was extracted. Extraction represents prenylated Rabs. Prenylated Rabs run faster than unprenylated, therefore the top and bottom bands represent unprenylated and prenylated Rab7 respectively. Simvastatin was used as a positive control for impairing protein prenylation. **(B)** Triton phase separation in N2a and N2aAPP^{swe}. Triton X-114 was used to separate prenylated (detergent phase, D) and unprenylated (aqueous phase, AQ) proteins. Rab7 was detected by immunoblot. Samples were normalized to cellular protein prior to separation. Simvastatin was used as a positive control for impairing protein prenylation. HSP90 and VDAC1 were blotted as controls for the separation, and should exclusively be in the aqueous and detergent phases respectively. **(C)** Exogenous administration of isoprenoid GGPP moderately restores N2aAPP^{swe}-induced inhibition of protein prenylation in preliminary experiments. GAPDH was blotted to confirm the separation, and should be enriched in the aqueous phase.